Experimental investigations into charge and spin carriers in polyaniline.

Devasagayam, Peter

EXPERIMENTAL INVESTIGATIONS INTO CHARGE AND SPIN CARRIERS IN POLYANILINE.

By

Peter Devasagayam

A thesis submitted to the faculty of science,

Durham University for the Degree of Ph.D.

Department of Physics

University of Durham

November 1998

ABSTRACT.

Conductivity and electron spin resonance measurements have been performed on solution doped polyaniline (PANi). It is proposed that both camphor-sulphonic acid (CSA) and 2-acrylamido-2-methyl-1-propanesulphonic acid (AMPSA) doped PANi can be described by the same model. It is suggested that the polyaniline materials are composed of differently ordered layers, a highly ordered region forming the core of the crystallites. The core of the crystallites are believed to be encapsulated within a semi-ordered region, with the crystallites themselves being dispersed in an amorphous polymer matrix.

The conductivity measurements and ESR results described in this work support the proposal that within the highly ordered region of doped polyaniline crystallites, a polaronic lattice exists. The polaronic lattice facilitates "free" carriers which are responsible for "metallic" conduction within the crystallites. Encapsulating the polaronic lattice is a semi-ordered region in which (partially) mobile polarons (and possibly bipolarons) are present. The highly conductive crystallites are randomly dispersed in a less conductive polymer matrix.

Charge transport within this heterogeneous system is well described by a heterogeneous metal - fluctuation induced tunnelling (FIT) model. The differences in the temperature dependent conductivities of the PANi-CSA and PANi-AMPSA materials are attributed to the systems having layers of different relative sizes (in the above model). AMPSA doped polyaniline films had a maximum room temperature conductivity of ~100 Scm^{-1}. This material also showed potential for use as an electrode layer in polymer LEDs, to replace ITO coated glass. The conductivity of PANi-AMPSA

was measured to be 50 ± 10 Scm^{-1} at thickness' of ~30nm. Layers of this thickness provide >90% optical transmission between 450 and 675 nm (most of the visible spectrum).

Faraday rotation measurements have shown that the recently reported large Faraday rotation of polyaniline can not be reproduced. The limited results of the Faraday rotation experiments described in this work provide support for the theory that charge carriers in polyaniline have an effective mass of at least 100 times that of a free electron. It has also been shown that the claims of a polyaniline derivative (namely the Marcoussis polymer) being an entirely organic ferromagnet are unsubstantiated, despite intense investigation.

DECLARATION.

The material in this thesis has not been submitted for examination for any other degree, or part thereof, at Durham University or any other institution. The material in this thesis is the work of the author except where formally acknowledged by reference.

ACKNOWLEDGEMENTS.

Thanks to the numerous technical staff whose patience in the face of panic have greatly aided the work described in this thesis. Thanks, Norman, Davey, Tom, Chris and Chris, Phil, George and Pete.

This thesis is dedicated to all those friends and relatives whose support has made this work possible. Most notable among these is my supervisor, Andy Monkman, for his relentless optimism at the times when it seemed nothing could be achieved. Similar gratitude must also be expressed to my colleagues for their great support over the past three years; thanks, Steve, Eggie, Phil, Ed, Anne, Eymard, Paul and Paul, Stu, Mounir and Ben. A special mention must be made of Dr Andreas Petr of IFW Dresden, for taking such good care of an Englishman abroad. Special thanks also to my housemates of the past three years for tolerating my numerous Ph.D. related mood swings; thanks Claire, Helen, Paul, Diane, Paul, Eggie, Stu and Catherine, especially Claire who had the misfortune to live with me for the entire three years of my Ph.D. studies.

Greatest thanks are bestowed upon my girlfriend Catherine for the numerous meals, lifts and expressions of love provided as I worked late into the night, and for her patience with my diabolical spelling and grammar whilst proof reading this thesis.

Thanks again everybody I could not have done it without you.

CONTENTS.

LIST OF FIGURES.

LIST OF TABLES.

List of Abbreviations.

AMPSA	-	2-Acrylamido-2-Methyl-1-PropaneSulphonic Acid
ANSA	-	5-Amino-2-NaphthaleneSulphonic Acid
ANSA	-	5-(1,4-Amino-Anilo)-2-NaphthaleneSulphonic Acid
APSA	-	AcrylamidoPropaneSulphonic Acid
CA	-	Cellulose Acetate
CA-PANi-HCl	-	(a blend of) CA and PANi (emeraldine base, doped with hydrochloric acid)
CSA	-	10-CamphorSulphonic Acid
DBSA	-	DodecylBenzeneSulphonic Acid
DCA	-	DiChloroacetic Acid
DNA	-	Deoxyribose Nucleic Acid
DMSO	-	DiMethylSulphOxide
ESR	-	Elxctron Spin Resonance
FIT	-	Fluctuation Induced Tunnelling
FTIR	-	Fourier Transform Infra-Red
IR	-	Infra-Red
ITO	-	Indium Tin Oxide
LCAO	-	Linear Combination of Atomic Orbitals
LED	-	Light Emitting Diode
MO	-	Molecular Orbital
NMP	-	N-Methyl-2-Pyrrolidinone
NMR	-	Nuclear Magnetic Resonance
PA	-	PolyAcetylene

PANi	-	PolyANiline
PANi-AMPSA	-	PolyANiline doped with 2-Acrylamido-2-Methyl-1-PropaneSulphonic Acid (A specific type of PANi-ES)
PANi-CSA	-	PolyANiline doped with 10-CamphorSulphonic Acid (A specific type of PANi-ES)
PANi-EB	-	PolyANiline - Emeraldine Base
PANi-ES	-	PolyANiline - Emeraldine Salt
PANi-LB	-	PolyANiline - Leucoemeraldine Base
PANi-PB	-	PolyANiline - Pernigraniline Base
PC	-	Personal Computer
PNA	-	PolyNaphthylamine
PP	-	PolyPyrrole
PPP	-	PolyParaPhenylene
PT	-	PolyThiophene
SSH	-	Su, Schrieffer, Heeger
VRH	-	Variable Range Hopping
VSM	-	Vibrating Sample Magnetometry

CHAPTER 1

CHAPTER 1

1. AN INTRODUCTION TO CONDUCTING POLYMERS - QUASI-ONE-DIMENSIONAL METALS.

1.1 THE HISTORY OF POLYACETYLENE.

The discovery that the conductivity of polyactylene could be increased by 13 orders of magnitude via doping [1] has led to considerable interest in the area of organic electro-active materials. This discovery has been one of the major driving forces behind research into electrically conductive polymers, and has led to the publishing of thousands of papers in the following years. Stretch-oriented polyacetylene samples with conductivites up to 10^5 Scm^{-1} have since been reported [2, 3]. Considering that the room temperature conductivity of copper is approximately $6x10^5$ Scm^{-1}, the highly conductive forms of polyactylene (PA) can be considered to be "metallic" in terms of magnitude, but the conductivity shows unusual temperature dependence. This anomalous temperature dependence showed that the electrical transport mechanism may not be metallic.

PA was first synthesised in 1958 [4] as a black or grey semi-crystalline powder, insoluble in any solvents, which decomposed before melting. A breakthrough came in 1974 when Shirakawa *et al.* [5], (rather fortuitously), devised an experimental technique in which the synthesised polymer was deposited as a free standing film. The discovery was instigated by a translation error whereby Shirakawa *et al.* blew one of the reactants

over the surface of the reaction mixture instead of bubbling it through, thus depositing a polymer layer on the surface of reaction medium. This black film with a "metallic lustre" is again insoluble and does not melt, but samples manufactured in this fashion have contributed greatly to the understanding of conducting polymers.

The motivation behind the interest in conducting polymers is two-fold. Firstly there is the purely theoretical challenge of trying to understand charge transport in what is inherently a quasi one-dimensional system. This is further complicated by the role of inter-chain charge transfer, which must obviously be present if there is to be bulk electrical conductivity. The other reason is associated with the fact that polymers have for a long time been used in a vast array of applications. One of their major attributes is the ease with which they can be processed once they have been synthesised. Unlike conventional metals, polymers do not require high temperature preparative techniques or high temperature thermal processing. Polymers (generally) can easily be cast or spun, (from a solution), into films or fibres and are often post-processed using low temperature techniques (compared to those used for metals) such as extrusion, injection moulding, etc..

The prospect of an electrical conductor that can be prepared from solution, and the anticipated applications associated with such a material [6,7] has led to intensive research. PA has been pivotal to this research due to its inherent simplicity as a polymer. A major drawback with PA is that it is not stable in oxygen or moisture rich environments, and hence has few (if any) practical applications. PA is therefore often viewed as a model compound.

1.2 PI - CONJUGATION.

The chemical structure of PA is very simple (figure 1.1). It is composed entirely of Carbon and Hydrogen (in the un-doped or "pristine" form) and is most easily described by the abbreviated notation $(CH)_x$. PA can exist in three forms (figure 1.2). For simplicity the *"trans-transoid"* isomer will be referred to as *trans*-PA, and the *"cis-transoid"* form *cis*-PA. It can be easily seen from figure 1.2 that the polymer backbone consists of alternating double and single bonds, creating what is known as a "conjugated" polymer. From now on any mention of PA will refer to *trans*-PA, unless explicitly stated otherwise.

At this point it is useful to introduce some nomenclature used by chemists to describe bonding. Excluding core electronic orbitals, which take no part in chemical processes, three basic types of bonding orbitals can be identified. Electrons in the "σ" orbitals are responsible for the strong "covalent" bonds associated with organic molecules, and are strongly localised between the two bonded nuclei. "π" electronic orbitals also contribute to chemical bonding, but tend to form weaker, less localised bonds. The other type of orbital, "n", refers to electrons in a "non-bonding" orbital, and is primarily associated with heteroatoms (i.e. O, N, S, P, etc., not C or H). Non-bonding orbitals are not considered to be important with respect to chemical bonding (obviously) but they do however influence chemical reactivity. A simple representation of the electronic structure of PA can be constructed when the arrangement of the chemical bonding is examined in greater detail. The three σ bonds around a single carbon atom (two connecting the adjacent carbon atoms and the other with the associated hydrogen atom) are formed from linear combinations of three in-plane atomic orbitals; namely

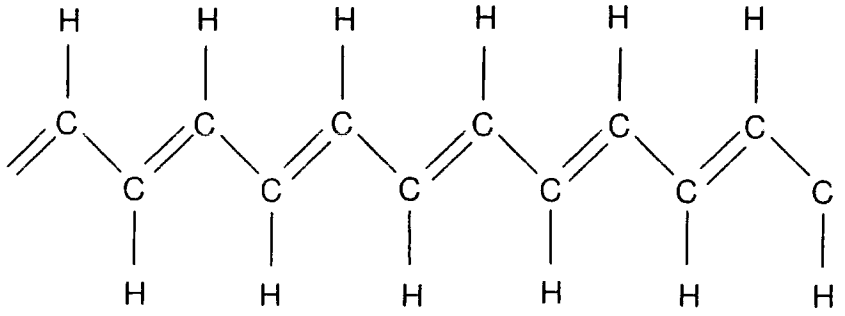

Figure 1.1. The chemical structure of ("*all trans*-") polyacetylene.

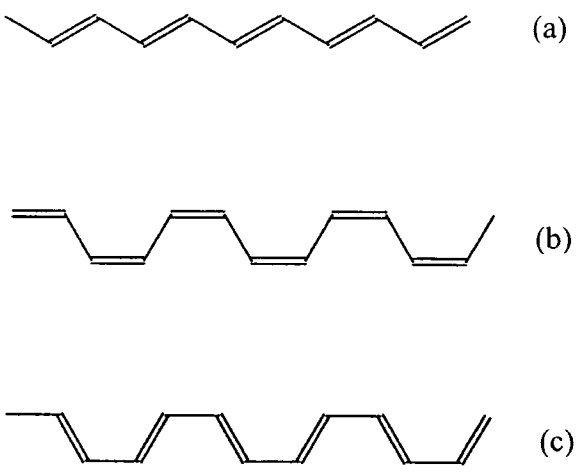

Figure 1.2. Skeletal representations of the three isomers of polyacetylene, (a) *trans-transoid*, (b) *cis-transoid*, (c) *trans-cisoid*.

the 2s, $2p_x$, and $2p_y$ (figure 1.3a). This combination of the atomic orbitals is termed "sp^2 hybridisation," and the resulting σ bonds are all equivalent and lie in the plane of the molecule (figure 1.3b). The π bond is formed by the sideways overlap of adjacent $2p_z$ orbitals which are orthogonal to the molecular plane. Unlike σ bonds, electrons in the π orbitals are not localised between particular carbon atoms; instead they are delocalised above and below the plane of the molecule, over the entire π-conjugated system (figure 1.3c). This delocalisation of electronic states is the very essence of possible conduction along the polymer backbone, and as a consequence many other π-conjugated polymeric systems have been investigated in some depth. For further information on bond hybridisation the reader is directed to standard organic chemistry texts, for example McMurry[8].

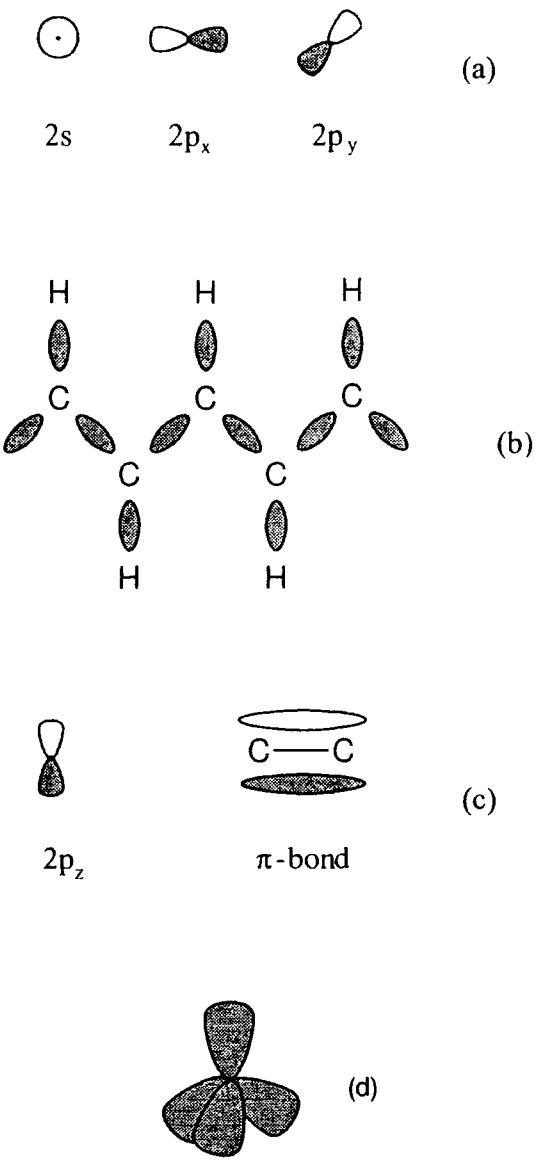

Figure 1.3. Diagrammatic representation of (a) the three in-plane atomic orbitals of carbon, (b) sp^2 hybridised σ bonds in the molecular plane, (c) π orbitals from the overlap of adjacent $2p_z$ orbitals, (the line represents the plane of the σ bond), and (d) the tetrahedral form of the sp^3 hydridised carbon orbital, often associated with diamond.

1.3 THEORETICAL MODELING OF POLYACETYLENE.

1.3.1 MOLECULAR ORBITAL THEORY.

Initial theoretical models for polyacetylene were based on the linear combination of atomic orbitals (LCAO) [9], commonly used in molecular orbital (MO) calculations. It was suggested that long chain lengths of PA would be metallic. This conclusion was arrived at by considering that all carbon-carbon bond lengths were equal. The increase in length of the polymer chain would add new states to both the π (ground state) and π^* (first excited state) molecular orbitals, as a result of the mixing of the new wave function with the system, thus forming bands. As the chain length tends to infinity, the gap between these two bands would eventually be filled by the additional states. Each carbon atom contributes one electron per site to the molecular orbital bands. The Pauli exclusion principle states that each site could be occupied by two electrons of opposing spins, hence the resultant infinite chain would have a half filled continuum band. The delocalised electrons within this band would produce a material that should exhibit metallic behaviour.

Polyacetylene, however, is at best semiconducting in the pristine form, and is only electrically conductive when doped with electron donating (nucleophilic) or withdrawing (electrophilic) species. The initial studies on short chain conjugated molecules [10], predicting that the band gap would tend to zero as chain length tended to infinity, were not, therefore, valid. Investigations into the reduction of the π to π^* band gap have shown that there is a minimum energy of ~1.4eV, even in long chain PA [1]. Therefore, a more complete model than LCAO is needed to understand the

electronic structure of conjugated polymers.

1.3.2 THE SU, SCHRIEFFER, HEEGER MODEL.

The major fault with the LCAO approach is the assumption that all carbon-carbon bond lengths are equal. The fact that a C=C (double) bond is shorter than a C-C (single) bond has been recognised for some time (C=C ~1.33Å and C-C ~1.54Å [8]). Chemists originally thought that long PA molecules would have equal carbon-carbon bond lengths as the π electron orbital was averaged over the entire molecule, (figure 1.4). This view was revised when it was revealed that high molecular weight PA was not metallic. The PA chain undergoes a distortion, by what is sometimes called the "quasi-Jahn-Teller" effect (originally suggested by Salem [11] based on the work by Pope and Walmsley [22]) and the molecule "dimerises" (figure 1.5). This can be likened to the case of a one-dimensional metal that has undergone a Peierls distortion [12,13]. Even in this dimerised form, however, it is wrong to think that a double bond on the PA chain consists of a σ and a π bond, and that a single bond is solely a σ bond. Both types of bond in PA contain elements of both types of bonding, it is just that the shorter carbon-carbon (double) bonds have a higher degree of π character.

Su, Schrieffer and Heeger constructed a model Hamiltonian (H_{SSH}) for the total energy of the PA system by considering the contributions of both the σ and π bands, [14] where $H_{SSH} = H_\sigma + H_\pi$. Hence the Hamiltonian is reduced into two parts, H_σ and H_π for the σ and π electrons respectively [15].

Figure 1.4. A schematic representation of the way in which the π orbital of PA was expected to average for long chain PA. The dotted lines represent a "half" π bond.

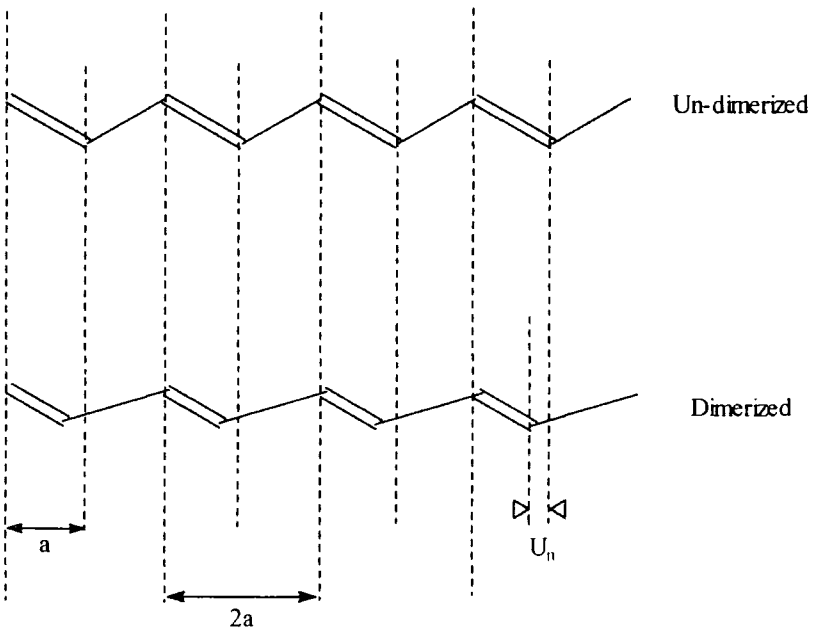

Figure 1.5. Schematic representation of the difference between the dimerised (real) and un-dimerised (originally suggested) structure of PA.

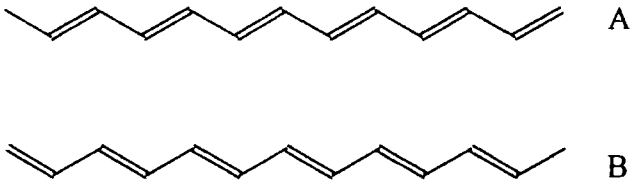

Figure 1.6. The two degenerate phases of PA, A and B.

$$H_\sigma = (K_0 / 2) \sum_n (u_{n+1} + u_n) \qquad \text{eqn. 1.1}$$

where u_n is the deviation of the n^{th} carbon site from the equilibrium position (figure 1.5). Taking the average bond length to be ~1.4Å, and the bond angle as 120°, then a ≈ 1.22Å (see figure 1.5). K_0 represents the lattice force constant, describing the potential energy of the displacement of an atom from the equilibrium position (more simply described as the spring constant due to σ bonding [16]).

H_π uses the tight binding approximation for the electrons in the π molecular orbital (i.e. only nearest neighbour interactions are considered).

$$H_\pi = -\sum_{n,s} t_{n,n+1}(c^+_{n,s}c_{n+1,s} + c^+_{n+1,s}c_{n,s}) \qquad \text{eqn 1.2}$$

where $t_{n,n+1}$ is termed the "hopping" (or transfer) integral and is a function of carbon-carbon separation, $c^+_{n,s}$ and $c_{n,s}$ are creation and annihilation operators (respectively) for a π electron with spin s at carbon site n. Linear expansion of the transfer integral gives:

$$t_{n,n+1} = t_o - \alpha(u_{n+1} - u_n), \qquad \text{eqn. 1.3}$$

α being a constant that relates electron transfer with carbon site displacement as a consequence of the electron transfer. Effectively α is an electron-phonon coupling constant for π electrons, and hence $t_{n,n+1}$ represents the π orbital (or π wavefunction) overlap between adjacent carbons; obviously, the greater the carbon-carbon separation the smaller the overlap.

For the case where $u_n=0$ (i.e. all carbon-carbon bond lengths are equal) then the above model predicts the formation of a tight binding, half-filled continuous π band of width $4t_0$, having the dispersion relation:

$$E_k = -2t_0\cos(ka). \qquad \text{eqn. 1.4}$$

However, since the Su, Schrieffer, Heeger (SSH) model is general, it can be used to take into account the alternation in bond lengths. It was shown by Peierls [12] that a lowering of the total system energy could be achieved in a one-dimensional metal. The distortion of the lattice into a dimerised state creates the formation of a gap in the band structure centred on the Fermi level. The dimerised state is more stable if the reduction in energy of the occupied states is greater than the energy required to dimerise the lattice. In the dimerised state (figure 1.5) the displacement of the carbon atoms from equilibrium is of the form:

$$u_{n0} = \pm (-1)^n u_0. \qquad \text{eqn. 1.5}$$

where (+) corresponds to phase A and (-) to phase B PA (see figure 1.6). Therefore, the hopping integrals for the perfect chain (consisting solely of PA in either the A or B phase) are:

$$t_{n,n+1} = \begin{cases} t_0 - t_1 & \text{-"single" bond} \\ t_0 + t_1 & \text{-"double" bond.} \end{cases} \qquad \text{eqn. 1.6}$$

The resultant band structure has a dispersion relation given by:

$$E_k = (4t_0^2\cos^2(ka) + \Delta^2\sin^2(ka))^{1/2} \qquad \text{eqn. 1.7}$$

where $\Delta = 4\alpha u_0$, and is known as the gap parameter. The gap separating the occupied π (valence) and unoccupied π^* (conduction) bands is of energy E_g, where $E_g = 2\Delta$. The change in energy of the system as a function of the displacement from equilibrium, u, can be calculated using the tight binding model; and takes the form:

$$E(u) = 2K_0u^2 - u^2\ln(t_0/\alpha u_0). \qquad \text{eqn. 1.8}$$

The first term representing the increase in potential as a result of lattice distortion and the second the decrease in energy of the π electron system. Equation 1.8 has minima (i.e. stable ground state configurations, see figure 1.7) for $u = \pm u_0$ referring to two degenerate resonance forms of polyacetylene.

Thus, Su, Schrieffer and Heeger's model fits the experimental observations of PA. Optical studies show that the absorption of pristine PA is similar to an inorganic semiconductor, with a band gap energy of ~1.4eV. It is also important to note that X-ray scattering [17] and NMR experiments [18] have shown that there is indeed a dimerisation of ~ 0.03-0.04Å, in agreement with theoretical expectation. Pristine PA also shows very low conductivity, as would be expected for a material with a fully occupied valence (π) band and an empty conduction (π^*) band. Metallic conductivity can only be induced in PA via chemical doping [3] in a similar way to the doping of conventional semiconductors.

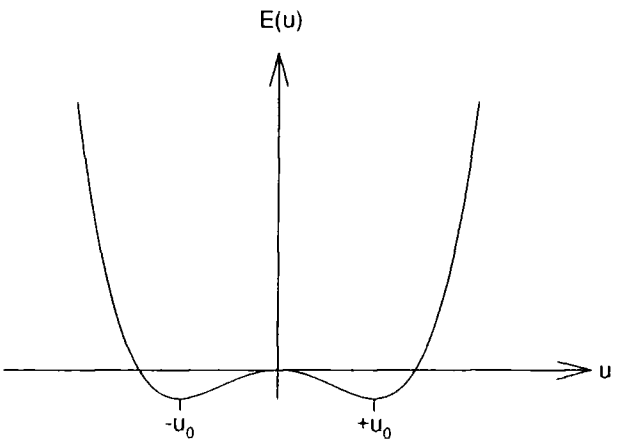

Figure 1.7. Graph showing the change in total energy, E(u), of the PA system with respect to the displacement, u, of carbon atoms from the equilibrium position. The energy tends to a minimum for $u=\pm u_0$, from equation 1.8.

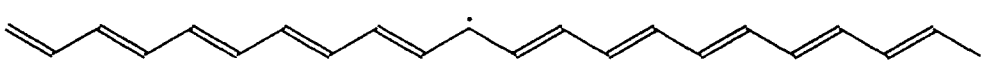

Figure 1.8. The meeting of A and B phase PA on a single chain. The dot represents a single un-paired π electron, but since there are the same number of electrons in the above molecule as there would be in a backbone of single phase, there is no charge associated with the lone electron.

1.4 SOLITONS IN POLYACETYLENE.

In section 1.3.2 it has been shown that the ground state of the dimerised chain has two degenerate forms, namely the A and B phases (figure1.6). Consider now a simple excitation associated with this degeneracy corresponding to a single molecule containing both A and B phases [19] (figure 1.8). The point separating the two phases is, in effect, a bond defect and is termed a "soliton" [20]. The carbon atom at this structural mismatch retains a single electron (in a $2p_z$ orbital) which is unable to form a π bond with either of the adjacent carbon atoms. Hence the soliton has an associated spin, s±½; but there is no net charge as a result of the defect.

Su, Schrieffer and Heeger [19], and (independently) Rice [21] modelled the properties of such a neutral soliton using the Heisenberg uncertainty principle (which describes the uncertainty associated with the position and momentum of a particle). The result was a suggested wave function of a soliton at site n (the n^{th} carbon site) and took the form:

$$\phi = u_0 \tanh(na/\xi) \qquad \text{eqn. 1.9}$$

where a is the length of a repeat unit of the dimerised polymer chain (i.e. equivalent to 2a in fig. 1.5) and ξ, the correlation length, corresponds to the number of lattice sites over which the soliton extends. Rice calculated correlation lengths for a number of different band gap energies and estimated that for E_g = 1.4eV, $\xi \approx 7a$, which is equivalent to 14 lattice sites. Thus Su *et al.* concluded that "...hence the wall [between

phases] is quite diffuse...". The same group [19] also calculated that the energy required to excite a PA molecule (from the ground state to a molecule containing a soliton) varied by only ~0.002eV as the position of the centre of the soliton was varied between carbon sites. This implies that at temperatures where the thermal energy is greater than ~0.002eV (between 20 and 40K) the soliton would be free to translate along the polymer backbone. The soliton thus converts regions of the chain from one phase to another with no change in the total energy of the system (as the two phases are degenerate). This is sometimes referred to as a non-dispersive solitonic excitation as the soliton defect is not changed by this process.

To investigate the effect of the soliton on the electronic band structure the density of states, N(E), as a function of energy, E, needs to be evaluated. Using the tight binding approximation in conjunction with equation 1.7 it can be shown [13] that the density of states takes the form:

$$N(E) = N / \pi.(4t^2 - (E - E_0)^2)^{1/2}. \qquad \text{eqn. 1.10}$$

This distribution of states is shown schematically in figure 1.9. The SSH model for solitons [19] showed that the presence of the bond alternation defect modified the band structure by the creation of a single sharp state at $E_0 = 0$, the mid-gap energy. Since the total number of electronic states in the π band must be conserved, it follows that both the valence and conduction bands contribute one half of this state. Su, Schrieffer and Heeger also showed that the valence band would be completely filled with or without the presence of a soliton and that the presence of a soliton reduces the number of available states in the valence band. Hence the midgap state is occupied by a single (unpaired) electron that could not be accommodated in the valence band (figure

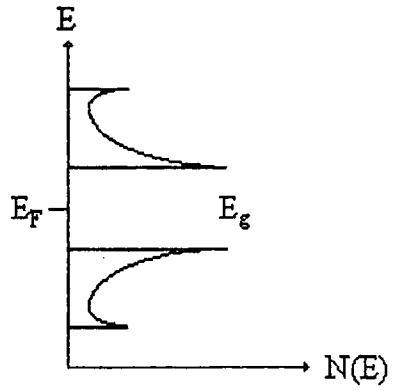

Figure 1.9. Schematic representation of the density of states as a function of energy. E_F is the Fermi level, and E_g the band gap.

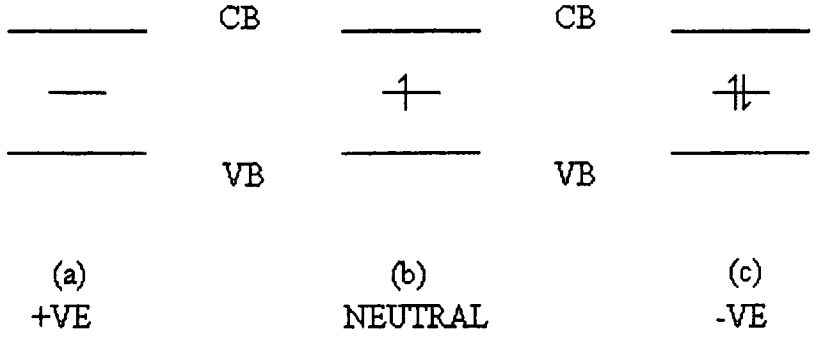

Figure 1.10. Diagram showing the relationship between charge and occupation of the non-bonding orbital that is associated with the soliton bond alternation defect. CB and VB refer to the Conduction and Valence Band respectively.

1.10). Note, however, that this mid-gap state is localised around the lattice distortion. The creation energy for the soliton state was also calculated and found to be roughly 0.6Δ, (note that $E_g=2\Delta$, equation 1.7), i.e., less than the creation energy of an electron-hole pair. This implies that the soliton is a more stable excitation than an electron in the conduction band, and as such should play an important role in the electronic properties of PA.

The form of this defect state had been reported as early as 1962 [22] with respect to long chain polyene molecules. Pope and Walmsley [22] even anticipated the presence of a localised spin associated with the bond alternation, but did not realise the reversed spin-charge relationship. Su, Schrieffer and Heeger summarised that the neutral soliton would have spin $\pm\frac{1}{2}$, occupying the non-bonding orbital mid way between the π (bonding) and π^* (anti-bonding) molecular orbital bands.

1.5 THE FORMATION OF CHARGE CARRIERS IN CONJUGATED POLYMERS.

1.5.1 DEGENERATE GROUND-STATE SYSTEMS.

The fact that polyacetylene is the simplest π-conjugated polymer has previously been mentioned, and as such it is again useful to consider PA as a model for the more complicated conducting polymers that shall be investigated further.

The chemical doping required to transform polyacetylene from a semi-conducting state to a conducting one is simple REDOX chemistry [9]. Simply put this is the REDuction (or OXidation) of the material to add (or remove) electrons from the polymer backbone. As discussed in section 1.4, the energy required to create a soliton excitation is smaller than the energy to create an electron in the conduction band. Hence it is energetically favourable to create a charged soliton state upon doping, as opposed to the formation of an electron or hole in the conduction or valence band respectively. Figure 1.10 shows the relationship between occupation of the mid-gap state and the charge of the defect. These combinations of charge and spin can be described simply as follows:

S^0 - neutral soliton, has no net charge and spin ±½ (figure 1.10b);

S^+ - positive soliton, has charge +1 and no net spin (figure 1.10a);

S^- - negative soliton, has charge -1 and no net spin (figure 1.10c).

It is immediately obvious that the presence of a few charged solitons would not instantly transform PA into a metallic conductor. The obvious reason being that neither

of the two charged species gives rise to a half filled band structure with an appreciable density of states at the Fermi level, as required for metallic conduction. It is, however, possible that a few mobile charges could lead to low electrical conductivity via a "hopping" mechanism such as variable range hopping (see section 1.7.4). Another reason is that solitons are localised, hence it is not unreasonable to assume that the charged species would reside on the parts of the chain close to the oppositely charged dopant counterion. In this case the mobility of the charge carrier would be restricted. How is it then, that there have been reports of such high conductivity [2,3,23] in doped PA?

It is simple to consider the case where the concentration of doping is great enough that there is no appreciable separation of charged solitons along the polymer backbone. If the correlation length of the soliton is ~14 sites, then it follows that a doping level of 1/14 (~0.07) dopant species per carbon atom will create chains in which there is significant overlap of the soliton wavefunctions. In terms of bond structure this can be considered as inducing a homogeneous displacement of carbon sites, not the dimerised structure expected in the pristine material. The interaction of the soliton states creates a band of delocalised states at the mid-gap energy. Note that this soliton band remains either completely filled or empty depending upon the type of doping.

It is the effect of the dopant counterions, however, that accounts for the conductive behaviour of doped PA. The creation of "pinning" sites along the chain causes extension of band tails into the gap regions between the valence-soliton and conduction-soliton bands, as proposed by Rice and Mele [24]. Hence there is a significant density of states at the Fermi level, and "metallic" conduction is possible. For a rigorous explanation of this effect the reader is referred to the above paper by Rice

and Mele [24].

1.5.2 NON-DEGENERATE GROUND-STATE SYSTEMS.

So far in this work the modelling of charge carriers in conducting polymers has only been considered for *trans*-PA, in which the ground-states are degenerate. At this point the author wishes to introduce the concept of systems with non-degenerate ground-states (non-degenerate for short).

The original SSH Hamiltonian was constructed to describe *trans*-PA, but the majority of conducting polymers (e.g. polypyrrole (PP), polythiophene (PT), polyparaphenylene (PPP), *cis*-PA, etc.) do not have a two-fold degenerate ground state (figure 1.11). Consider, for simplicity, *cis*-PA (figure 1.12). The *cis-transoid* isomer is a slightly lower energy state than the *trans-cisoid* form. Unlike the all *trans* case, the symmetry between the two kinds of bonds is broken: there are bonds parallel to the chain direction and bonds at ~60° to it. Hence, it is possible that there is some dimerisation due to the σ bonding, without involving the π electrons. It is, therefore, natural to assume that the three parameters in the SSH model are different for parallel and tilted bonds [25], namely the hopping integral t_0, the electron-phonon coupling constant α and the spring constant K. Wang *et al.* [25] evaluated such a modified Hamiltonian. They found that the energy of the system, E(u), as a function of displacement (u) from equilibrium contained two inequivalent minima at u_0 = 0.054Å and $-u_0$ = -0.049Å, with an energy difference of 0.0148eV. A generic model for the SSH Hamiltonian was proposed by Takayama, Lin-Liu and Maki (the TLM model [26]), and independently by Brazovskii [27]; and the correct boundary conditions were

suggested by Kivelson, Lee, Lin-Liu, Peschel and Yu [28]. This model predicts that a bond alternation defect due to the addition or removal of electrons from the polymer would form a new type of defect.

In a non-degenerate conjugated polymer, with phase A being lower in energy than phase B, it is not possible for a single soliton to exist. Since solitons are mobile the above state would be unstable to the case where the soliton moves to convert all the B phase to the A phase, hence reducing the energy of the system. Therefore the bond alternation defects in non-degenerate systems must be such that it returns to the lower energy configuration either side of the defect, and such a defect is termed a "polaron." In *cis*-PA for example, a polaron is represented by a region of phase B bounded by one charged and one neutral soliton (figure 1.13). Hence, in general terms a polaron is often described as a bound pair of one charged and one neutral soliton.

The effect of a polaron on the band structure can also be considered as a charged-neutral soliton pair. Consider trans-PA, for example; at infinite separation the two species would remain discrete, each occupying a localised mid-gap state. As the solitons are moved closer (to around one bond) the interaction causes a splitting of the mid-gap state. The two new energy levels are distributed symmetrically about the centre of the π–π^* band gap (figure 1.14), this is the general form of the band structure for polarons. Takayama *et al.* [26] calculated the creation energy of a polaron in *cis*-PA, (E_p, analogous to E_s for a soliton) and found $E_p \approx 0.9\Delta$. Hence, an electron (hole) excitation caused by doping is unstable with respect to the formation of a negative (positive) polaron [16]. This is the general case for non-degenerate conjugated polymers.

The creation of a pair of energy levels in the mid-gap region gives rise to the

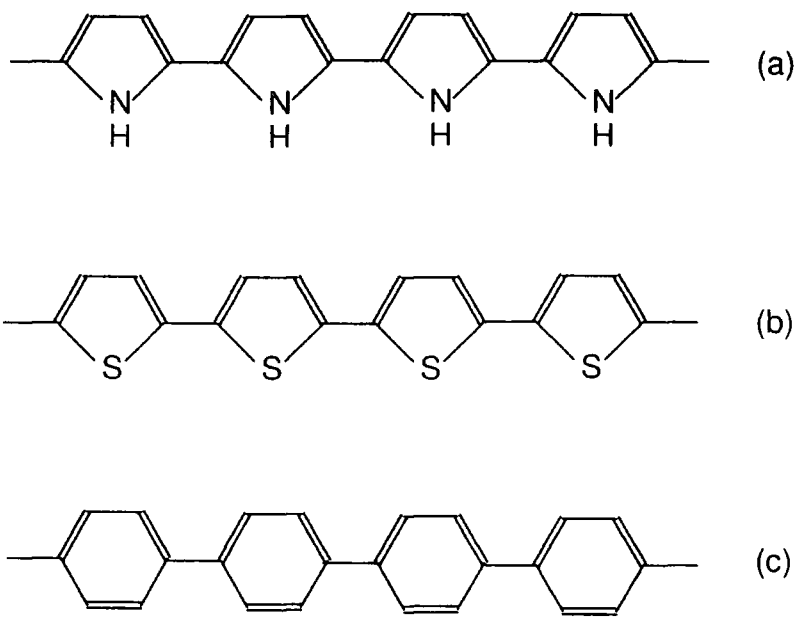

Figure 1.11. Structural configurations of (a) polypyrrole, (b) polythiophene and (c) polyparaphenylene.

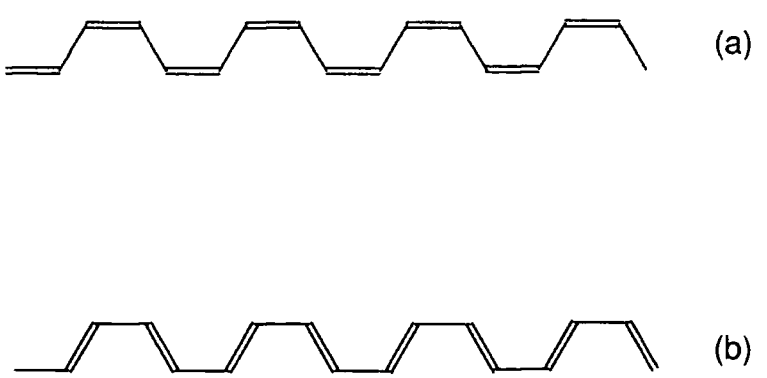

Figure 1.12. The ground-state structures of *cis*-PA, (a) *cis-transoid*, (b) *trans-cisoid*.

possibility of five electronic states (as illustrated in figure 1.15). As in the case of solitons, the formation of a polaron induces a change in the structure of the molecular lattice. Hence it can be viewed that the energy required for lattice distortion is less than the energy gained by the formation of a polaron, thus formation of polarons reduces the energy of the system as a whole. Further addition (removal) of electrons to the polymer chain can result in either production of more polarons, or the formation of "bipolarons," (figure 1.15). The formation of bipolarons occurs when further modification of the lattice structure is favourable compared to the increase in electrostatic repulsion energy associated with the proximity of two like-charges. The polaron, therefore, is similar to the soliton in that it can be envisaged as a charge carrier bound to a lattice deformation. It is useful to summarise the occupation of the polaron energy levels, and the associated charge of the defect, as follows:

P^+ - positive polaron, has charge +1 and spin ±½ (figure 1.15b),

Bp^{2+} - positive bipolaron, has charge +2 and no net spin (figure 1.15a),

P^0 - polaron-exciton, has no net charge and no net spin (figure 1.15c),

P^- - negative polaron, has charge -1, and spin ±½ (figure 1.15d),

Bp^{2+} - negative bipolaron, has charge -2 and no net spin (figure 1.15e).

It is immediately obvious that there are two types of charge carrier, singularly and doubly charged. As stated above, there are different spin-charge relations in polarons and bipolarons. This distinction makes it possible to investigate the majority charge carriers in different polymeric systems. In *trans*-PA the formation of bipolarons is not expected due the above considerations, and this is supported by the Pauli paramagnetic susceptibility for highly doped samples [29]. PPP and PP, however (figure 1.11) show diamagnetic properties at high doping concentrations [16], thus

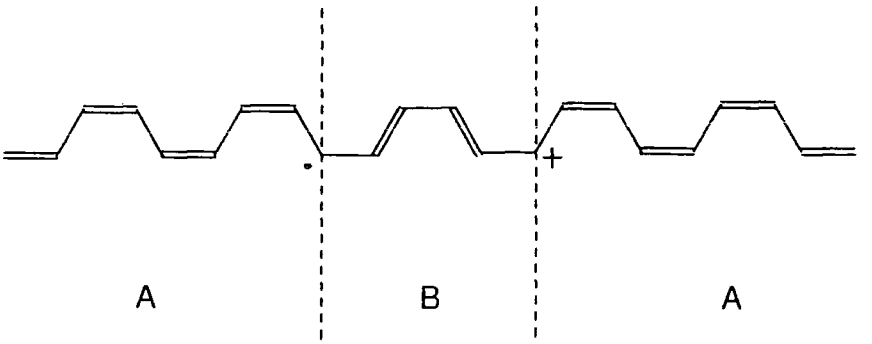

Figure 1.13 Polaron defect in *cis*-PA, a pair of one neutral and one charged soliton separate the higher energy B phase from the A phase polymer either side.

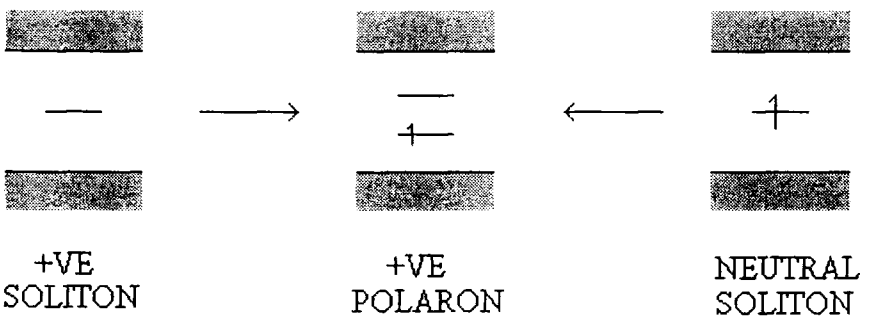

Figure 1.14. Schematic representation of the splitting of the mid-gap energies as two solitons approach each other on the polymer backbone.

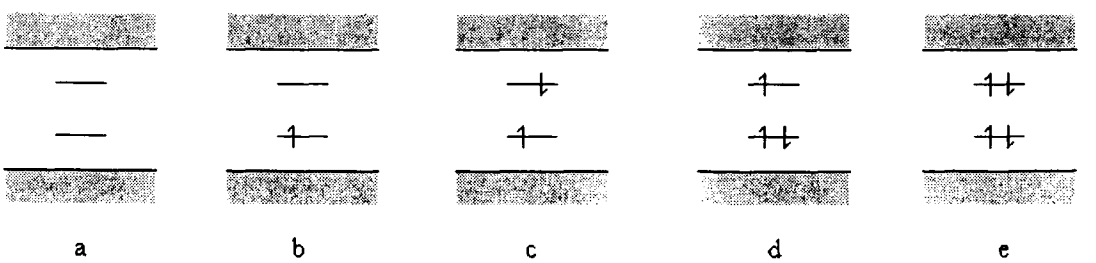

Figure 1.15. Electron occupation of the energy levels in the polaron state; (a) positive bipolaron, (b) positive polaron, (c) polaron-exciton, (d) negative polaron, (e) negative bipolaron.

suggesting the presence of bipolarons.

It is useful to point out that charge transport via polarons (or bipolarons) can be produced by two different mechanisms. The first (and perhaps most obvious) being the propagation of polarons along the polymer backbone, i.e., a quasi-one-dimensional mechanism. This "mobile polaron" model would result in charge carriers with an effective mass much greater than that of a free electron (or hole) as scattering would occur as a result of vibrational and rotational motion of the polymer chain. The three-dimensional "polaron lattice," on the other hand, would result if polaron defects were fixed in a regular array and electrons (or holes) "hopped" between polaron sites. This could (theoretically) lead to essentially free carriers analogous to inorganic metallic and semiconducting systems. Macroscopic charge transport mechanisms are discussed in more detail in section 1.7.

1.6 THE POLYANILINE FAMILY.

So far this work has considered (in the main) polyacetylene as a basis for the theories describing the formation of charge carriers in polyacetylene. There are, however, conducting polymers that could be used as electrical conductors (e.g., polypyrrole and polythiophene). Perhaps one of the most notable series of conducting polymers to date are the "polyanilines." The polyaniline family of polymers can be considered as being based upon a simple molecular chain consisting of 1,4- coupled aniline monomers [30] (figure 1.16). This polymer, and its' derivatives, have been reported as early as 1862 [31] and numerous times since, (see, for example, [32-34]). The general formula of the polymer is shown in figure 1.17. It is generally accepted that there are three basic oxidation states of polyaniline (PANi) [35] (shown in figure 1.18). The oxidation states are summarised as follows:

a) fully reduced (figure 1.18a) - the polymer consists only of "benzenoid" groups (corresponding to x = 1 and y = 0 in figure 1.17) "Leucoemeraldine base" or PANi-LB;

b) half oxidised (figure 1.18b) - there is a 3:1 ratio of "benzenoid" to "quinoid" groups in the polymer backbone (x = 0.5 and y = 0.5 in figure 1.17) "Emeraldine base" or PANi-EB;

c) fully oxidised, (figure 1.18c) - a 1:1 ratio of "benzenoid" to "quinoid" groups (x = 0 and y = 1) "Pernigraniline base" or PANi-PB.

Study of the molecular structure of these forms of PANi reveals two important observations. Firstly the heteroatom (in this case nitrogen) is an integral part of the

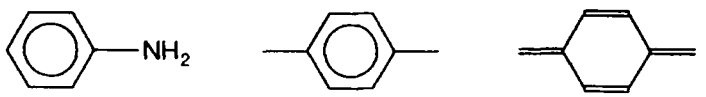

(a) (b) (c)

Figure 1.16. (a) The aniline molecule. The "4" position is "*para*-" to the amine group, which occupies the "1" position. (b) A "benzenoid" group. (c) A "quinoid" group.

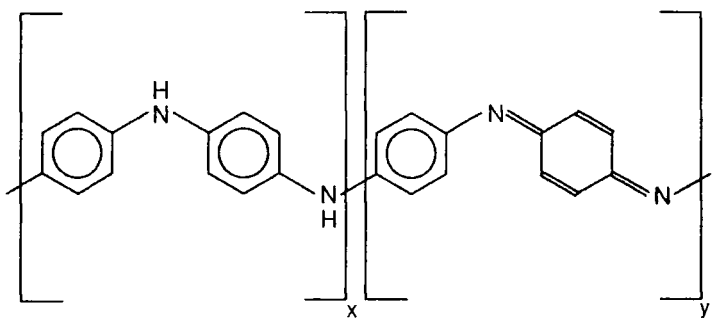

Figure 1.17. General formula for the polyaniline family of polymers.

$x + y = 1$.

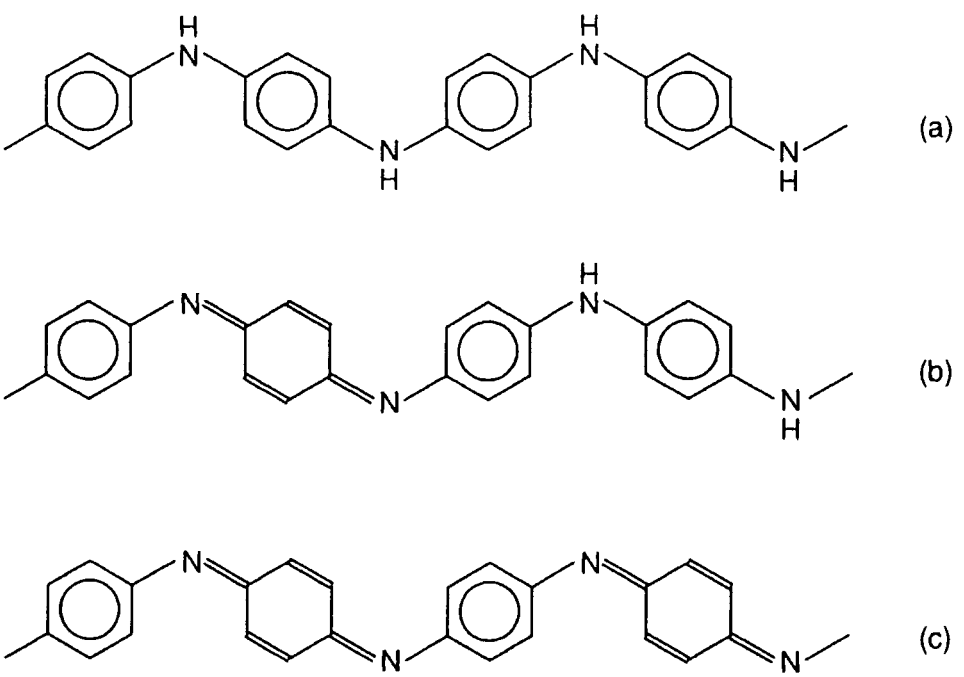

Figure 1.18. The different oxidation states of PANi, (a) Leucoemeraldine base, fully reduced, (b) Emeraldine base, half oxidised, (c) Pernigraniline base, fully oxidised.

polymer backbone and secondly, only the PANi-PB form is conjugated along the full length of the chain.

The former of these two observations is perhaps the major factor that distinguishes PANi from the vast majority of other conducting polymers. The fact that the nitrogen atoms occupy primary sites in the polymer lattice, (i.e. there is no continuous carbon-carbon bonding), infers that the heteroatom plays a key role in the electronic structure of the system. This is not the case with many of the pyrrole and thiophene derivatives (see figure 1.11).

The fact that pernigraniline base is conjugated (and has a two-fold degenerate ground state due to the symmetry of the two isomers) might lead the reader to believe that it is the form of PANi that is used in the investigations comprising this work. PANi-PB is, however, virtually impossible to synthesise due to the propensity of the quinoid groups to hydrolyze. The Leucoemeraldine base can be synthesised with relative ease (compared to PANi-PB at least) but is unstable to oxidation in air. PANi-EB, on the other hand, is simple to produce and is stable in normal atmospheric conditions. This stability, combined with its solution processibility (from some polar solvents) makes PANi-EB a viable material for electrical applications. The Emeraldine base, however, is only conjugated over the quinoid group and adjacent benzene rings i.e. the conjugation of the polymer backbone is broken at the -NH- (secondary amine) groups. How, therefore, is it possible to produce a conducting material from PANi-EB?

All of the three polyaniline molecular systems described above are inherently electrically insulating, in the same way as pristine PA. The PANi-EB form, however, forms a salt (known as emeraldine salt or PANi-ES) when treated with an acid of pH less than ~3. This "acid doping" can increase the conductivity of the polymer by a

factor of 10^{12} [30]. The highest reported conductivities from such PANi-ES systems are in the region of 200-400 Scm^{-1} [36,37]. This transition from insulating to conducting is quite remarkable since the protonation of the polymer does not change the number of electrons on the polymer chain.

Doping of the emeraldine base such that one half of the nitrogen sites are protonated creates what is effectively one bipolaron per repeat unit (see figure 1.19a). Stafström *et al.* showed that this structure is unstable with respect to formation of a polaron lattice, due to disproportionation of the bipolaron [38] (figure 1.19b). This "polysemiquinone radical cation" structure has alternative resonance structures giving rise to the possibility of significant delocalisation of the charge carriers along the polymer backbone. The mixing of polaron states in such close proximity, in a similar way to soliton over-lap explained in section 1.5.1, leads to a partially filled delocalised mid-gap band. Thus, PANi-ES can be considered to be a pseudo-one-dimensional conductor.

Initial experiments investigating the conducting emeraldine salt concentrated on the effect of acids, such as hydrochloric acid (HCl) on free standing films of PANi-EB (these films were generally cast from a solution of PANi-EB in N-methyl-2-pyrrolidinone, NMP for short) [39]. It has been widely accepted that the maximum doping level would correspond to protonation of half the nitrogen sites on the polymer backbone (the imine sites) and hence is termed "50% doped" (see figure 1.19). The post-process doping of the film, however, is only controlled by the pH of the dopant solution and the time for which the film is immersed in it. Thus properties of the undoped film (such as thickness, density, solvent content and homogeneity) play a major part in determining the final properties of the doped film. These properties are often the indirect result of differential drying rates from varying solution concentrations and

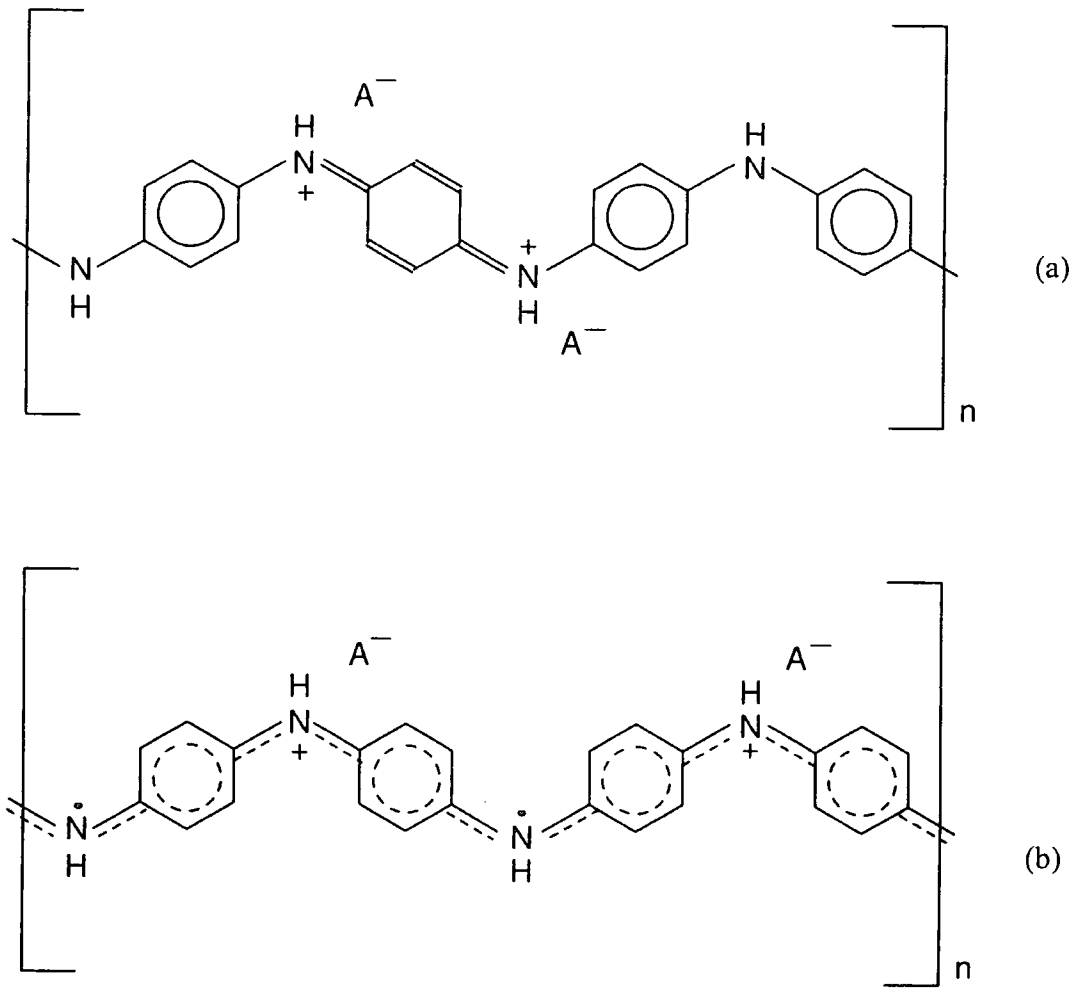

Figure 1.19. Skeletal representation of (a) the bipolaron and (b) polaron (polysemiquinone radical cation) forms of Emeraldine Salt.

drying temperatures, and these may go some way to explaining the range of conductivities reported for PANi-HCl and similar systems [40].

Recently, however, the doping problem of PANi-ES has been overcome by the development of solution-state doping of emeraldine base initially suggested by Cao *et al.* [41]. The routes use 10-Camphorsulphonic acid (CSA) and dodecylbenzene sulphonic acid (DBSA) to dope PANi-EB in organic solvents. Hence direct control of the doping level (via the ratio of acid to polymer in solution) is achievable. Thus, investigation of the properties of PANi-ES as a function of doping can yield important information about charge transport mechanisms. Greater detail of the polymer processing techniques will be given later in the appropriate experimental chapters, but one of the most interesting systems of recent note has been that of polyaniline (emeraldine base) doped with CSA.

1.7 CHARGE TRANSPORT ON A MACROSCOPIC SCALE.

So far charge transport has only been considered in terms of carrier propagation along the polymer backbone. It is obvious, however, that inter-chain charge transfer is essential if the previously discussed systems are to exhibit bulk electrical conductivity. In amorphous polymers there must also be mechanisms whereby charge carriers can cross chemical defects (such as mis-bonding, chain-ends and cross-links) in the chain. Similarly, in the case of "crystalline" polymeric systems, there must be other transport processes such that crystallographic defects do not inhibit all macroscopic charge transport. Defects such as grain boundaries (i.e., the boundaries between crystalline grains, in the context of conducting polymers) and charge transfer between crystalline regions would, however, cause some modification to the bulk electrical properties that would be experimentally observable. Defects in the crystalline regions themselves (again caused by mis-bonding, cross-linking and chain ends) may also affect charge transport within the crystalline "grains."

As mentioned earlier, the possibility of varying the conductivity by more than ten orders of magnitude is one of the most interesting properties of conducting polymers. Trying to understand this remarkable charge transport transformation has been one of the major stimuli for the recent interest in conjugated polymers, but the interpretation of transport data is still one of the most controversial aspects of the field. One of the main reasons for this is the inherent lack of periodic structure in amorphous conducting polymers, compared with inorganic conductors and semiconductors at least. This has lead to ambiguity in the interpretation of experimental data in terms of specific models. Over the past three decades, however, there has been an appreciable increase in

the understanding of amorphous solids. Hence the concepts developed for non-crystalline conductors are often applicable to conducting polymers in general. A good starting point in understanding the electronic properties of amorphous conductors is the book by Mott and Davis [42] that discusses the theories developed for non-crystalline inorganic metals and semiconductors.

In this section some concepts relevant to non-crystalline solids will be discussed. Some experimentally measurable properties will be presented, along with a few of the models used to explain the experimental findings.

1.7.1 ANDERSON LOCALISATION.

Although polymers are not periodic in nature, solutions to the Schrödinger equation must exist, and hence, the concept of "density of states" is still applicable. (The density of states at an energy E is often referred to by the notation N(E).) A crystalline solid can only be an insulator or semiconductor if the density of states at the Fermi level, $N(E_F)$, is zero. In non-crystalline solids, however, the conductivity can be zero even if $N(E_F) \neq 0$ and wave function overlap between neighbouring sites is significant.

N(E) is defined such that N(E)dE is the number of eigen states per unit volume for an electron of given spin within the system between energies E and E + dE. Thus, for a given temperature, T, the number of electrons in the energy range is, for each spin direction, N(E)f(E)dE, where f(E) is the Fermi distribution function given by:

$$f(E) = \frac{1}{\exp\{(E - E_F) / k_B T\} + 1} \qquad \text{eqn. 1.11}$$

where E_F is the Fermi energy and k_B the Boltzman constant. The Fermi energy is a function of T and tends to a limiting value as $T \rightarrow 0$, whereby E_F represents the energy separating occupied and un-occupied states.

Calculation of N(E) in disordered systems can be considered for two limiting cases. The first being that charge carriers are not strongly scattered (i.e. the free electron approximation) due to little disorder, e.g. lightly doped inorganic semiconductors. Thus the electron energy can be written as:

$$E = \hbar^2 k^2 / 2m^* \qquad \text{eqn. 1.12}$$

where $\hbar$ is Planck's constant over 2π, k the wavevector and m* is the effective mass of the charge carrier. In this case the density of states in each spin direction is given by the free electron formula:

$$N(E) = \frac{(Em^3 / 2)^{1/2}}{\pi^2 \hbar^3}. \qquad \text{eqn. 1.13}$$

The free electron approximation is only applicable to systems in which the lattice contains only small amounts of defects, such that the mean free path of the electron, L, is large compared to the lattice spacing. Hence for the free electron approximation scattering is weak and it follows that L is large, such that $L >> 1/k$ (where k is the

reciprocal of the lattice spacing).

Consideration of the other limiting case, namely that scattering is strong due to the inherent disorder in non-crystalline media, then there is considerable deviation from the density of states given in equation 1.13. Ioffe and Regel [43] proposed that L~1/k in this case (L being the mean free path) and cannot be shorter than 1/k in any case. If scattering becomes extremely strong each wavefunction becomes confined to a small region of space (i.e. localised) and falls off exponentially with distance (R) from the well as exp(-αR). This was first recognised in 1958 by Anderson.

Anderson [44] considered the tight binding model with respect to a regular array of rectangular potential wells, with random well depths. Anderson proved that there was no quantum diffusion of electrons between wells if the randomness of well potential, V_0, was great compared to well separation, a (figure 1.20). Non-crystalline materials which exhibit insulating behaviour at low temperature and have a finite value of $N(E_F)$ were thus termed "Fermi glasses" [45].

Anderson showed that the width of the band, B, formed by such an array of potential wells would take the form:

$$B = 2zI \qquad \text{eqn. 1.14}$$

where z is the lattice co-ordination number and I is the transfer integral. I is dependent on the shape of the wells, but takes the general form:

$$I = I_0\exp(-\alpha R). \qquad \text{eqn. 1.15}$$

The rate at which the wavefunction of a single well falls off with distance is

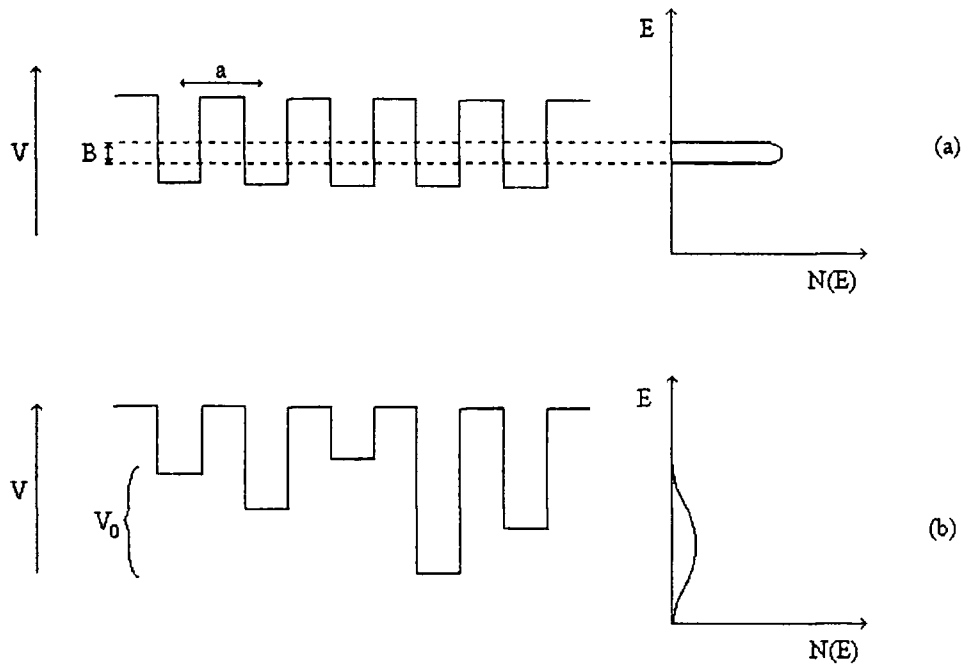

Figure 1.20, schematic representation of the change in the density of states as a result of a disordered system. (a) Potential wells for a crystalline lattice, (b) Potential wells for the Anderson random potential lattice.

defined by α.

Mott and Davis [42] considered what happened to this band of energies when the potential energy function, V, is non-periodic. Aperiodicity can be achieved in two ways; the first being the randomisation of the well potentials in a regular array, as in figure 1.20b. Anderson considered that the wells were all of a depth between $\pm\frac{1}{2}V_0$, such that V_0 was the spread of energies. If V_0 is small, then L is large, and it can be shown that [42]:

$$\frac{a}{L} = \frac{(V_0 / I)^2}{32\pi}. \qquad \text{eqn. 1.16}$$

The Ioffe-Regel rule (that $L < 1/k$ is not allowed) effectively means that the shortest mean free path is the distance between atoms, or to be more precise, scattering species. In this case the mean free path is approximately the lattice spacing, i.e., $L \sim a$. Hence equation 1.16 becomes:

$$V_0/I \approx \sqrt{32\pi} \sim 10, \qquad \text{eqn. 1.17}$$

or, substituting equation 1.14 for a system with a co-ordination number of 6 (as a simple example used by Mott and Davis [42]),

$$V_0/B \approx 0.83. \qquad \text{eqn. 1.18}$$

Mott suggests that when the value of V_0/B is greater than ~2, for three

dimensional systems [42], the perturbation of a wavefunction by that of a neighbouring well becomes negligible. Thus the diffusion of electrons between wells becomes impossible as $T \rightarrow 0$, and conductivity tends to zero.

The second way in which a lattice can be considered non-periodic is when the lattice sites are randomly distributed spatially. Spatial disorder is an inherent property of all polymers, even those classified as crystalline. In these systems it is not possible to define a co-ordination number. Mott proposed [42] that each atom be paired with it's nearest neighbour, the separation of the pair being defined as the distance r_1. The nearest neighbour separation can be derived in terms of the number of sites per unit volume, N:

$$\tfrac{4}{3}\pi r_1^3 = 1/N. \qquad \text{eqn. 1.19}$$

Mott, roughly approximated V_0 in the Anderson formula (equation 1.16) for spatially disordered systems. The energy of an electron on either of the two centres in the pair is $I_0\exp(-\alpha r_1)$, and Mott approximated this to V_0. The mean distance between pairs, r_2, is given by:

$$r_2 = 1/(\tfrac{1}{2}N)^{1/3}. \qquad \text{eqn. 1.20}$$

So it follows that the band-width takes the form:

$$B = 2zI_0\exp(-\alpha r_2). \qquad \text{eqn 1.21}$$

Mott argues that due to the low dimensionality of the pair, the value for z can be approximated to a value close to 2. In terms of polymeric systems, however, the nature of the molecular electronic orbitals, (as opposed to the atomic orbitals used in the above derivations), means that quantitative analysis is not possible. The Anderson theory is, however, very useful as a qualitative illustration of disorder induced localisation.

1.7.2 CHARGE CARRIER MOBILITY NEAR BAND EDGES.

In the early sixties it was realised that the majority of electronic states close to band edges, especially in band tails, would be localised [46,47]. Mott later pointed out that an energy separating the localised states from the delocalised ones, E_C, must exist [48] such that the conductivity of an electron with an energy E, σ_E, is given by:

$$\langle\sigma_E\rangle = 0 \quad \text{when} \quad E < E_C \text{ and}$$

$$\langle\sigma_E\rangle \neq 0 \quad \text{when} \quad E > E_C \qquad \text{eqn. 1.22}$$

where $\langle\ \rangle$ denotes the configurational average. Mott showed that there must be a sharp boundary where this occurs, as σ_E cannot be both zero and non-zero for wavefunctions of the same energy [48]. Cohen *et al.* first introduced the concept in terms of the conduction band of amorphous semiconductors [49], terming the critical energy , E_C, the "mobility edge."

The general density of states for non-crystalline solids near the band is schematically represented in figure 1.21 [16]. Here E_F is the Fermi level, E_C and E_V refer to the mobility edges in the conduction and valence band respectively, similarly E_A

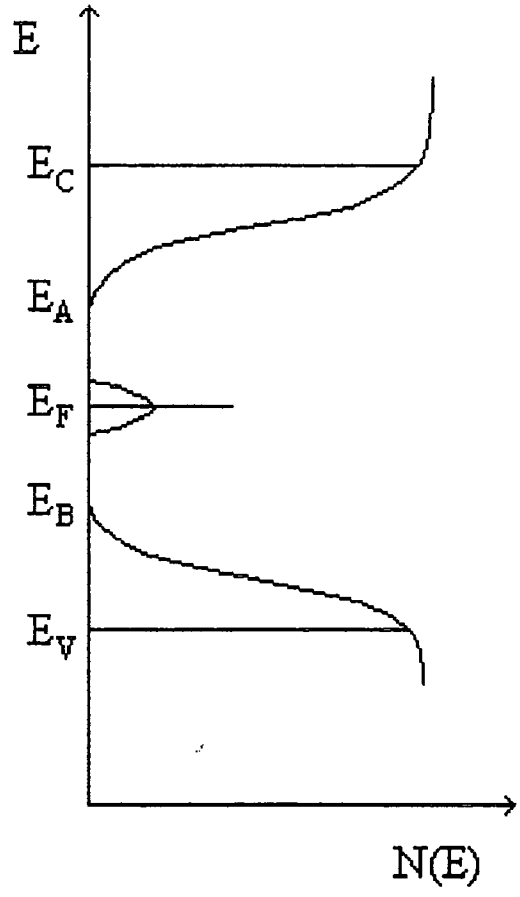

Figure 1.21. Schematic representation of the density of states as a function of energy for a general non-crystalline solid. The shaded area represents localised states.

and E_B are the band edges.

If the Fermi level lies in the region of the localised states (as depicted in figure 1.21) then two forms of d.c. conduction are possible. The first is thermal hopping between the localised states (see section 1.7.4), whilst the other is excitation to the extended states above the mobility edge, E_C. The second of these mechanisms has an activation energy (ε) and gives a conductivity of the form:

$$\sigma = \sigma_{min}.\exp\{-(E_C - E_F)/k_BT\} \qquad \text{eqn. 1.23}$$

where σ_{min} is the "minimum metallic conductivity," i.e., the lowest conductivity, which occurs when $E_F = E_C$ ($E_C - E_F = \varepsilon$). In systems of the Fermi glass type in which E_F can move from below E_C to above it (as a result of compositional change or some similar transformation) a sharp change in σ_{min} is expected; i.e. from zero below E_C to some finite value above it.

The descriptions of the Anderson localisation (in the preceding section) and the mobility edge are derived for a particle, but are equally valid for any excitation [42]. Thus the concepts outlined so far in this chapter are of obvious importance when trying to understand charge transport by, for example, polarons in PANi-ES.

1.7.3 SOME EXPERIMENTALLY OBSERVED PROPERTIES OF CONDUCTING POLYMERS.

There are two major experimental procedures that are often used to investigate charge carrier transport in conducting polymers. The first being conductivity, which is self explanatory. The second is "thermoelectric power" (thermopower for short) for which a basic outline is given below. These two techniques are very much complementary due to the fact that one is dependent upon an applied electric field (conductivity) and the other is a zero current measurement, i.e. no external field is applied (thermopower).

Dugdale, in his book "The Electrical Properties of Metals and Alloys," [50] describes the thermopower of a conductor to be the potential difference between two sections of a conductor at temperatures T and T+ΔT. This potential can be measured by any device that does not draw current from the circuit, as is the case with the majority of modern digital voltmeters. This effect is termed the Seebeck effect after its' discoverer. The thermopower of a conductor is given by:

$$S(T) = \frac{\Delta E}{\Delta T} \qquad \text{eqn. 1.24}$$

where S(T) is the Seebeck coefficient, (commonly called the thermopower), and is measured in μVK^{-1}. ΔE is the potential difference across the thermal gradient ΔT.

The thermopower of a material is directly dependent upon its electronic structure and is characteristic of each metal and semiconductor. The author does not feel that this

work necessitates a detailed derivation of thermopower, interested readers are therefore referred to the afore-mentioned book by Dugdale [50]. The thermopower does, however, contain information about the electronic states within a conductor or semiconductor and as such it is useful to outline some of the major conclusions that can be drawn from thermopower measurements. Although it is the Seebeck effect that is most usually measured, it is useful to consider the case of a current flow from one conductor to another.

To illustrate the thermopower qualitatively Dugdale considers the passage of current through two different conductors joined in series. Since there cannot be an accumulation or dispersion of charge at the junction, the current through the two conductors must be the same. Although this electrical current must be the same, there is no reason why the thermal energy carried to the junction by the charge carriers of the first conductor must be the same as that removed from the junction by those of the second material. Thus, even though the *electrical currents* must be equal, the *thermal currents*, in general, are not. This manifestation, for a two conductor system, is known as the Peltier effect. Although this effect is a result of a junction between two materials, it arises directly from the difference in bulk properties of the charge carriers in the different media.

The thermopower of an individual material is referred to as the absolute thermopower and is characteristic of that material. In simple terms, a non-zero thermopower arises only when there is a differential thermal conductivity, as a result of there being occupied electronic states with energies above and below the Fermi energy, E_F. A general derivation of the "absolute" thermopower of a conductor, in which there is elastic scattering of the charge carriers, is given by Dugdale as:

$$S = k_B T.(\pi^2/3).(k_B/e).(\delta \ln\sigma(E)/\delta E) \qquad \text{eqn. 1.25}$$

where the constants have their usual physical meaning, except for e, which can be either positive or negative (depending upon the charge carrier, hole or electron) and $\sigma(E)$ which is the same as σ_E in equation 1.22. Dugdale suggests that this is one of the most valuable ways of interpreting the thermopower of a metal, as it has a general validity. Thus for an ideal metal we would expect a negative coefficient, linear with respect to temperature, as predicted by equation 1.25. Dugdale also states that it is non-trivial to calculate S from equation 1.25 due to inherent difficulty in calculating $\sigma(E)$ itself, let alone its energy dependence, $d\ln\sigma(E)/dE$.

There is, however, a wide deviation from equation 1.25 in the measured thermopower of many metals. The noble metals (Cu, Ag and Au) all have a positive value of S at low T and exhibit a peak at around 50K. This phenomenon has been explained (partly at least) by the contribution of phonons to thermal current. Consider the case where electrons and phonons are associated, then motion of one "drags" the other. In the case of electron diffusion (the Peltier effect outlined earlier) the electrons drag the phonons as they move under the affect of the applied field. In the Seebeck effect, however, there is no applied field, but a temperature gradient. This effectively induces a "phonon current" from the hotter part of the material to the colder. Thus, if there is some association between electrons and phonons, the phonons drag electrons and hence the effect is named phonon-drag. Thus Dugdale concludes that any carrier of thermal energy that interacts with electrons can contribute to the thermopower of the conductor or semiconductor. What then, do thermopower and conductivity

measurements reveal about the structure of the electronic states in conducting polymers?

For heavily doped PA [51-53] and PANi-ES [54,55] the thermopower varies almost linearly with temperature, as would be expected for extended, ("metallic"), states. The d.c. conductivity for most conducting polymers, however, has a temperature dependence that does not fit simple metallic models. Generally conductivity measurements on conducting polymers reveal an exponential dependence on temperature [36,56,57] which contrasts the thermopower measurements. How, then, can we model these opposing transport properties of conducting polymers?

1.7.4 THERMALLY ACTIVATED CHARGE CARRIER "HOPPING."

In section 1.7.2 the concept of the mobility edge was introduced for the case where E_F lies in the region of the localised states. Two mechanisms for charge carrier transport were suggested, namely excitation of charge carriers to states above the mobility edge and thermally activated hopping. Equation 1.23 describes the conductivity in the former case, which is expected to be dominant at high temperatures or when $E_C - E_F$ is small.

The thermally activated hopping process is limited by the probability of an electron hopping from a state below the Fermi level, to an un-occupied one above it. (Note this is not the same as excitation to a state above the mobility edge in the case $E_F < E_C$, as depicted in figure 1.21.) Since this is a thermal process around the Fermi energy, the number of electrons within the range k_BT of the Fermi energy (i.e., $2N(E_F)k_BT$) is a major factor in the hopping process. The hopping probability is given

by Mott as [42]:

$$\nu_{HOP} = \nu_{PH}.\exp\left\{-2\alpha R - \frac{W \pm eRF}{k_B T}\right\} \qquad \text{eqn. 1.26}$$

where ν represents the frequency of the event, the suffixes HOP and PH refer to hopping and phonons respectively. α is the tail-off of wavefunction with distance, and R the hopping distance. The $\exp(-W/k_BT)$ is the Boltzman factor where W is the difference between the energies of the two states. The $\pm$ refers to the hopping in both directions relative to the applied field, F. Note that the inclusion of the ν_{PH} term is due to the approximation to the conduction of semiconductors as a result of impurity doping. In such systems each time an electron hops it must either emit or absorb a phonon, it is therefore obvious that the process involving the absorption of a phonon is rate limiting. Mott proposes that this phonon interaction is a prerequisite of all electronic hopping processes in similar localised states.

To obtain the resultant current the forward and backward hopping rates are multiplied by the distance, R, and the electric charge, e. For weak fields $eRF << k_BT$ and the conductivity is given by:

$$\sigma = 4e^2R^2N(E_F).\ \nu_{PH}\exp\left\{-2\alpha R - \frac{W}{k_B T}\right\} \qquad \text{eqn. 1.27}$$

Two types of hopping process are thus available, and dependent upon the degree of localisation within the system. The first is nearest neighbour hopping, and is the only

mechanism available when localisation is strong, such that $\alpha R_0 >> 1$ (R_0 being the nearest neighbour distance) and the mobility edge is in the higher (conduction) band. For this case equation 1.27 reduces to show the temperature dependence of hopping to be proportional to $\exp(-T_0/T)$. T_0 is defined as the characteristic temperature of the conductor, and is a function of the localisation length, L_c, the average distance over which an electron can hop in a three dimensional conduction system:

$$T_0 = 16 / (k_B N(E_F) L_c^3) \qquad \text{eqn. 1.28}$$

Mott suggested that in the case where localisation is weak (i.e., $\alpha R_0 \sim 1$, or even less) or in any case, at very low temperatures, "variable range hopping" (VRH for short) is always to be expected. In this mechanism the hopping distance, R, increases with decreasing temperature [58].

There are two competing factors; as the hopping distance increases the wavefunction overlap decreases, but the energy difference of the states, W, reduces due to the relation:

$$W = \frac{3}{4\pi R^3 N(E_F)}. \qquad \text{eqn. 1.29}$$

By balancing these two factors the maximum hopping rate becomes:

$$\nu_{HOP} = \nu_{PH}.\exp(-B/T^{1/4}), \qquad \text{eqn. 1.30}$$

where

$$B = B_0(\alpha^3 / k_B N(E_F))^{1/4}, \qquad \text{eqn. 1.31}$$

B_0 being a numerical constant derived from Mott's rigorous treatment combining equation 1.26 with equation 1.29 [42], (which has the approximate value of 1.66). The form of the conductivity as a result of VRH is thus given as:

$$\sigma = \sigma_0.\exp[-(T_0/T)^{1/4}]. \qquad \text{eqn. 1.32}$$

A more general form of this equation is also proposed by Mott such that

$$\sigma = \sigma_0.\exp[-(T_0/T)^x] \qquad \text{eqn. 1.32}$$

where $x = \frac{1}{1 + d}$,

in which d takes the value of the number of dimensions in which electron transport occurs, i.e. for three dimensional conduction systems x = ¼, as in equation 1.31. It can be seen that VRH thus has a much weaker dependence on temperature, ($\propto T^{-1/4}$), compared to the linear dependence of nearest neighbour hopping.

Early studies of PANi-HCl often showed that there was a temperature dependent conductivity that is a good fit to VRH models, and it appeared that $\sigma \rightarrow 0$ with $T \rightarrow 0$. It was often observed that the temperature dependence was characteristic of a x=½, i.e. a

quasi-one-dimensional system (see for example [54] and [59]). Lightly doped PA also exhibits a temperature dependent conductivity predicted by VRH, [56] as would be expected for a system in which there is an inherently low charge carrier density. This fit to quasi-1-D VRH would appear to be supported by the observed increase of conductivity along the stretch direction in PANi-EB samples that have been uniaxially stretch oriented prior to acid doping [60] and uniaxially aligned PA [3].

The thermopower measurements for both of the above systems also fit that expected from Mott's modelling of thermopower due to VRH mechanisms [51-55] (see reference [42] for this derivation). The VRH model is obviously not the only model that can be used to describe electrical transport in disordered conductors and is limited in its usefulness (in terms of this work at least) to the above systems.

The PANi-CSA system shows behaviour that cannot be explained adequately by variable range hopping in a one dimensional system. These samples are generally an order of magnitude more conductive than PANi-HCl (often around $300Scm^{-1}$) and it is claimed that these systems are close to the metal-insulator transition [36,57]. At temperatures above ~135K certain PANi-CSA samples have an observable negative coefficient of the temperature dependence of the conductivity, but below ~100K they exhibit behaviour that is a close fit to VRH in three dimensions.

X-ray diffraction experiments on PANi-CSA have revealed that there is a high degree of crystallinity and it is believed that within the crystalline regions there is metallic transport [36,57]. This is analogous to the formation of "fibrils" in PA (fibrils are "bundles" of highly aligned polymer chains which form fibre-like structures in PA [16]). If this is the case then there must be some other transport processes involved in the charge transfer within and between the crystalline regions, (or fibrils in the case of

PA). Thus, the concept of small metallic islands in an amorphous insulating (or semiconducting) host matrix can be envisaged. This system is often named a "granular metallic" system.

1.7.5 FLUCTUATION INDUCED TUNNELING.

In 1980 Sheng proposed a mechanism of fluctuation induced tunnelling (FIT) as a model for granular disordered systems [61]. The model considered the case where granular metallic regions were separated by potential barriers, in effect, small insulating regions. The effective height of the barriers to tunnelling from one metallic island to another was shown to be reduced by thermally induced fluctuations of the charge distribution of the islands either side of the insulating barrier. Thus, FIT is a temperature dependent mechanism.

Sheng went on to show that at low temperatures (i.e. where fluctuations in charge distribution do not occur) that the FIT model becomes the same as simple elastic tunnelling, i.e. the probability of a particle tunnelling from one well to another through a potential barrier. For a random network of grains and barriers the conductivity is given by [62]:

$$\sigma = \sigma_0 . \exp\left(\frac{-T_1}{(T + T_0)}\right) \qquad \text{eqn. 1.33}$$

where T_0 is a representation of the temperature at which there is a significant

contribution to the conductivity of FIT, as opposed to elastic tunnelling which dominates below this temperature. T_1 is dependent on the average barrier potential, i.e. the spacing of the metallic islands. Sheng and Klafter later considered the limiting case when the metallic grains became small [61]. It was shown that the energy required to overcome the electrostatic force opposing a hop from one island to another became large compared to the thermal energy, k_BT, available. Thus the conductivity of this type of composite is expected to be of the form:

$$\sigma = \sigma_0.\exp[-T_0/T]^{1/2} \qquad \text{eqn. 1.34}$$

where the symbols represent the same as in equation 1.33.

Fitting the conductivity data of PA (from around that time) to this model showed that there was a very close fit to equation 1.33. This is supported by the belief that the fibrils in PA are not thought to be so small that the limiting case in equation 1.34 is reached [16].

1.7.6 THE NEED FOR A HETEROGENEOUS MODEL.

So far, this chapter has considered transport along the polymer chain, and some models that have been used to explain the macroscopic properties observed in conducting polymers, namely d.c. conductivity and thermopower measurements. It can be seen, however, that these models alone cannot explain the transport properties displayed by the most highly conductive polymer samples to date (e.g. stretched PA [3]

and PANi-CSA [36,57] materials).

A series of publications (primarily) by Kaiser [53,55,63-65] argues the case for a heterogeneous model to explain the transport properties of the above systems. He proposes that VRH is adequate to describe amorphous systems (such as un-stretched PANI-HCl and lightly doped PA) but cannot predict accurately the properties of the systems close to the metal-insulator boundary. In particular there is support for the FIT model put forward by Sheng, [62] as this accommodates the observation of a finite σ_{min} at the low temperature limit. But Kaiser argues that this model only considers conduction through the barrier regions, and thus must be combined with a term for conduction through the metallic islands.

Due to the linear dependence of the thermopower in the highly conductive forms, indicative of metallic diffusion, Holland *et al.* proposed that a simple heterogeneous model where charge transport through the granular regions was considered as metallic [37], i.e. Ohmic conduction. Kaiser suggests that in the case where the insulating boundaries were thin, thermal conduction through these regions is possible. Their contribution to thermopower would therefore be negligible, and the observed thermopower would (essentially) be that of the highly conductive regions. Conversely the conductivity measurements would be dominated by the properties of the insulating matrix and thus electrical transport in the highly conductive regions would be masked. This simple qualitative concept, therefore, is able to reconcile the apparently contradictory conductivity and thermopower data from investigations into conducting polymers.

Holland *et al.* used this heterogeneous model in the form [37]:

$$1/\sigma = AT + B[\exp(-T_0/T_1 + T)]^{-1} \qquad \text{eqn. 1.35}$$

to fit data from temperature dependent conductivity of highly conductive PANi-CSA (A and B are constants). It can be seen that the total resistivity in equation 1.35 is a simple summation of the resistivity due to the metallic (AT) and fluctuation induced tunnelling ($B[\exp(-T_0/T_1 + T)]^{-1}$) mechanisms. Similar models have been used to fit conductivity measurements of highly conducting PA [53] and also show good agreement of theory with experiment.

It is the development and application of this model by Kaiser [53,55,63-65] and (separately) Holland [37] that has allowed transport data in conducting polymers to be explained. This heterogeneous nature is supported by the observation of a composite structure in conducting polymers, i.e. crystalline regions in PANi-CSA, and the formation of fibrils in PA.

1.8 SUMMARY.

The aim of the work presented here is to determine the nature of the charge carriers within solution doped polyaniline materials. The conductivity measurements presented in chapter 2 concentrate mainly on "solution doped" polyaniline (see chapter 2 section 2.1.2). These conductivity measurements may show whether charge transport in PANi-ES is governed by one of the transport mechanisms outlined in the previous section of this chapter (Fermi-glass, thermally activated or variable range hopping, Sheng's FIT model or a heterogeneous model).

A comparison of conductivity measurements from solution doped polyaniline doped with 10-Camphorsulphonic acid (PANi-CSA) and 2-acrylamido-2-methyl-1-propanesulphonic acid (PANi-AMPSA) is made. It is hoped that both these systems can be explained by the same transport mechanism, and that any observed differences are easily attributable to some factor within this transport mechanism.

On a lower level this work aims to determine the properties of the charge carriers themselves. Two more experimental techniques are discussed in chapters three and four, Electron Spin Resonance (ESR) and Faraday rotation respectively. The ESR experimentation (chapter 3) concentrates on the PANi-CSA material since the measurements were performed prior to the investigation of the PANi-AMPSA material studied in other chapters. The object of the ESR work was to determine whether charge transport was best described by a three dimensional "polaron lattice" model, or the migration of charge carriers along the polymer chain. ESR investigations could also determine whether polarons or bipolarons were the majority charge carriers in doped

polyaniline.

The Faraday rotation investigation (chapter 4) was undertaken in the hope that information about the effective mass of the majority charge carrier could be determined. The Faraday rotation results could also confirm that the charge carriers in doped polyaniline are indeed positively charged.

The final experimental chapter (chapter 5) presented in this work regards a possible "ferromagnetic" derivative of polyaniline. Although incongruous at first it is hoped that this work will provide an insight into the charge and spin carriers in polyaniline (and its derivatives). The work discussed in chapter five is chronologically out of step with the other investigations described in this thesis. One of the main reasons for including chapter five is the fact that it comprised a major portion of the overall research time.

It is hoped that the information provided by the diverse experimental techniques used will lead to the formation of a simple theory for charge transport in solution doped polyaniline systems. The study of the other materials described in this thesis will hopefully support the conclusions reached in this work.

1.9 REFERENCES.

1. Chiang, C.K., Fincher, C.R., Park, Y.W., Heeger, A.J., Shirakawa, H., Louis, E.J., Gau, S.C., MacDiarmid, A.G., *Electrical conductivity in doped polyacetylene.* Phys. Rev. Lett., 1977. **37**(17): p. 1098 - 1101.
2. Park, Y.W., Park, C., Lee, Y. S., Yoon, C. O., Shirakawa, H., Suezaki, Y., Akagi, K., *Electrical-Conductivity Of Highly-Oriented-Polyacetylene.* Solid State Communications, 1988. **65**(2): p. 147-150.
3. Schimmel, T., Riess, W., Gmeiner, J., Denninger, G., Schwoerer, M., Naarmann, H., Theophilou, N., *Dc-Conductivity On a New Type Of Highly Conducting Polyacetylene, N- $(CH)_x$.* Solid State Communications, 1988. **65**(11): p. 1311-1315.
4. Natta, G., Mazzani, G., Corradini, P., *Synthesis of original PA.* Alti. Acad. Naz. Lincei Rend. Sci. Fis. Mat. Nat., 1958. **25**.
5. Shirakawa, H., Ikeda, S., *Preparation and morphology of as-prepared and highly stretch aligned polyacetylene.* Synth. Met., 1979. **1**: p. 175 - 184.
6. Miller, J.S., *Conducting Polymers - Materials Of Commerce.* Advanced Materials, 1993. **5**(7-8): p. 587-589.
7. Horowitz, G., Peng, X. Z., Fichou, D., Garnier, F., *The Oligothiophene-Based Field-Effect Transistor - How It Works and How to Improve It.* Journal Of Applied Physics, 1990. **67**(1): p. 528-532.
8. McMurry, J., *Organic Chemistry.* 2nd ed. 1988: Brooks/Cole Publishing.
9. Atkins, P.W., *Physical Chemistry.* 4th ed. 1990: Oxford Press.
10. Kuhn, H., *Free Electron Model for Absorption Spectra of Organic Dyes.* Journal of Chemical Physics, 1948. **16**: p. 840.
11. Salem, L., *The Molecular Orbital Theory of Conjugated systems.* 1966, N.Y.: Benjamin.
12. Peierls, R.E., *Quantum theory of Solids.* 1955: Oxford University Press.
13. Petty, M.C., Bryce, M.R., Bloor, D., *Introduction to molecular electronics.* 1995: Edward Arnold.
14. Su, W.P., Schrieffer, J.R., Heeger, A.J., *Solitons in Polyacetylene.* Physical

Review Letters, 1979. **42**: p. 1698 - 1701.

15. Friend, R.H., *Physics and Chemistry of Electrons and Ions in Condensed Matter.* 1984: D. Riedel Publishing Company.
16. Yu, L., *Solitons and Polarons in Conducting Polymers.* 1988: World Scientific.
17. Fincher, C.R., Chen, C.E., Heeger, A.J., MacDiarmid, A.G.,, *Structural determination of the symmetry-breaking parameter in trans-PA.* Physical Review Letters, 1982. **48**: p. 100 - 104.
18. Yannoni, C.S., Clarke, T.C., *Molecular geometry of cis- and trans- PA by Nutation NMR spectroscopy.* Physical Review Letters, 1983. **51**: p. 1191 - 1193.
19. Su, W.P., Schrieffer, J.R., Heeger, A.J., *Soliton Excitations in Polyacetylene.* Physics Review B - Condensed Matter, 1980. **22**: p. 2099 - 2111.
20. *Solitons in Condensed Matter Physics*, ed. A.R. Bishop and T. Schnider. 1978: Springer-Verlag.
21. Rice, M.J., *Charged pi-phase kinks in lightly doped Polyacetylene.* Physics Letters, 1979. **71a**: p. 152 - 154.
22. Pope, J.A., Walmsley, S.H., *Bond alternation defects in long polyene molecules.* Molecular Physics, 1962. **5**: p. 15 - 20.
23. Park, Y.W., Yoon, C. O., Lee, C. H., Shirakawa, H., Suezaki, Y., Akagi, K., *Conductivity and Thermoelectric-Power Of the Newly Processed Polyacetylene.* Synthetic Metals, 1989. **28**(3): p. D 27-D 34.
24. Rice, M.J., Mele, E.J., *The role of the Peierls instability in doped polyacetylene.* Chemica Scripta, 1981. **17**: p. 121-126.
25. Wang, C.L., Su, Z.B., Martino, F., *Bipolaron dynamics in nearly degenerate quais-one-dimensional polymers.* Physical Review B, 1986. **33**: p. 1512.
26. Takayama, H., Lin-Liu, Y.R., Maki, K., *Continuum model for solitons in PA.* Physical Review B, 1982. **21**: p. 2388.
27. Brazovski, S.A., *Self-localized excitations in the Peierls-Frohlich state.* Soviet Physics JETP, 1980. **51**: p. 342.
28. Kivelson, S., Lee, T., Lin-Liu, Y.R., Peschel, I., Yu, L., *Boundary conditions and optical absroption in the soliton model of polyacetylene.* Pysical Review B, 1982. **25**: p. 4173-4184.
29. Weinberger, B.R., Kaufer, J., Heeger, A.J., Pron, A., MacDiarmid, A.G.,

Magnetic susceptibility of doped polyacetylene. Physical Review B, 1979. **20**: p. 223 - 230.

30. Lux, F., *Properties of electronically conductive polyaniline: a comparison between well-known literature data and some experimental findings.* Polymer, 1994. **35**: p. 2915 - 2926.
31. Letherby, H., Journal of the Chemical society, 1862. **15**: p. 161.
32. Green, A.G., Woodhead, A.E., Journal of the Chemical Society, 1910: p. 2388.
33. Surville, R.d., Josefowicz, M., Yu, L.T., Perichon, J., Buvet, R., Electro Chim. Acta., 1968. **13**: p. 1451.
34. Chiang, J.C., Macdiarmid, A. G., *Polyaniline - Protonic Acid Doping Of the Emeraldine Form to the Metallic Regime.* Synthetic Metals, 1986. **13**(1-3): p. 193-205.
35. MacDiarmid, A.G., Epstein, A.J., Faraday Discussions of the Chemical Society, 1989. **88**: p. 317.
36. Menon, R., Yoon, C. O., Moses, D., Heeger, A. J., Cao, Y., *Transport In Polyaniline Near the Critical Regime Of the Metal- Insulator-Transition.* Physical Review B-Condensed Matter, 1993. **48**(24): p. 17685-17694.
37. Holland, E.R., Pomfret, S. J., Adams, P. N., Monkman, A. P., *Conductivity Studies Of Polyaniline Doped With Csa.* Journal Of Physics-Condensed Matter, 1996. **8**(17): p. 2991-3002.
38. Stafström, S., Bredas, J.L., Epstein, A.J., Woo, H.S., Tanner, D.B., Huang, W.S., MacDiarmid, A.G., *Polaron Lattice in Highly Conducting Polyaniline - Theoretical and Optical Sudies.* Physical Review Letters, 1987. **59**: p. 1464.
39. Macdiarmid, A.G., Chiang, J. C., Richter, A. F., Epstein, A. J., *Polyaniline - a New Concept In Conducting Polymers.* Synthetic Metals, 1987. **18**(1-3): p. 285-290.
40. Monkman, A.P., Adams, P.N., *Observed Anisotropies in Stretch Oriented Polyaniline.* Synthetic Metals, 1991. **41-43**: p. 627.
41. Cao, Y., Smith, P., Heeger, A.J., *Counterion Induced Processibility of Conducting Polyaniline and Conducting Polyblends of Polyaniline in bulk Polymers.* Synthetic Metals, 1992. **48**: p. 91.
42. Mott, N.F., Davis, E.A., *Electronic processes in Non Crystalline Materials.*

1979, Oxford: Clarendon Press.

43. Ioffe, A.F., Regel, A.R., *Amorphous and Liquid Electronic Semiconductors.* Progress in Semiconductors, 1960. **4**: p. 237.

44. Anderson, P.W., *The Absence of Diffusion in certain Random Lattice.* Physical Review, 1958. **109**: p. 1492.

45. Anderson, P.W., *The Fermi Glass, Theory and Experiment.* Comments Solid State Physics, 1970. **2**: p. 193.

46. Gubanov, A.I., *Quantum Electron Theory of Amorphous Conductors.* 1963, New York: Consultants Bureau.

47. Banyai, L., in *Physiques des Semiconductors*, M. Hulin, Editor. 1964, Dunod: Paris. p. 417.

48. Mott, N.F., *Electrons in Disordered Systems.* Advances in Physics, 1967. **16**: p. 49.

49. Cohen, M.H., Fritzsche, H., Ovshinsky, S.R., *Simple Band Model for Amorphous Semiconducting Alloys.* Physical Review Letters, 1969. **22**: p. 1065.

50. Dugdale, J.S., *The Electrical Properties of Metals and Alloys.* The Structures and Properties of Solids, ed. B.R. Coles. Vol. 5. 1977: Edward Arnold.

51. Su, W.P., Schrieffer, J.R., *Fractionally Charged excitations in charge-density-wave systems having commensurability 3.* Physical Review Letters, 1981. **46**: p. 738.

52. Park, Y.W., Han, W. K., Choi, C. H., Shirakawa, H., *Metallic Nature Of Heavily Doped Polyacetylene Derivatives - Thermopower.* Physical Review B-Condensed Matter, 1984. **30**(10): p. 5847-5851.

53. Kaiser, A.B., *Metallic Behavior In Highly Conducting Polymers.* Synthetic Metals, 1991. **45**(2): p. 183-196.

54. Zuo, F., Angelopoulos, M., Macdiarmid, A. G., Epstein, A. J., *Transport Studies Of Protonated Emeraldine Polymer - a Granular Polymeric Metal System.* Physical Review B-Condensed Matter, 1987. **36**(6): p. 3475-3478.

55. Kaiser, A.B., *Electronic Properties of Conjugated Polymers.* 1989, Berlin: Springer Verlag.

56. Park, Y.W., Heeger, A.J., Druy, M.A., Macdiarmid, A.G., *Electrical Transport in Doped Polyacetylene.* Journal of Chemical Physics, 1980. **73**: p. 946-957.

57. Reghu, M., Cao, Y., Moses, D., Heeger, A. J., *Counterion-Induced Processibility Of Polyaniline - Transport At the Metal-Insulator Boundary.* Physical Review B-Condensed Matter, 1993. **47**(4): p. 1758-1764.

58. Mott, N.F., Journal of Non-Crystalline solids, 1968. **1**: p. 1.

59. Wang, Z.H., Li, C., Scherr, E. M., Macdiarmid, A. G., Epstein, A. J., *3 Dimensionality Of Metallic States In Conducting Polymers - Polyaniline.* Physical Review Letters, 1991. **66**(13): p. 1745-1748.

60. Adams, P.N., Laughlin, P.J., Monkman, A.P., Bernhoeft, N., *A Further Step Towards Stable Organic Metals - Oriented Films of Polyaniline with High Electrical Conductivity and Anisotropy.* Solid State Communications, 1994. **91**: p. 875.

61. Sheng, P., Klafter, J., *Hopping Conductivity In Granular Disordered-Systems.* Physical Review B-Condensed Matter, 1983. **27**(4): p. 2583-2586.

62. Sheng, P., *Fluctuation Induced Tunneling in Disordered Materials.* Physical Review B - Condensed Matter, 1980. **21**: p. 2180 - 2195.

63. Kaiser, A.B., *Thermoelectric-Power and Conductivity Of Heterogeneous Conducting Polymers.* Physical Review B-Condensed Matter, 1989. **40**(5): p. 2806-2813.

64. Kaiser, A.B., *Physical Models For Electronic Transport In Highly-Conducting Polymers.* Abstracts Of Papers Of the American Chemical Society, 1991. **201**(APR): p. 175-PMSE.

65. Kaiser, A.B., *Metallic Polymers - Interpretation Of the Electronic Transport-Properties.* Synthetic Metals, 1991. **43**(1-2): p. 3329-3334.

CHAPTER 2

CHAPTER 2

2 CONDUCTIVITY MEASUREMENTS OF POLYANILINE SYSTEMS.

2.1 INTRODUCTION.

If conducting polymers are to be used in applications as diverse as "transparent electrodes" for "all polymer LEDs" [1, 2] and "RADAR avoidance coatings," [3] then they must take the form of highly stable, highly conductive materials. As discussed in the first chapter, PA is definitely not stable under normal atmospheric conditions, and as such has limited use as anything other than a theoretical model. Acid doped PANi, on the other hand, displays resilience to atmospheric oxygen and moisture, thus opening it up to a range of possible applications.

The d.c. conductivity of a "conductive" polymer sample is perhaps its' most important attribute (in terms of practical applications at least) and accurate measurement techniques are therefore essential. (Note that all the references to conductivity will be with respect to the d.c. measurement.) Although many techniques exist, the "four-in-a-line" technique is perhaps one of the simplest and most reliable of ways of determining the conductivity of conducting and semiconducting materials.

2.1.1 THE "FOUR-IN-A-LINE" TECHNIQUE.

This technique has been considered as one of the definitive characterisation methods (with respect to conductive polymers) and is widely used throughout the field. Essentially, the four-in-a-line measurement uses Ohms law to calculate the conductivity of a sample of known dimensions from its' resistance. (Note that *resistance* is determined by sample dimensions whereas *resistivity* is a property of the material in question.) Consider a conductive bar of uniform rectangular cross-section, width w and thickness t. Four equally spaced "zero resistance" electrical contacts, of separation ℓ, are made across the entire width of one face of the sample, perpendicular to the length of the "bar" (see fig. 2.1). A current, I, is passed between the outer two contacts and the resultant voltage, V, between the inner two is measured. Hence, the conductivity of the sample is given as:

$$\sigma = \frac{I\ell}{Vwt} \qquad \text{eqn. 2.1}$$

where ℓ in this case, refers to the separation of the centre (voltage) contacts.

The use of precision digital voltmeters and current sources in the above experimental set-up minimises the error associated with these measurements. The exact determination of the sample dimensions, therefore, governs the overall accuracy in the calculation of σ, the conductivity.

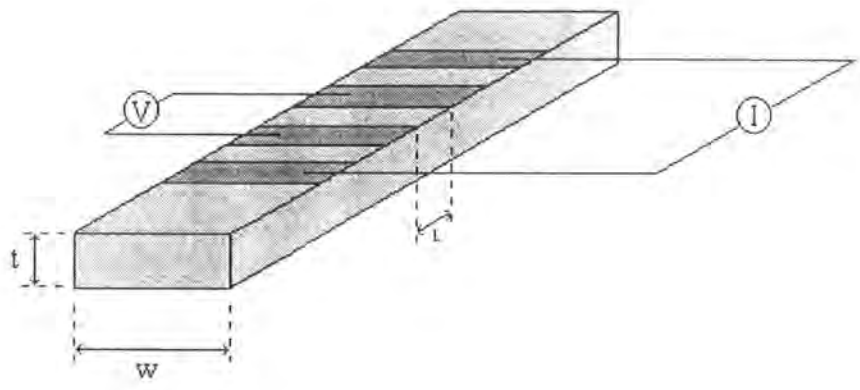

Figure 2.1. Schematic representation of the "four-in-a-line" technique for measuring d.c. conductivity, the darker areas being "zero resistance" contacts to the sample.

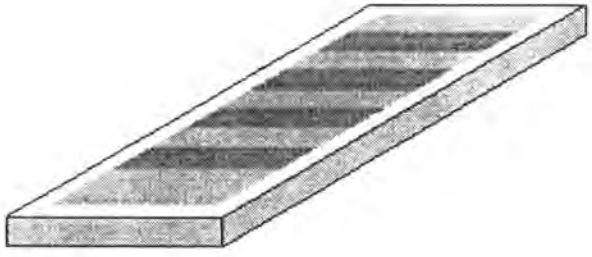

Figure 2.2. Diagram showing a thin polymer film (light grey) on a glass substrate, the dark stripes representing gold contacts. The diagram shows that the polymer round the edge of the substrate has been removed to eliminate the posibility of short-circiuts. By this method only the thin films' resistance, and hence conductivity, is measured.

The four-in-a-line measurement of sample resistance, and hence conductivity, is thus straight forward. The method can be used to measure the conductivity of samples of almost any shape, if they have a uniform cross-sectional area. It also reduces greatly the errors associated with contact resistance in the simpler "two-point" measurement method.

2.1.2 THE SYNTHESIS OF POLYANILINE.

The emeraldine base form of polyaniline that was used throughout this work described in this thesis was synthesised by Dr. P.N. Adams (Durham University). The synthesis of PANi-EB is well documented [4,5] and has been optimised by Adams *et al.* [6]. The polyaniline synthesis route (from reference [6]) is outlined for the typical synthesis conditions used by the research group.

0.1 moles (9.313g) of AnalaR grade aniline were added to 100g of 1.0M AnalaR HCl solution. The pH of the mixture was adjusted to +1.0 by the addition of a few more drops of concentrated HCl. To this reaction mixture 0.489 moles (20.76g) of LiCL were added (just sufficient to stop the reaction media from freezing at -25°C [6]). The reaction mixture was then transferred to a 1-litre jacketed reaction vessel (with removable lid and "anchor" stirrer paddle). The reaction vessel was connected to a Haake F3K circulating chiller unit, which pumped a chilled water/methanol mixture at -25°C through the jacket of the reaction vessel. The reaction mixture was left to stir while cooling to -25°C.

0.125 moles (28.52g) of AnalaR $(NH4)_2S_2O_8$ was dissolved in 51.5g distilled water. This ammonium persulphate solution was added dropwise to the reaction mixture over a 14 hour period (using a peristaltic pump running at ~5ml/hour). The reaction mixture was left to stir for a total of 46 hours. After this time the precipitated reaction product was recovered by filtration. The filtrate was washed with distilled water (10 × 200ml) and deprotonated by stiring in 100ml of 33% w/v aqueous ammonia solution. The solid product was filtered again and washed with distilled water (8 × 200ml) and finally washed with isopropyl alcohol (2 × 200ml). The filtrate was then dried under vacuum at 60°C for 24 hours, giving a final brown powder.

The product is best described as a high molecular weight polymer (emeraldine base) with a weight average molecular weight of 2×10^5 daltons. The polymer has some ring chlorination, about 1% by weight (corresponding to approximately 1 chlorine atom per 30 C-6 rings). For full details of the low temperature synthesis of polyaniline the reader is referred to the comprehensive paper by Adams *et al.* [6].

2.1.3 THE DOPING OF POLYANILINE.

There are two main methods by which the base form of polyaniline can be protonated to yield the conductive polyaniline salt, these are outlined below. PANi-EB was found to be soluble in only a few organic solvents, the most notable of these being NMP (N-methyl-2-pyrrolidinone) [7]. When doped with common acids (e.g. hydrochloric and sulphuric acid) however, the resultant polymer salt is found to be insoluble in a wide range of organic solvents [8].

The original studies of the conductivity of PANi-ES were thus from "post-doped" samples. In this process the emeraldine base was dissolved in NMP and the solution poured over a flat substrate and dried under dynamic vacuum, often at a temperature between 60 and 100 degrees Celsius. The resultant film is then peeled from the substrate and doped by either immersion into an acid solution, or exposure to an acid vapour. The percolation of the acid through the sample is an obvious barrier to homogeneous doping of the polymer, and for this reason physically small inorganic acids were often used, the acid halides being among the most common.

In this work the above type of post-doping method was only used for the study of 50-50 weight percent blends of polyaniline and cellulose acetate (CA) post-doped with HCl vapour. These samples were in the form of "ultra-thin" films for electrochemical studies, the process by which they were prepared is discussed in the next section. "Post-doped" polyaniline-cellulose acetate blends will be referred to as CA-PANi-HCl henceforth.

In 1992 Cao *et. al.* presented work showing that careful selection of an organic acid and solvent would allow production of a soluble polyaniline salt [9]. Cao and co-workers used m-cresol as a solvent for the PANi-ES formed from solution doping with camphorsulphonic acid (CSA) or dodecylbenzenesulphonic acid (DBSA). The PANi-CSA salt (as it will be referred to from now on) was shown in numerous studies to be about an order of magnitude more conductive than samples prepared by post-doping methods [9-12]. This form of polyaniline, therefore, has been of particular interest in terms of its' transport properties. It is also possible to control directly the protonation level of the solution doped polymer by varying the molar ratio of

polyaniline to acid. In this way it is possible to study the effect of doping at levels other than the assumed "50% doping" of the post-doped samples [4].

Since the discovery by Cao *et al.* intensive research has been conducted to find other acids and solvents that can be used to form polyaniline salt solutions, giving rise to polymers with different physical properties. One of the most recently discovered systems uses dichloroacetic acid (DCA) as a solvent for the salt formed by protonation of emeraldine base with 2-acrylamido-2-methyl-1-propanesulphonic acid (AMPSA) [13]. The temperature dependent conductivity of the PANi-AMPSA system is presented in this work. One reason for the interest in the PANi-AMPSA system is the fact that its solvent (DCA) is cheaper and simpler to work with (as well as being less toxic) than m-cresol (which is required for PANi-CSA materials). Investigation into "ultra-thin" films was spurred by their possible application as electrodes for polymer LED's (currently being investigated by other members of this group at a research level [14]).

2.2 EXPERIMENTAL TECHNIQUES.

2.2.1 SAMPLE PREPARATION.

Although different solids and solvents are used in the different polyaniline systems (as explained in the previous section) the preparation of the solutions contains similarities. As such, direct comparisons between samples can be made. The methods used to create the different solutions are outlined below.

(i) CA-PANi-HCl. This preparation involves the making of films from polymer blends of polyaniline and cellulose acetate (CA), followed by post-doping the samples with HCl vapour. Equal masses of PANi-EB and CA were weighed and dissolved in NMP, such that the resultant solution contained 1.5% solids by weight. This solution was then homogenised for approximately 15 minutes using a Janke and Kunkel "Ultra-Turrax T-25" homogeniser. The solution was then centrifuged at 4000 r.p.m. for one hour in an Eppendorf "Chermle z 320" centrifuge to remove any un-dissolved particles.

Measurements of thin film CA-PANi-HCl blends were undertaken in collaboration with of Dr. C.M.A. Brett (University of Coimbra, Portugal). Dr. Brett was investigating CA-PANi blends for use in "in-situ electrochemical spectrophotometric" measurements.

(ii) PANi-CSA (from m-cresol) and PANi-AMPSA (from DCA). The polyaniline was mixed with the desired molar ratio of acid (dopant) and dissolved in the respective solvent, to again give a solution of 1.5% solids by weight. (In the case of

CSA a receamic mixture of 10-camphorsulphonic was used). The solution was then homogenised and centrifuged as described above.

Two main types of sample were prepared for conductivity measurements, the first being "ultra-thin" films "spin-coated" onto glass substrates. Glass substrates 12mm by 25mm were cut from microscope slides for use in this sample preparation. The films were "spun" onto these substrates using a "Solent Semiconductor Services" programmable spinner. The desired solution was deposited on the glass substrate and spun until dry, typically, at ~1700r.p.m. under an IR heat lamp heating the sample to 120°C. The spin speed was varied to control the thickness of the sample produced. Samples requiring post-doping were exposed to HCl vapour from concentrated hydrochloric acid for one hour.

The other type of samples investigated were "free standing films," such that the bulk properties of the polymer systems could be studied. Free standing films of "solution doped" polyaniline were formed by solution casting on silicon substrates, dried under atmosphere at ~80°C; this usually took 2-3 days. The resultant films were subsequently peeled from the substrates. Samples of approximately 12mm by 25mm were cut from the free standing film for use in the conductivity experiments.

To ensure low contact resistivity, gold strips were evaporated onto all the samples using an Edwards "Auto 306" vacuum evaporator. A mask was used to create four contact stripes on each sample, 3mm wide with a separation of 3mm between stripes. Gold was used to provide a chemically inert low resistance contact over the entire width of the samples.

The ultra-thin samples required one further stage in preparation, namely the removal of a ~1mm strip of the sample around the edge (see fig. 2.2, earlier). This

was done to ensure that the measured resistance was that of the thin film, not the excess polymer that had accumulated around the edge of the glass substrate.

As discussed in section 2.1.1, the greatest source of error in the four-in-a-line measurement of conductivity is the determination of sample's dimensions. The length ℓ (eqn. 2.1) is the same for all samples since all the masks used in the evaporation process were identical, nominally ℓ=3.00mm. The sample widths can be measured with a high degree of precision using a travelling microscope, thus reducing errors from this measurement. The largest single source of error is therefore the sample thickness. For the free standing films a "Matsuo digital micrometer" was used to measure thickness with an estimated error of 5%. In the case of the "ultra-thin" films, the thickness was measured using an "Alpha Step 2000." This instrument traversed the surface of the sample with a stylus and the step between the un-coated glass and the deposited polymer film was measured (the step is formed by removing a small section of the sample from the substrate). Due to the thinness of the samples, the estimated error from the Alpha Step measurements is between 10-20%. Multiple measurements were made, therefore, and the results averaged giving an error of approximately 10%. Note that all the measurements of sample dimensions were made after the conductivity experiments to reduce damage and contamination of the sample.

2.2.2 EXPERIMENTAL SET-UP.

Two types of conductivity measurement were made during the course of this work. Namely, room temperature conductivity and conductivity measured as a function of temperature. The measurements were all made using the same apparatus, namely the modified head of a Leybold "closed loop helium refrigeration cryostat." To the head of the cryostat a small aluminium plate was added, upon which was mounted a very thin sheet of mica (to provide electrical insulation). The sample under investigation was placed on the mica and pressure contacts were made to the gold stripes on the sample. The pressure contact consisted of four parallel platinum wires stretched over an insulating plate, the spacing of these wires exactly matched that of the gold stripes. The contact plate was held in place over the sample using six fixing screws, ensuring good contact throughout the experiment (see fig. 2.3).

Room temperature measurements were made manually, using a Keithley "220 programmable current source" and Keithley "196 digital multimeter." The temperature dependent measurements used the same system, but the experiment was fully automated (schematically shown in fig. 2.4). An IBM compatible 386 PC running "Turbo Pascal 6.0" controlled the previously mentioned "Keithleys" as well as an Oxford Instruments "ITC4" temperature controller. Using this set-up it was possible to measure conductivity at any temperature between 15 and 300K. The system was programmed to set the temperature of the sample to the user specified minimum, wait for 20 minutes to ensure thermal equilibrium, then measure the conductivity at that temperature. The temperature would then be increased by a user

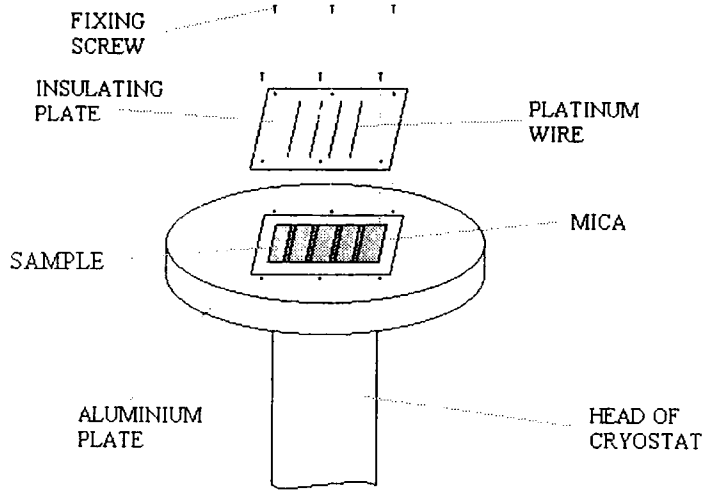

Figure 2.3. Diagram showing how the samples were clamped between electrical contacts and the head of the Leybold cryostat.

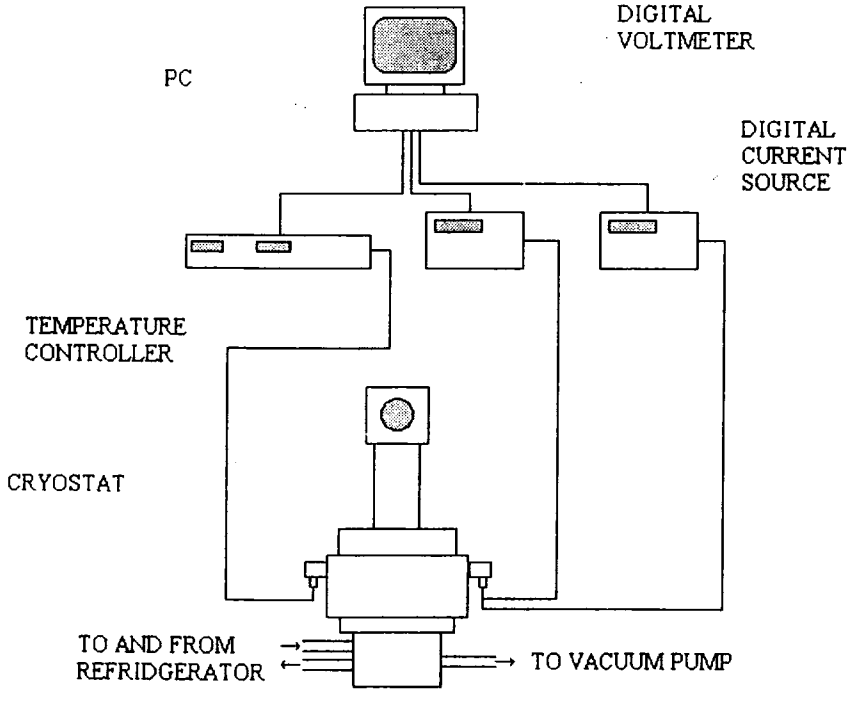

Figure 2.4. Schematic diagram of the set-up used to measure temperature dependent conductivity.

defined increment, and the process repeated up to the users specified maximum temperature. The data from this system is, therefore, a recording of a given samples' conductivity as a function of temperature.

The cryostat was kept under dynamic vacuum ($<10^{-4}$ Torr) for the duration of the experiment (note that below 200K "cryo-pumping" ensures that the sample is in an atmosphere below 10^{-7} Torr). To ensure that any excess moisture had been removed, the sample was heated to 300K under dynamic vacuum for 3 hours prior to the experiment.

A suitable magnitude of current needed to be selected for each sample under investigation such that "Joule heating" during the measurement was minimised. In the case of the room temperature measurements of the ultra-thin films, currents between 1μA and 10nA were used. For the free standing films the measurements were made using a current of 1mA above 70K, and 0.1mA below (typically). This took into account the increased effect of Joule heating at lower temperatures.

2.3 THE CONDUCTIVITY OF "BULK" PANi-AMPSA FILMS.

2.3.1 RESULTS.

Polyaniline films from the AMPSA-DCA solution state doping route have different electrical properties to PANi-CSA and PANi-HCl. The most conductive AMPSA doped samples have a room temperature conductivity of ~100Scm^{-1}, about 30-40% the conductivity of the most conductive PANi-CSA samples. PANi-AMPSA is, in effect, an analogue of PANi-CSA and direct comparisons between the two forms could reveal whether the solution doped PANi has a generic model in terms of transport mechanisms.

The temperature dependent conductivity of PANi-CSA is well documented [11,12,15,16] and the system is considered to be disordered granular metal close to the metal-insulator boundary. Holland *et al.* investigated PANi-CSA samples with different protonation levels, hence the investigation of PANi-AMPSA in this work is directly comparable. Holland expressed the level of doping as a percentage of nitrogen sites that would be protonated due to the presence of an acid at a given molar ratio to PANi-EB. Hence, a fifty percent doped sample would have a molar ratio (in solution) such that half the nitrogen sites in the polymer should be protonated (i.e., all the imine nitrogens).

To ensure that any differences between PANi-AMPSA (investigated here) and Holland's PANi-CSA materials were due solely to the different acid-solvent systems and not any difference in the PANi-EB used, a series of doped PANi-CSA films were prepared.

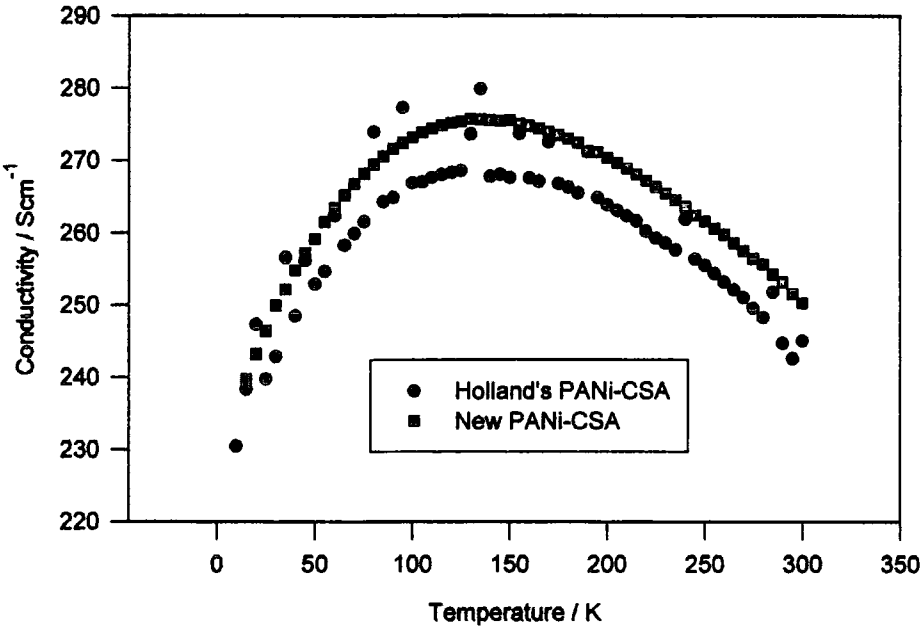

Figure 2.5. Comparison between Holland's 60% doped PANi-CSA [12] and a 60% doped PANi-CSA sample prepared for this work.

The samples were prepared and the measurements made as described in section 2.2. After the 3 hour period under dynamic vacuum (at 300K) the conductivity of the samples dropped by ~15%. This was attributed to the removal of excess water that had been absorbed from the atmosphere. After the experiment hadbeen performed and the samples were again exposed to the atmosphere, their original conductivities were regained. This suggests that conduction is enhanced by the presence of moisture, and that the dopant is not removed from the sample by the experiment. This contrasts with reported data from post-doped PANi in which conductivities do not return to their original value after exposure to high vacuum, thus implying that some dopant is lost, (see for example reference [17]). The result for post-doped PANi is not surprising since diffusion of the dopant into the polymer must have taken place initially, hence the loss of dopant under vacuum is to be expected.

Figure 2.5 shows that Holland's PANi-CSA and the PANi-CSA material measured here are well within experimental error of each other. Table 2.1 (below) compares the peak conductivities, the temperature of the peak conductivity and the ratio of $\sigma_{max}/\sigma_{300K}$ of Holland's PANi-CSA with a series of PANi-CSA materials produced for this work. It is obvious that both PANi-CSA materials are almost identical with respect to the temperature dependant conductivity. Hence, the author is confident that any differences between the PANi-AMPSA material studied in this work and the PANi-CSA investigated by Holland *et al.* [12] are due entirely to the different dopant-solvent systems used.

	Holland's PANi-CSA			New PANi-CSA		
% Doping	Peak σ (Scm^{-1})	Temp. of Peak σ (K)	$\sigma_{10K}/\sigma_{300K}$	Peak σ (Scm^{-1})	Temp. of Peak σ (K)	$\sigma_{15K}/\sigma_{300K}$
30	90	270	0.13	88	275	0.14
40	160	225	0.44	157	225	0.44
50	178	190	0.67	187	185	0.69
60	268	135	0.94	276	130	0.96
70	184	185	0.75	186	180	0.77
90	121	185	0.71	117	185	0.74

Table 2.1. Comparison of characteristic temperature dependent conductivity values for Holland's PANi-CSA and PANi-CSA materials produced for this work.

The temperature dependent conductivities of PANi-AMPSA samples with different doping levels are shown if figures 2.6 and 2.7. It can be seen that the samples at doping densities between 40% and 70% have very similar profiles, and that all the samples display the same general shape as a function of temperature. All the samples also show a discontinuity in the gradient of temperature dependence between 240K and 260K. The slope of this change in gradient is displayed better by the normalised conductivity shown in figure 2.8, where the graphs are normalised such that:

$$\sigma(\text{Normalised}) = \sigma(T) / \sigma(300K). \qquad \text{eqn. 2.2}$$

Figure 2.9 shows the shape of the temperature dependent conductivity of the 50% doped sample alone.

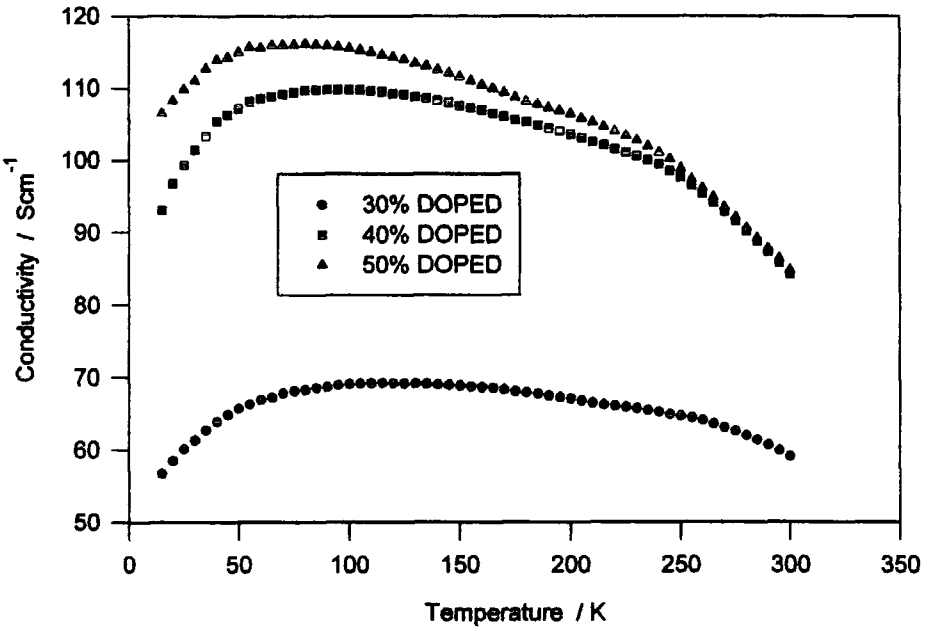

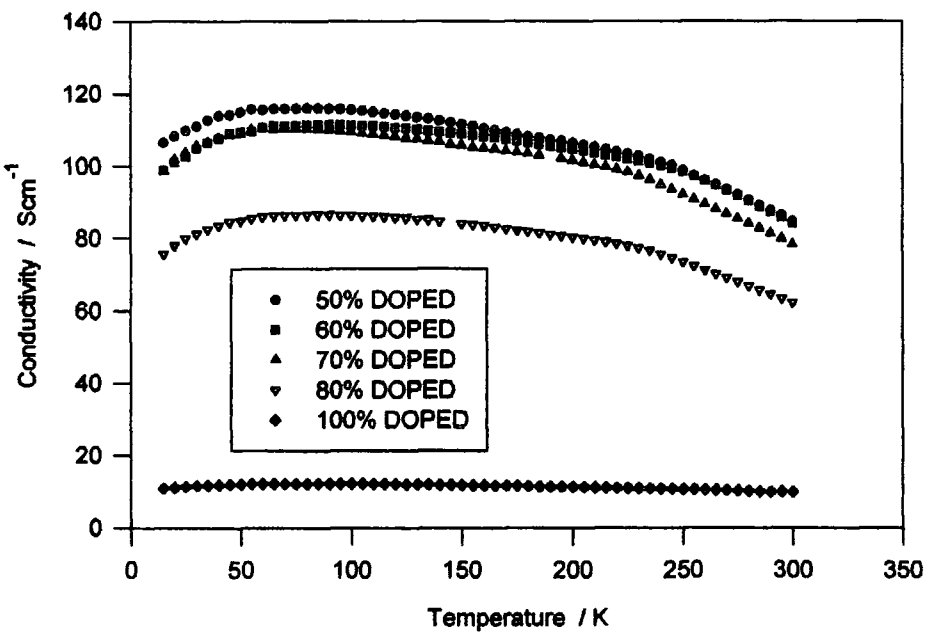

Top: Figure 2.6. Conductivity vs. Temperature for 30-50% doped PANi-AMPSA samples.

Bottom: Figure 2.7. Conductivity vs. Temperature for 50-100% PANi-AMPSA doped samples.

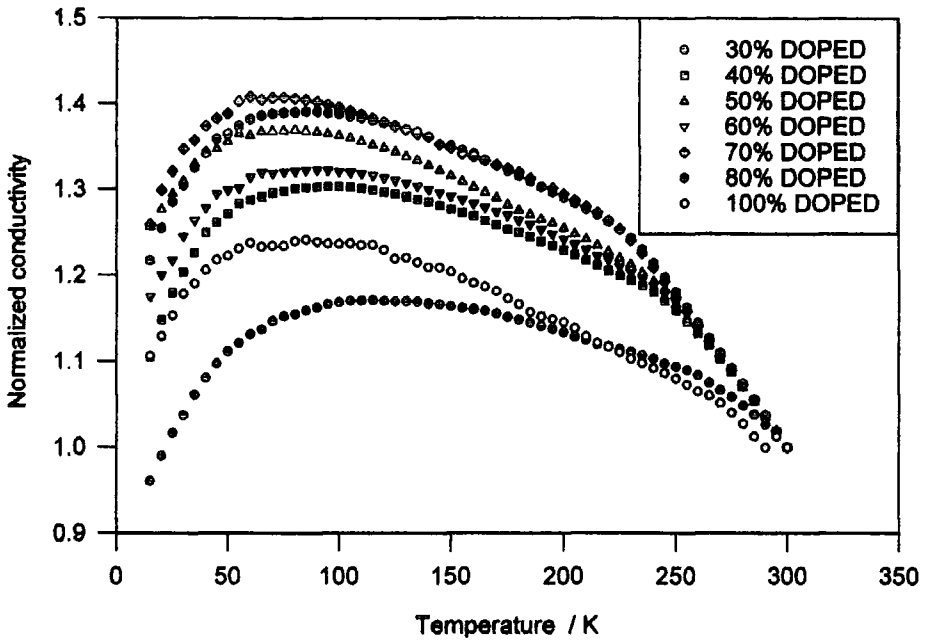

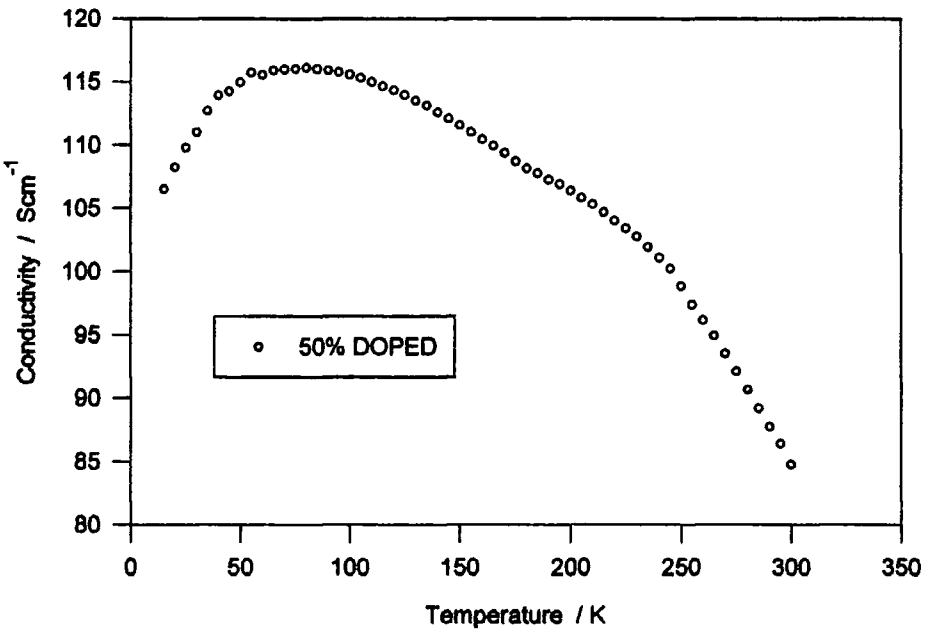

Top : Figure 2.8. Normalised Conductivity vs. Temperature for all PANi-AMPSA samples.

Bottom : Figure 2.9. Expanded view of the temperature dependent conductivity of the 50% doped PANi-AMPSA sample.

2.3.1 DISCUSSION.

The PANi-AMPSA materials exhibit a negative temperature coefficient of conductivity at temperatures greater than 100K for the most conductive samples. This is very similar to the trend exhibited by the PANi-CSA materials investigated by Holland *et al.* [12], thus implying that a metallic transport mechanism may be present in AMPSA doped polyaniline.

There are two models that can be used to describe protonation of the polymer, the first being a random distribution leading to homogeneous doping throughout the system. At low concentrations the conduction band states formed by the protonated imine sites would be widely spaced, thus little interaction between the states is possible. In this picture, charge carriers would be localised, and conduction via thermally activated hopping (e.g. VRH) would be expected. Increasing the doping level would have the effect of increasing the interactions between conduction band states and increasing the density of charge carriers in the material. This change would be manifested as an increase in conductivity and charge carrier mobility. At high doping levels the system may become a Fermi glass (containing both localised and de-localised states within the conduction band, section 1.7.2). In the Fermi glass state (where the Fermi level lies in the region of the localised states but is close to the mobility edge) the conductivity at low temperatures is expected to follow a power law with respect to temperature [18]:

$$\sigma(T) \propto T^{1/2} \qquad \text{eqn. 2.3}$$

where $1 < Z < 3$. At high temperatures conduction by carriers excited above the mobility edge could be limited by phonon scattering. Power-law modified VRH models were suggested as the transport mechanisms for early polyaniline [16,19,20], but these models do not describe adequately the charge transport observed in either the PANi-CSA or PANi-AMPSA systems.

Holland *et al.* [12] proposed that a second type of "non-homogeneous" doping process was occurring in PANi-CSA, along the lines of Kaiser *et al.* [28-30,33]. Protonation of the emeraldine base may favour repeated doping of the polymer chains, or conglomeration of doped chains during the drying process. In such a case the material will contain "granular metallic islands" in a less conducting polymer matrix. As the level of doping is increased, the size and density of the metallic grains within the polymer would increase, and a state could be reached where significant percolation of charge carriers between islands occurs. In this system macroscopic charge transport would be governed by the properties of the metallic region, as well as tunnelling through the amorphous "barrier" regions. Tunnelling between islands still dominates, thus the conductivity is only a few hundred Siemens per centimetre. The temperature dependence of the tunnelling mechanism is weak compared to that of the metallic regions, hence a negative temperature coefficient of conductivity is observed above ~100K. It was this second model that provided the best fit to Holland's' data from PANi-CSA systems.

The fitting of any particular model to PANi-AMPSA is somewhat complicated by the presence of (what the author will tentatively suggest as) the glass transition within the measured range. It can be seen from the normalised data that the slope of

the graphs above 260K are all approximately the same, indicating that the discontinuity between 240-260K is independent of doping (for the highly conducting samples at least). This feature indicates that, at temperatures above 260K, there is a change in the samples such that the conductivity is more strongly dependent upon temperature. Adams *et al.* [13] have measured differential scanning calorimetry (DSC) on PANi-AMPSA, this shows that there is a transition at about 30 to 35 degrees below zero Celcius (roughly the same temperature as the conductivity discontinuity). Adams *et al.* suggest that this transition is possibly the "glass transition" of the PANi-AMPSA system. This theory is supported by the fact that films and fibres produced by the PANi-AMPSA route can be "cold-drawn" [13]. The conductivity of these "stretched fibres" has been measured by Adams *et al.* to be about $1000Scm^{-1}$ for the most highly conductive samples (currently).

Below this transition temperature, T_g, the dependence of the conductivity displays a similar shape to the heterogeneous model suggested by Holland [12], although differences are apparent. Perhaps the most obvious of these differences is that the lowest measured conductivity of PANi-AMPSA is at room temperature, (for the samples with doping levels of 40% or greater, at least). In contrast the PANi-CSA data presented by Holland shows that the low temperature conductivity (of even the most conductive samples) is less than the room temperature measurement. Table 2.2 shows $\sigma(15K)/\sigma(300K)$ for PANi-AMPSA compared with $\sigma(10K)/\sigma(300K)$ for PANi-CSA*.

DOPING LEVEL (%)	30	40	50	60	70	80	90	100
σ(15K)/σ(300K) AMPSA	0.96	1.10	1.26	1.18	1.26	1.22	-	1.11
σ(10K)/σ(300K) CSA*	0.13	0.44	0.67	0.94	0.75	-	0.71	-

Table 2.2. σ(low T)/σ(room T) for PANi doped with AMPSA and CSA*.
*CSA data from Holland *et. al.* [12].

This trend suggests that the thermal scattering of charge carriers at high temperatures is stronger in the AMPSA doped material than in PANi-CSA. One probable explanation for this is that PANi-AMPSA is much less crystalline than PANi-CSA and, therefore, the density of scattering species is higher in the former material. The observation that the peak conductivity of PANi-AMPSA is about 1.4 times its room temperature conductivity (much greater than observed in PANi-CSA) suggests that the AMPSA doped material may have a different crystal structure, phonon interaction or barrier formation compared with PANi-CSA. X-ray analysis of PANi-AMPSA at different doping densities is currently being undertaken by this group [21].

Another difference between the two systems is the temperature at which the peak conductivity is observed. For PANi-CSA samples the temperature at which the turn-over occurs decreases with increasing doping, to a minimum for the most conductive samples. At higher doping (>50%) levels the peak conductivity occurs at a slightly higher temperature, but the turn-over point shows little (if any) dependence upon doping (table 2.3).

DOPING LEVEL (%)	PEAK CONDUCTIVITY (Scm^{-1})		TEMPERATURE OF PEAK CONDUCTIVITY (K)	
	CSA	AMPSA	CSA	AMPSA
30%	90	69	270	115
40%	160	110	225	95
50%	178	116	190	75
60%	268	111	135	85
70%	184	110	184	80
80%	-	87	-	85
90%	121	-	185	-
100%	-	12	-	85

Table 2.3. Conductivity maxima and the temperature at which they occur for the differently doped PANi-CSA* and PANi-AMPSA systems.

*CSA data from Holland *et al.* [12].

The PANi-AMPSA samples show the same rough trend as the CSA doped systems (table 2.2), with two important differences. Firstly the most highly conductive samples from the PANi-AMPSA route are those doped to 50%, the optimum theoretical doping level for polyaniline (see section 1.6 and references such as [8, 22]). PANi-CSA, however, has a maximum conductivity for samples prepared from 60% doped solutions (see table 2.3 and reference [12]). Holland proposed two explanations for this seemingly anomalous maximum in conductivity with respect to doping [23].

1. All the CSA does not dissociate fully in the m-cresol solution, hence an excess of acid is required to fully protonate all the imine sites.

2. Protonation beyond the theoretical "50% optimum" leads to further generation of conduction band states, thus allowing a higher charge carrier density within the material.

The author wishes to expand upon this list.

3. The CSA is not fully soluble in m-cresol. In this case an excess of CSA would need to be added to the solution to create the 2:1 molar ratio of PANi to solvated CSA. The majority of the excess CSA crystallites would be removed from the solution by the centrifuge, and would not be present in the films produced. The films produced by a 60% doping level (in terms of the acid added to solution) may, therefore, be closer to 50% doped. The validity of this theory can be evaluated simply by performing x-ray analysis on PAN-CSA materials produced from non-centrifuged solutions, to determine whether CSA crystallites are present or not.

4. X-ray diffraction experiments by Abell *et al.* [24-26] have shown that the 60% doped PANi-CSA system exhibits a high degree of crystallinity. Perhaps the excess CSA (if it is present in excess) complexes with solvent and polymer to aid creation of the "metallic" crystalline regions that are thought to be present in this system [11,18,27]. In this case the CSA is important in the crystal structure, but a small fraction of it is not involved in the protonation of the polymer, again leaving the material closer to 50% doped than 60%.

The investigation of the PANi-AMPSA system seems to support the explanations that imply that excess acid is required to protonate PANi-CSA to the desired level, or to enhance the crystallinity of the polymeric system. This conclusion is supported by the direct comparisons that can be drawn between the two systems (PANi-AMPSA and PANi-CSA) as they have identical processing techniques.

It should be noted, however, that the PANi-AMPSA system may also require excess doping. It could be suggested that the traces of water in the solvent (dichloroacetic acid) could lead to its' dissociation, thus limited protonation of the polymer without the addition of a "dopant" may occur. Dichloroacetic acid is itself a weak acid, but it is a stronger acid than m-cresol. In this case the requirement of an excess of acid would be masked. It is, therefore, possible that protonation of the polymer backbone above 50% does occur, leading to increased conductivity in the (nominally) 50% doped PANi-AMPSA system.

It is clear from the above arguments that there are still unresolved issues regarding the optimum doping level of salt solution polyanilines. Further studies of this form of PANi are required to determine which (if any) of the above theories are correct.

The second difference between the conductivity's of the CSA and AMPSA systems is that the peak conductivity occurs at a much lower temperature in PANi-AMPSA (table 2.3). This suggests that the thermally activated conduction mechanism has a smaller activation energy in PANi-AMPSA than that in PANi-CSA. If the density of scattering species (i.e. polymeric and crystallographic defects) is much higher in PANi-AMPSA than its' CSA doped analogue, then it is possible that the turn-over is a result of the increased scattering. The two systems, therefore, may have very similar activation energies. Optimisation of the production of PANi-AMPSA materials (i.e., drying temperature, solution concentration, etc.) may lead to PANi-AMPSA materials with higher conductivities than those recorded here.

The data from the PANi-AMPSA materials has been fitted with a heterogeneous model similar to one suggested by Kaiser [28-30] and used by Holland

[12] (section 1.7.6) for the fitting of PANi-CSA curves. The model takes the form of equation 1.35, reproduced below:

$$1/\sigma = AT + B[\exp(-T_0/(T_1+T))]^{-1} \qquad \text{eqn. 2.4}$$

where A and B are fitting parameters and T_0 and T_1 are the characteristic temperatures of the FIT model. (T_0 and T_1 represent the temperature at which there is a significant contribution to the conductivity by FIT and the effective barrier potential of the insulating regions respectively, see section 1.7.5.) The fits were made for the regions below the observed discontinuity and extrapolated to 300K (figures 2.10-2.13). As Holland pointed out, there is no justification for the use of the suggested heterogeneous model, other than the fact that it provides the most satisfactory fit to the experimental data. The same is true for the data from the PANi-AMPSA materials, and thus it is the model used. Table 2.4 lists the parameters of equation 2.4 as a function of doping.

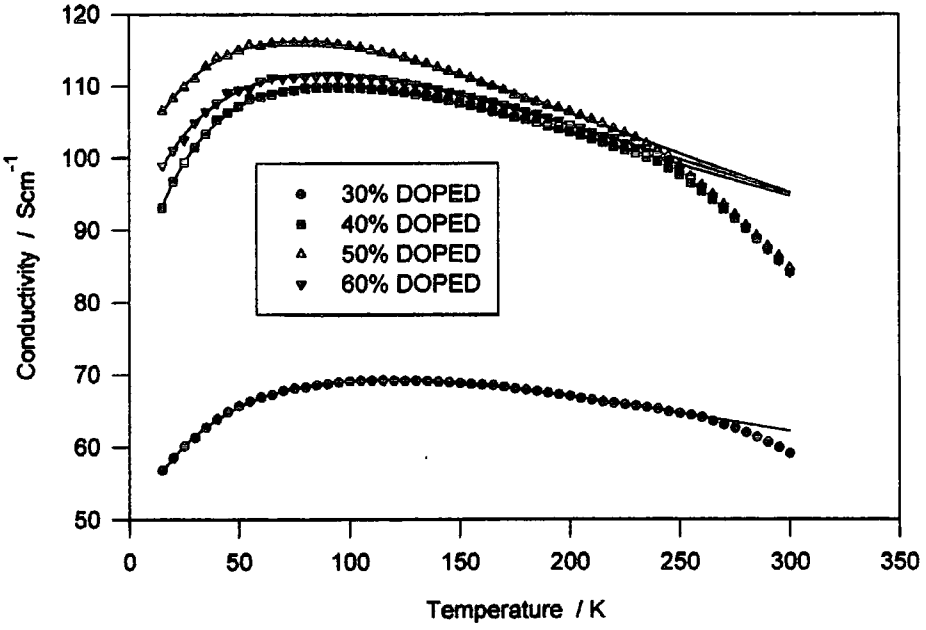

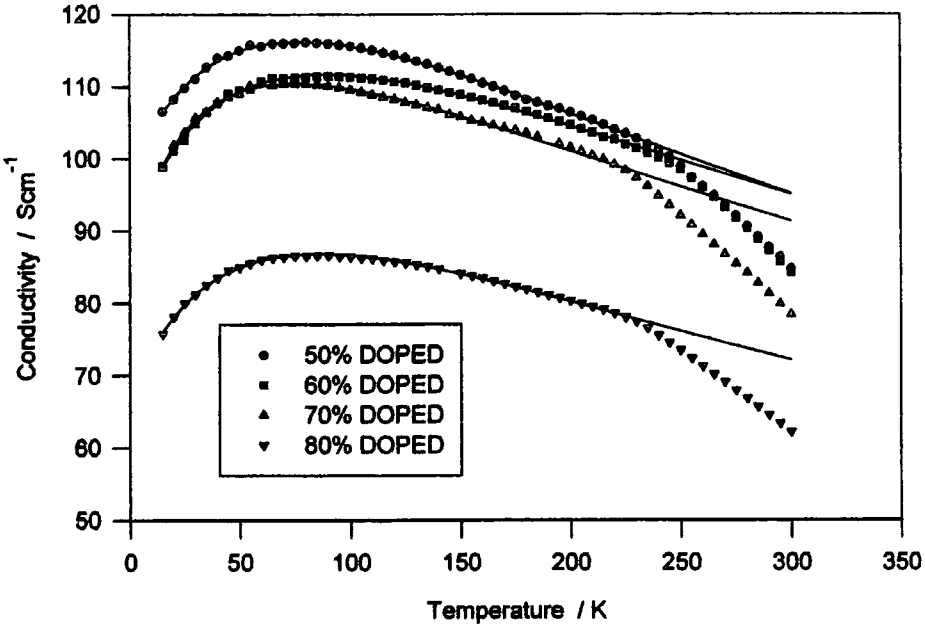

Top : Figure 2.10. Heterogeneous fit to samples doped from 30-60%.

Bottom : Figure 2.11. Heterogeneous fit to samples doped from 50-80%.

The lines are the curves fitted to the data in both figures.

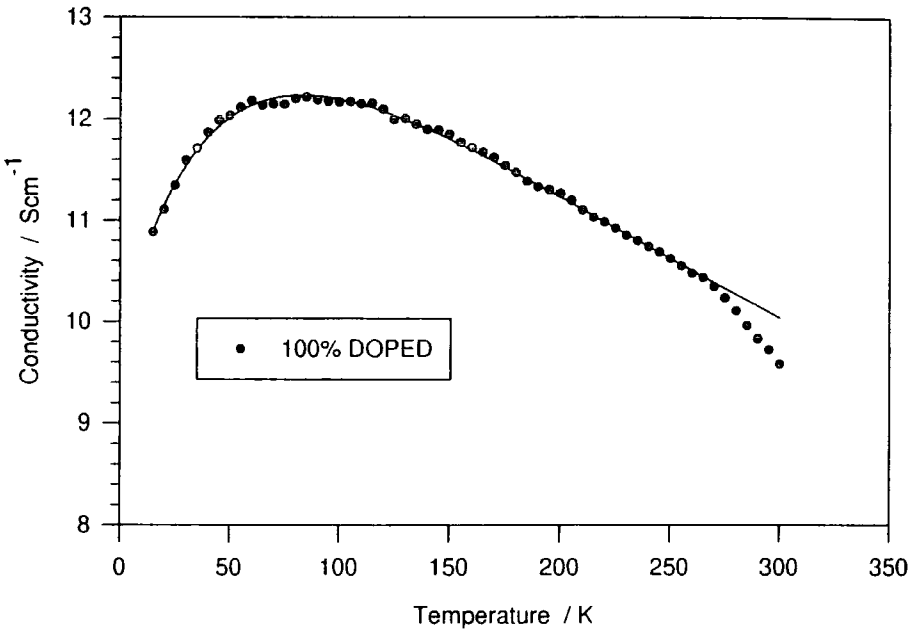

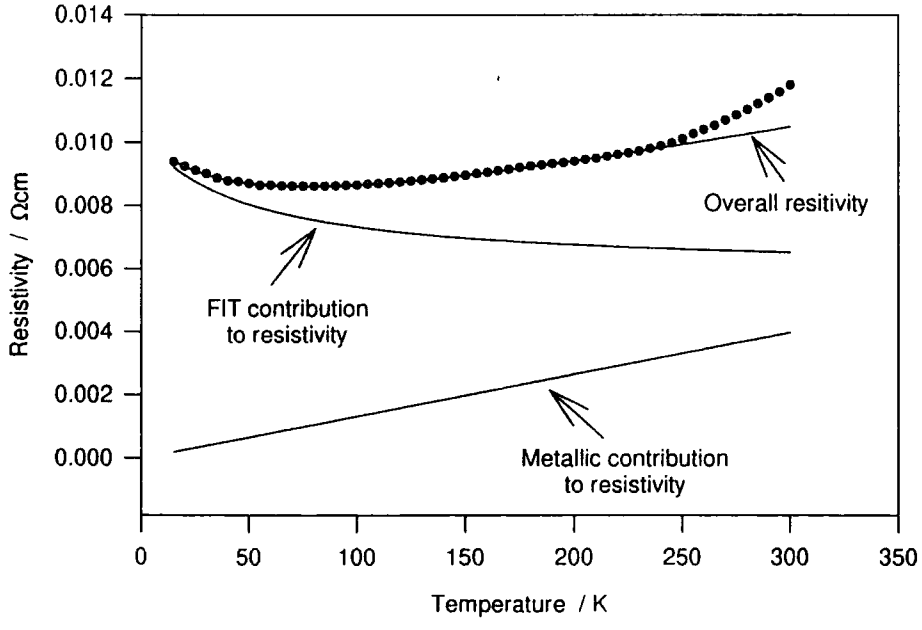

Top : figure 2.12. Curve fitted to data from the 100% doped material.

Bottom : figure 2.13. Expanded view of the individual resistivities from the curve fitting parameters of the 50% doped material. The fitted line is simply the sum of the two individual resistivities.

DOPING LEVEL %	A $x10^{-5}$ ΩcmK^{-1} (+/- 5%)	B $x10^{-3}$ Ωcm (+/- 5%)	T_0 K (+/- 10%)	T_1 K (+/- 10%)
30	1.63	10.1	37.5	53.3
40	1.09	6.84	20.9	33.3
50	1.33	5.93	34.5	63.6
60	1.18	6.41	29.6	52.7
70	1.21	6.92	17.9	34.7
80	1.71	7.98	31.6	50.8
100	12.8	54.9	37.0	60.0

Table 2.4. Fitting parameters from equation 2.4 for PANi-AMPSA.

The parameters listed in table 2.4 do not reveal any trends with respect to doping, except for B, which tends to a minimum for the most conducting samples (the 50% doped materials). This is the case for the parameter B listed by Holland for PANi-CSA [12], but in this case there is also a trend for the other parameters. For PAN-CSA the two temperature variables tend to a maximum and the fitting parameter A has a minimum (with respect to doping) for the most conductive (60%) samples. The same is not true for PANi-AMPSA (as seen in table 2.4) where no discernible trends are obvious. The parameter B is the maximum resistivity at T=0, i.e. the reciprocal of the minimum metallic conductivity outlined in section 1.7.2.

SAMPLE	A $x10^{-5}$ ΩcmK^{-1} (+/- 5%)	B $x10^{-3}$ Ωcm (+/- 5%)	T_0 K (+/- 10%)	T_1 K (+/- 10%)
50% DOPED PANi-AMPSA	1.33	5.93	34.5	63.6
60% DOPED PANi-CSA*	0.66	0.931	519	332

Table 2.5. Comparison between PANi-AMPSA and PANi-CSA* with respect to the parameters from equation 2.4.

*CSA data from Holland *et al.* [12].

Comparison of the values of the parameters between the most conductive samples of the two dopant systems (table 2.5) shows some differences between the systems. Firstly T_0 and T_1 for the 50%-AMPSA doped samples about an order of magnitude smaller than those for 60% CSA. For PANi-CSA T_0 is roughly twice the size of T_1, whereas the converse is true for PANi-AMPSA. This result seems to suggest that conduction through the non-crystalline "barriers" is better in PANi-AMPSA than PANi-CSA, thus implying that the former has a lower activation energy for FIT than the latter. Also, the value of A for PANi-AMPSA is approximately twice that of the CSA doped polymer, inferring that phonon scattering is stronger in the AMPSA system. The increased scattering could be due to an increased density of scattering species in PANi-AMPSA compared with PANi-CSA. The author is, however, cautious as to whether these observations are meaningful or merely just mathematical necessities for the fitting of the data.

Figure 2.14 shows a modification of Holland's metal-FIT model to try and encompass the discontinuity due to the phase transition at ~250K. Modification of A and B to be different values above and below the discontinuity leads to the curve overlaid on the 50% doped data in figure 2.14. The difference between the values of A and B for the different temperature regimes is given in table 2.6. At temperatures above the phase change it can be seen that the parameter A increases by a factor of ~2.5 whereas parameter B decreases by a factor of ~3. If the temperature dependence of conductivity is expected to be dominated by scattering in the metallic islands at the phase transition temperature, it is obvious that a change in A will lead to a modification of the gradient.

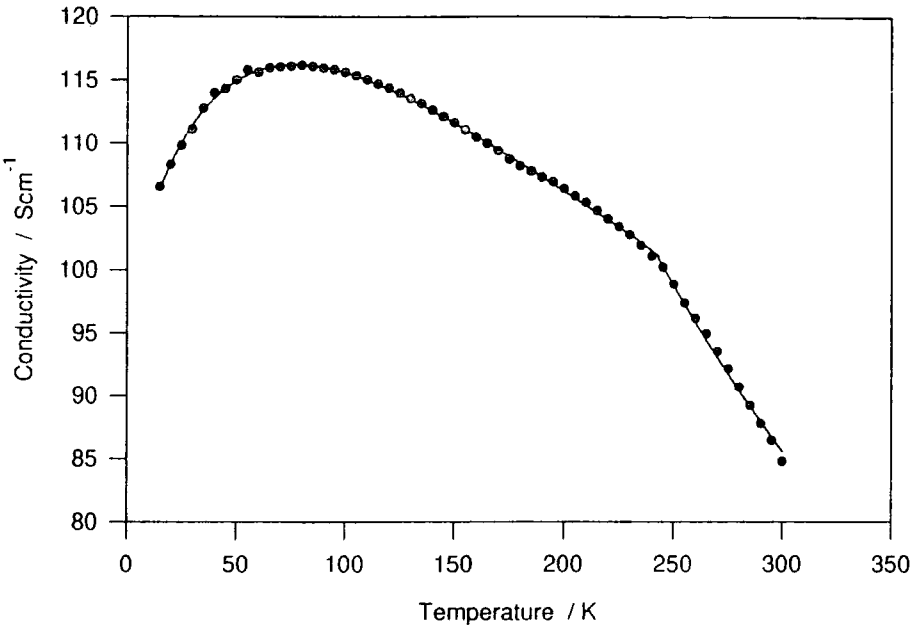

Figure 2.14. Modified fit to the 50% doped material to include the phase change discontinuity at ~250K. The model uses two different values of A and B for temperatures below and above the discontinuity. The values of T_0 and T_1, however, are unchanged for the entire fit.

of the conductivity. The parameter B, must therefore be modified at temperatures greater than T_g since it is little more than an extrapolation of the curve back to T=0.

TEMPERATURE K	A $x10^{-5}$ ΩcmK^{-1} (+/- 5%)	B $x10^{-3}$ Ωcm (+/- 5%)
<250K	1.33	5.93
>250K	3.19	1.91

Table 2.6. Comparison of the modified parameter as a result of fitting around the phase transition discontinuity observed in the 50% doped PANi-AMPSA.

As previously mentioned, B is effectively the reciprocal of the minimum metallic conductivity, σ_{min}, described in chapter 1.7.2. The value of σ_{min}, therefore, changes from ~170 Scm^{-1} below to ~520 Scm^{-1} above the transition temperature for the 50% doped material. It is obvious, however, that the change in B is necessitated by the fitting of a different metallic coefficient A. Since no fit to the curve could be made by significantly changing T_0 and/or T_1, it is suggested that the phase change has little effect (if any) on the FIT mechanism. This seems intuitively correct since it is expected that the metallic term would be dominant (with respect to the temperature dependence) at such temperatures, thus, the phase change at about ~250K increases scattering within the metallic regions.

It is perhaps simplest to ascribe phase transition to the temperature at which a degree of rotational or vibrational freedom is frozen. If this transition has a great effect on intrachain transport, it would be expected that the conductivity of the metallic regions would be affected more than the barrier regions. It is suggested that further work be carried out on the PANi-CSA system at temperatures higher than

those measured by Holland. The glass transition temperature of CSA has been reported to be ~145 to 150°C [31], thus investigation of the conductivity around this temperature may reveal whether the discontinuity observed in PANi-AMPSA also occurs in the CSA doped materials. If this is not the case then another explanation for the discontinuity must be found. CSA, however, becomes unstable at temperatures greater than 120°C, hence investigation of this transition may be impossible.

Although the change in σ_{min} at Tg can be considered as a mathematical by-product of the curve fitting process, the value it has at temperatures below the discontinuity is notable. In his book [32], Mott proposed that the σ_{min} of a disordered conductor was the minimum value of conductivity that could be reached before the onset of localisation. Mott calculated this value to lie in the range of 100-300 Scm^{-1}. It can be seen, therefore, that the reciprocal of B for all the highly doped PANi-AMPSA samples are within this range, thus suggesting that conduction via extended metallic states does occur.

Kaiser *et al.* have recently suggested a slightly different model for the conductivity of PANi-CSA seen by Holland [33]. Kaiser suggests that the conduction in the metallic regions is quasi-one-dimensional, and therefore scattering is only possible as the "back-scattering" of charge carriers. This model is derived from an expression initially devised to explain the conductivity of polyacetylene. A heterogeneous model was used to describe quasi-one-dimensional conduction in the metallic "fibrils," with a second term representing hopping/tunnelling between metallic regions. The modification of Holland's' "FIT-metal" model by Kaiser is shown in equation 2.5.

$$1/\sigma = A\exp(-T_m/T) + B[\exp(-T_0/(T_1+T))]^{-1} \qquad \text{eqn. 2.5}$$

where T_m represents the energy of a phonon that is required for the back-scattering of a charge carrier. This mechanism requires phonons of relatively high energy that are not easily excited below room temperature. Kaiser fitted this to the PANi-CSA data, taking a value of T_m of around 1000K. Kaiser admits, however, that the quasi-one-dimensional model does not provide as good a fit as Holland's' to the PANi-CSA data at low temperatures. Fits of equation 2.5 to the PANi-AMPSA data could not be made for the value of T_m ~1000K. Values of T_m ~400K accommodated reasonable fits to the data (for the region between 80 to 250K), but were also unsatisfactory with respect to the low temperature region. The author, therefore, doubts the validity of Kaisers' model with respect to PANi, especially considering the low temperatures at which phonon scattering appears to dominate in the PANi-AMPSA materials. Kaiser himself points out that phonons of the energy required to back-scatter charge carriers are not readily excitable below room temperature. The author also expresses concern with both Kaiser's and Holland's models as they contain so many variables, and as such might provide reasonable fits to almost any curve of the general shape exhibited by the PANi-CSA data.

It is possible, however, that the heterogeneous "granular 3-D-metal" model (above) is not the actual combination of mechanisms that govern transport in either the PANi-CSA or PANi-AMPSA materials. The lack of any other model to provide comparably good fits to the experimental data (for either of the dopant systems), however, suggests that Holland's model is at least useful at a conceptual level. The model used above is especially useful in understanding how combinations of

individual mechanisms can lead to a coherent transport model for extended temperature regimes.

It is perhaps useful at this point to describe in some detail what is meant by a crystalline polymer. Long chain polymers can not form single crystals in the same way as smaller organic (and inorganic) molecules. Sections of polymer chains become aligned and a "lamella" structure is formed. Single layers consist of aligned polymer segments which can fold at the surface of the ordered layer such that another section of the same chain can become part of the crystal layer. Obviously some polymer chains have segments which constitute part of different crystalline layers. Between the layers is an amorphous tangle of polymer chains weaving between the various layers. It is thought that different lamella group together around a crystal "nucleation" site, thus forming a macroscopic polycrystalline grain. Within this grain there must be chain-ends, mis-bonding and cross-linking, all contributing to the properties of the grain. In crystalline polyaniline it is possible that a polaron lattice exists within the lamella structure, thus the crystalline grains may exhibit metallic conductivity on a microscopic scale. It is also possible that highly mobile polarons exist in the ordered layers, thus accounting for metallic conduction within the crystalline regions. It is, however, not possible to distinguish between these two possibilities from temperature dependent conductivity measurments alone.

2.4 THE CONDUCTIVITY OF "ULTRA-THIN" POLYANILINE FILMS.

The conductivity of the thin films was only measured at room temperature, the reasons for this being two-fold. Firstly, the interpretation of the temperature dependence is subject to the question "are the samples two or three dimensional?" in terms of transport modelling. Secondly the applications for which the samples were being prepared did not require high conductivity over an extended temperature range.

Three different polyaniline salts were used to coat glass substrates, as outlined in section 2.2.1. Although the final applications of the solution doped and post-doped samples were somewhat different, the requirements of each were similar. In each case the films produced had to be of a low optical density such that visible light could easily propagate through the sample and substrate. For the PANi-AMPSA and PANi-CSA materials a compromise between high conductivity (thicker films) and maximum optical transmission (thinner films) had to be reached. Only films displaying the most satisfactory fit to this compromise were produced for further investigation into their suitability as electrodes for organic polymer LEDs. A comparison with the conductivity of Indium Tin Oxide (ITO) coatings on glass was made for the PANi-CSA and PANi-AMPSA systems.

The CA-PANi-HCl materials did not require such high optical transmission, indeed it is changes in the optical absorption spectrum of the system that would be measured in the "in-situ" electrochemical experiments of Dr. C.M.A Brett. The post doped polyaniline cellulose acetate blends, therefore, were spun to give optimum uniformity and surface quality.

2.4.1 CA-PANi-HCl - RESULTS AND DISCUSSION.

The samples of the polyaniline cellulose acetate blend were prepared as outlined in section 2.1.2. The quality of the films was dependent on the speed and temperature at which they were spun, and hence only a limited range of spin conditions yielded uniform defect free films. It was not possible, therefore, to study the thickness dependence of conductivity within this material. The measured conductivities and thickness' of the CA-PANi-HCl system are given in table 2.7.

SAMPLE THICKNESS nm (+/- 15%)	CONDUCTIVITY Scm^{-1} (+/- 20%)
50	5.2
70	3.3
40	6.0
40	3.1
60	3.0

Table 2.7. Thickness and conductivity measurements of CA-PANi-HCl thin films.

It can be seen that the error in thickness measurement has led to a large error in the conductivity of the material. The only result that can be drawn from this experiment is that CA-PANi-HCl films of ~50nm thickness have a conductivity of around 4 ± 2 Scm^{-1}. This result, however, is non-trivial when it is considered that the material is a 50-50 weight percent polymer blend of polyaniline with an insulating polymer, namely cellulose acetate. The conductivity of CA-PANi-HCl, therefore, is comparable to samples of similar thickness spun from 60% doped PANi-CSA (see section 2.4.2).

Kaiser *et al.* [33] reported data from 50% doped PANi-CSA dispersed in insulating polymers at various ratios of PANi to insulating polymer. They showed that the conductivity of the samples decreased as the fraction of PANi in the blend was reduced. It is noticeable, however, that the temperature dependence of the conductivity was different to that of pure PANi-CSA in that it tended to zero at T=0. Kaiser modelled the data with a similar heterogeneous model to the one he suggests for PAN-CSA (eqn. 2.5, above) with the FIT exponential term replaced with a tunnelling/hopping term of the form $\exp[(T_0/T)^{½}]$. The use of this form of model is justified by the expectation that granules of PAN-CSA would be dispersed throughout the polymer system (due to phase segregation) and hopping or tunnelling between these mesoscopic grains would be the dominant charge transport mechanism.

The CA-PANi-HCl blend, however, is not expected to consist of grains within an insulating polymer matrix. Since the films are formed from undoped PANi in a host polymer, a homogeneous random distribution of PANi chains entangled with those of CA is more likely, hence a different model must be adopted. Temperature dependent measurements of CA-PANi-HCl should reveal further information about the charge transport properties of the system and need to be undertaken.

It is possible, however, that the observations made here relate to PANi-CSA polymer blends. If charge transport in CA-PANi-HCl shows the same temperature dependence as the blends studied by Kaiser *et al.* then it is possible that his model is not justified. The assumption that there are discrete PANi-CSA grains dispersed in pure insulating polymer is disputable. It is, perhaps, more likely that a system where PANi-CSA grains are dispersed in a homogeneous blend of PANi-CSA and insulating polymer exists. Transport, in this case, could be limited by conduction along quasi-

one-dimensional PANi chains linking the PANi-CSA islands, and hopping from one chain to another in the amorphous region. Alternatively the above polymeric structure may be limited by a hopping/tunnelling process (as suggested by Kaiser) where the presence of PANi-CSA in the host matrix modifies the energy of the barrier to hopping/tunnelling.

Further study of the CA-PANi-HCl system present here may provide insight into which of the above systems provides a general model for the structure of polyaniline blends. It should also be noted that one other form of polymer blend is possible. It could be the case that all the blends described above are of non-miscible polymers, hence it is possible that discrete granules of the insulating polymer are dispersed in an amorphous or semi-crystalline PANi matrix. The latter structure is, however, unlikely from Kaisers' data showing that $\sigma \rightarrow 0$ as $T \rightarrow 0$ inferring that the insulating polymer (or a blend of it with PANi) is the host material.

2.4.2 PANi-CSA AND PANi-AMPSA THIN FILMS - RESULTS AND DISCUSSION.

Thin films were prepared from solutions of 60% doped PANi-CSA and 50% doped PANi-AMPSA, the most conductive materials from the respective systems (from the bulk measurements shown in section 2.3). Unlike CA-PANi-HCl, it was possible to produce a range of film thickness' for both the solution doped polymers. Indeed, the film quality (in terms of surface roughness and thickness uniformity) of the CSA and AMPSA doped materials was measurably better than the post-doped polymer blend described in the previous section.

Figures 2.15 and 2.16 show the "sheet resistance" as a function of film thickness for the PANi-CSA and PANi-AMPSA films. Sheet resistance (resistance per square, R_{SQ}) is often quoted for thin film conductors such as ITO on glass, and a comparison between the above materials and ITO is made (ITO data from Merck Balzers, manufacturers of coatings for flat panel displays). Consider a square sample of thickness t and length and width x. Substitution into equation 2.1 gives:

$$\sigma = \frac{I}{Vt} = \frac{1}{R_{SQ}t} \qquad \text{eqn. 2.6}$$

$$\Rightarrow \quad R_{SQ} = \frac{1}{\sigma t}. \qquad \text{eqn. 2.7}$$

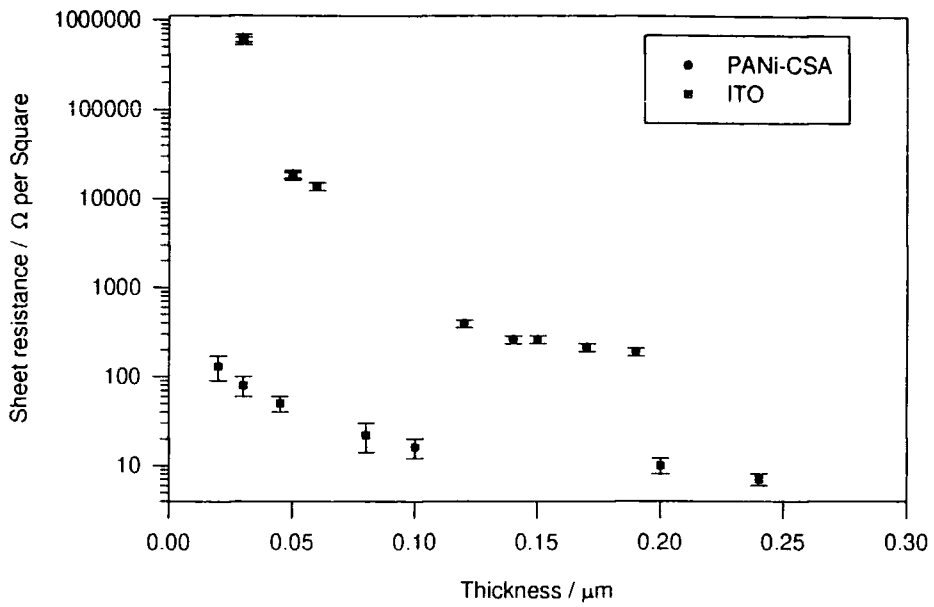

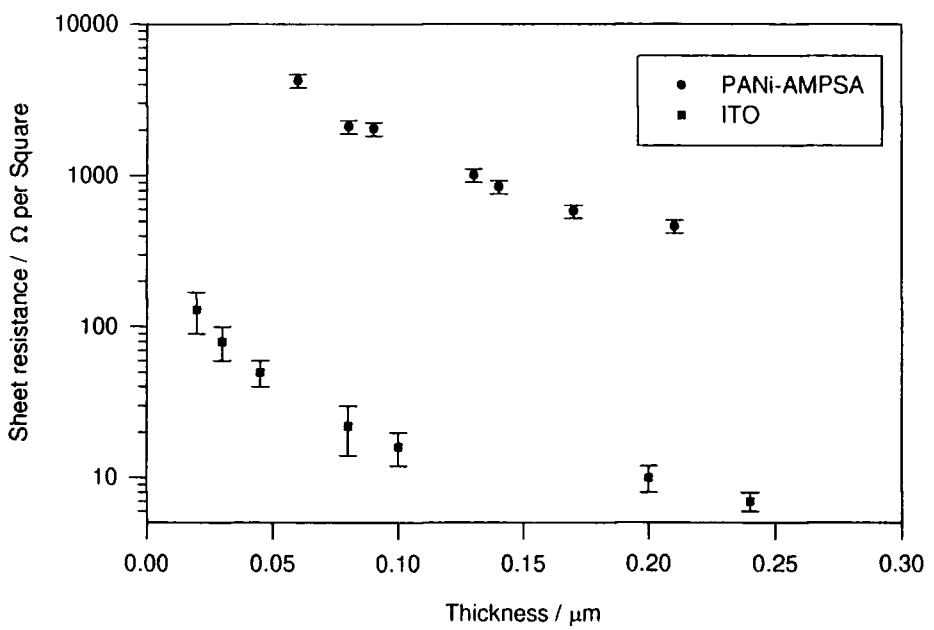

Top : Figure 2.15. Sheet resistance vs. thickness for PANi-CSA, compared with ITO.

Bottom : Figure 2.16. Sheet resistance vs. thickness for PANi-AMPSA, compared with ITO.

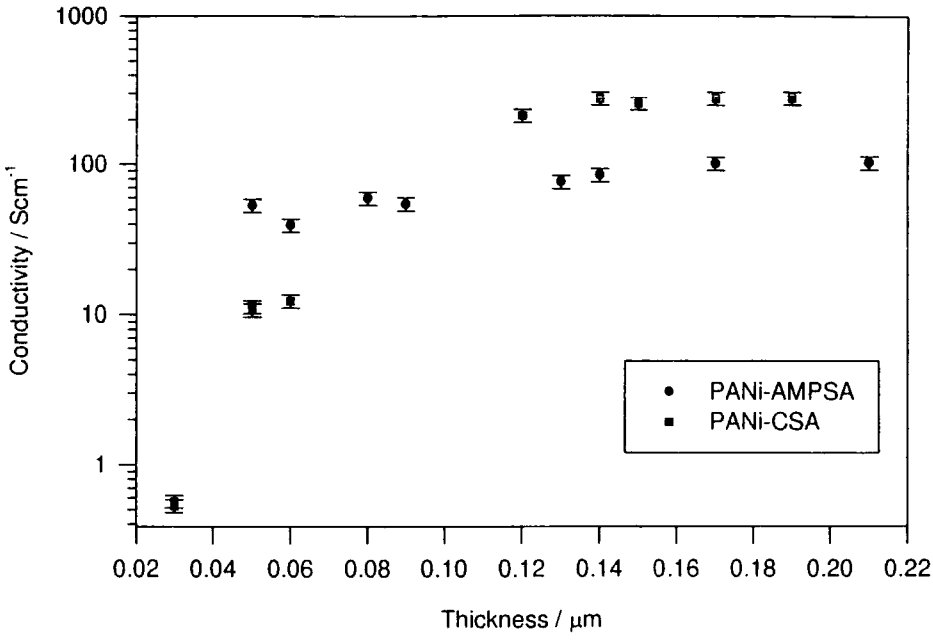

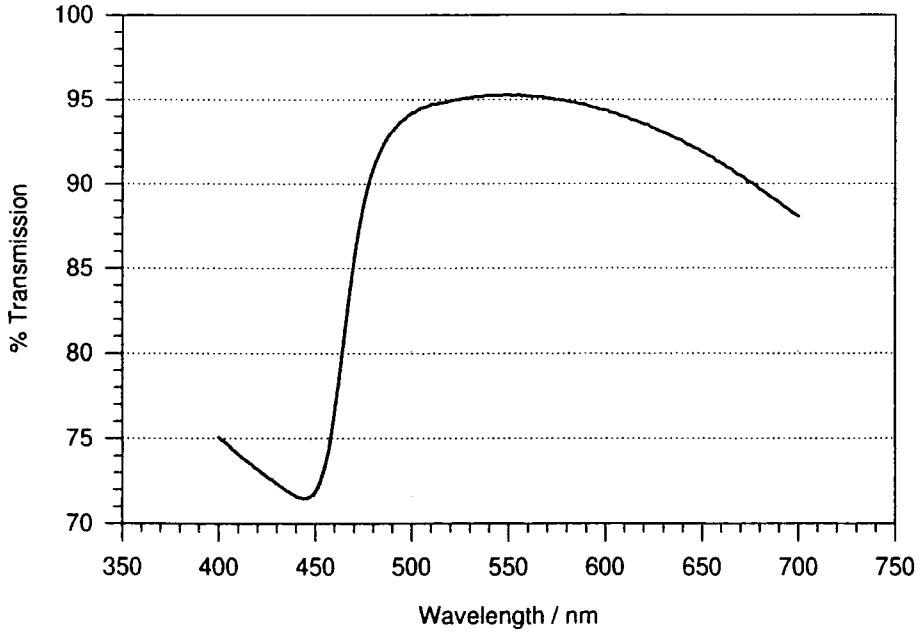

Top : Figure 2.17. Conductivity vs. thickness for PANi-CSA and PANi-AMPSA.

Bottom : Figure 2.18. Transmission spectrum of a 70nm thick film of PANi-AMPSA.

Thus conductivity and resistance per square are easily calculated from each other if the sample thickness is known. Figure 2.17 shows the conductivity of all the systems as a function of thickness.

The most obvious difference between PANi-CSA and PANi-AMPSA is that while the AMPSA doped materials display only limited thickness dependence whereas the CSA samples exhibit a discontinuity between roughly 70nm and 100nm. The CSA samples have conductivities of the same order as those measured in the bulk material at thicknesses greater than ~100nm (a conductivity of approximately 300 Scm^{-1}). At around 50nm thick the conductivity has dropped by an order of magnitude to ~10Scm^{-1} and decreases still further to <1Scm^{-1} for thicknesses of ~30nm. This variation of conductivity compares un-favourably with ITO for which conductivity decreases from ~6000Scm^{-1} to ~4000Scm^{-1} as its' thickness is reduced from 240nm to 20nm, a mere 30% decrease. One explanation for the discontinuity observed in the PANi-CSA samples is that the material undergoes a transition, from a three dimensional array of "metallic grains" in the bulk to a two dimensional system in thin films. It is widely accepted that (60% doped) PANi-CSA materials exhibit a high degree of crystallinity, and that the system is composed of crystallites dispersed in an amorphous matrix. Thus, it is not unreasonable to consider that a reduction in conductivity may occur as the thickness of the sample approaches the same order of magnitude as the crystallite diameter. The results from ultra-thin PANi-CSA films, therefore, may fit a 2-D FIT model. The author suggests that temperature dependent conductivity measurements should be made on samples of PANi-CSA at thickness' around 30nm to investigate this proposition.

In contrast, the PANi-AMPSA doped materials do not display a discontinuity in conductivity as a function of sample thickness (to the lowest thickness measured here). This material is reported to display a lower degree of crystallinity than PANi-CSA [21], thus suggesting that the metallic regions within the AMPSA doped polymer are smaller that those in the CSA doped analogue. If PANi-AMPSA is indeed composed of crystallites of a smaller size than those in PANi-CSA, then it is unlikely that the samples investigated above would be anything other than a three dimensional array of granules in an amorphous matrix. As such, no discontinuity would be expected for the measured thickness range.

The optical transmission of PANi-CSA films with thickness' greater than 100nm is at best 80%, thus making the system similar to ITO currently used, (peak transmission for 100nm of ITO ~ 85% at 500nm). The 70nm thick PANi-AMPSA materials, however, exhibit a >90% transmission window between 480nm and 670nm with a peak transmission of ~95% at 560nm (figure 2.18), as well as a conductivity of ~50 ± 10Scm^{-1}. The LEDs under investigation by this group emit around a peak at 550nm, very close to the maximum transmission of the PANi-AMPSA thin films. Although not as conducting as ITO, ultra-thin PANi-AMPSA films may, therefore, provide superior electrodes for polymer LEDs.

Carter *et al.* [34] recently published supporting data to that presented above, showing that 100nm films of PANi-CSA and PANi-APSA (APSA = acrylamidopropanesulphonic acid, obviously very similar to AMPSA) had conductivities of 200Scm^{-1} and 100Scm^{-1} respectively. In the LEDs produced by Carter *et al.* the PANi layer was used as the anode since it has been suggested that the use of a "hole injecting" polymer anode would enhance device lifetime. One of the

major problems associated with ITO as an electrode is the leeching of indium and oxygen into the emitting layer, hence PANi and other conducting polymers have been used to provide a barrier layer between ITO and other layers of a polymer diode, thus increasing the longevity of the devices. Carter *et al.* [34] also showed that polymer electrodes with a conductivity of $>2Scm^{-1}$ could be used as the only necessary contact, and not just as an extra coating on ITO substrates, thus the materials invesigated here (σ $\sim 50Scm^{-1}$) could easily be used as electrodes, fabrication permitting. It was also shown that the use of doped PANi electrodes produced a marked increase in device performance (i.e., life-time and brightness).

The results presented in this section show that PANi-AMPSA materials would provide higher conductivity electrodes than PANi-CSA at thickness' <100nm. They also show good agreement with the data presented by Carter's' group, although they did not investigate conductivity as a function of electrode thickness. The AMPSA doped PANi system is currently under investigation (by this group) as a single electrode for polymer LEDs. The system gives rise to the possibility of all organic LED's and the simple manufacturing techniques associated with (most) polymers.

2.5 CONCLUSIONS.

The measurement of the temperature dependence of conductivity (as a function of doping) for the bulk PANi-AMPSA material shows good agreement with the heterogeneous metal-FIT model proposed by Holland *et al.* [12]. It is apparent that conductivity is not a result of the system being a Fermi glass since it is seen that σ does not tend to zero with $T \rightarrow 0$. It might, however, be prudent to take conductivity measurements at milli-Kelvin temperatures to verify this since the observation is made from an extrapolation of the available data to T=0. Similarly, it is unlikely that conductivity is well described by variable range hopping since neither the 1-D-VRH nor 3-D-VRH models provided good fits to the experimental data. The author, therefore, proposes that Holland's model [12] is the best available model to fit temperature dependent conductivity measurements of polyaniline doped (in solution) with functionalised sulphonic acids.

The differences between the shapes of the fits made to the data from the PANi-CSA and PANi-AMPSA materials do, however, highlight the fact that the systems are not identical. It is proposed that the differences are a result of the systems having different physical properties. The discontinuity observed in the PANi-AMPSA samples supports this explanation by showing that a phase transition occurs for the AMPSA doped material at a temperature where no similar discontinuity is observed in PANi-CSA. The most intuitive cause of this discontinuity is the freeing of a vibrational or rotational degree of freedom within the polymer chains at temperatures

above the discontinuity. Phonons created above the discontinuity temperature increase the scattering of charge carriers and conductivity is reduced, as observed.

Another important difference between the two materials is that PANi-AMPSA exhibits a peak conductivity for the 50% doped material, whereas the conductive PANi-CSA materials are 60% doped. It is again proposed that this difference is due to the systems having different physical properties, i.e., size and concentration of crystallites. It is also possible, however, that protonation of the polymer backbone such that more than half of the nitrogen sites are protonated occurs in both materials. Since dichloroacetic acid is a stronger acid than m-cresol it is possible that the solvent protonates to a greater extent in the PANi-AMPSA material than the CSA doped analogue. Fifty percent "doped" PANi-AMPSA may, therefore, be protonated to a similar extent as 60% "doped" PANi-CSA (where "doping" in this sense refers only to the molar ratio of AMPSA added) and each may be protonated beyond the 60% level.

The conductivity measurements of the thin-film polyaniline material support the suggestion that AMPSA and CSA doped polyaniline have different physical properties. The observed reduction in conductivity with decreasing thickness of PANi-CSA may show that this material contains larger crystallites than PANi-AMPSA. Alternatively, It may just be an indication that "spinning" does not produce as high quality films from PANi-CSA as PANi-AMPSA. This could be due to the solutions having different viscosities and drying rates as a result of the different solvents and dopants used. From the results presented here it is apparent that PANi-AMPSA could easily be used as the electrode layer in polymer LED's instead of ITO (currently used). The high optical transmission and electrical conductivity of this material ($\sigma \sim 50 Scm^{-1}$ with a peak transmission of ~95% for the ~30nm thick layers)

could lead to an improvement in the quality of the LEDs (with respect to those fabricated on ITO substrates). Comparisons between efficiency and longevity for LED's with ITO and/or PANi-AMPSA electrodes are currently being undertaken by this group.

The post-doped blend of polyaniline with cellulose acetate resulted in a material with a surprisingly high conductivity. Since the post-doped material is not expected to contain crystallites it would be interesting to measure the temperature dependent conductivity of CA-PANi-HCl materials to investigate whether they exhibit different temperature dependencies to the solution doped polymers. Such data would also indicate whether Kaiser *et al.*'s [33] model for solution doped polyaniline dispersed in an insulating polymer matrix provides a good description for charge transport in CA-PANi-HCl. If this is the case, Kaiser's model can not be valid as the model assumes the dispersion of highly conducting crystallites within an insulating/semiconducting polymer matrix. Such a system is not expected for CA-PANi-HCl since post doped polyanilines are unlikely to contain crystallites.

2.6 REFERENCES.

1. Dodabalapur, A., *Organic light emitting diodes.* Solid State Communications, 1997. **102**(2-3): p. 259-267.
2. Burroughes, J.H., Bradley, D. D. C., Brown, A. R., Marks, R. N., Mackay, K., Friend, R. H., Burns, P. L., Holmes, A. B., *Light-Emitting-Diodes Based On Conjugated Polymers.* Nature, 1990. **347**(6293): p. 539-541.
3. Miller, J.S., *Conducting Polymers - Materials Of Commerce.* Advanced Materials, 1993. **5**(7-8): p. 587-589.
4. Macdiarmid, A.G., Chiang, J. C., Richter, A. F., Epstein, A. J., *Polyaniline - a New Concept In Conducting Polymers.* Synthetic Metals, 1987. **18**(1-3): p. 285-290.
5. Mattoso, L.H.C., *Polyanilines - Synthesis, Structure and Properties.* Quimica Nova, 1996. **19**(4): p. 388-399.
6. Adams, P.N., Laughlin, P.J.,Monkman, A.P., Kenwright, A.M., *Synthesis of High Molecular Weight Polyaniline.* Synthetic Metals, 1996. **83**: p. 379
7. Angelopoulos, M., Asturias, G.E., Ermer, S.P., Ray, A., Scherr, E.M., MacDiarmid, A.G., Akhtar, M., Kiss, Z., Epsein, A.J., *Polyaniline - Solutions, Films and Oxidation States.* Journal of Molecular and Liqiud Crystals, 1988. **160**: p. 151.
8. Lux, F., *Properties of electronically conductive polyaniline: a comparison between well-known literature data and some experimental findings.* Polymer, 1994. **35**: p. 2915 - 2926.
9. Cao, Y., Smith, P., Heeger, A.J., *Counterion Induced Processibility of Conducting Polyaniline and Conducting Polyblends of Polyaniline in bulk Polymers.* Synthetic Metals, 1992. **48**: p. 91.
10. Lee, K.H., Heeger, A. J., Cao, Y., *Reflectance Of Polyaniline Protonated With Camphor Sulfonic-Acid - Disordered Metal On the Metal-Insulator Boundary.* Physical Review B-Condensed Matter, 1993. **48**(20): p. 14884-14891.

11. Reghu, M., Cao, Y., Moses, D., Heeger, A. J., *Counterion-Induced Processibility Of Polyaniline - Transport At the Metal-Insulator Boundary.* Physical Review B-Condensed Matter, 1993. **47**(4): p. 1758-1764.

12. Holland, E.R., Pomfret, S. J., Adams, P. N., Monkman, A. P., *Conductivity Studies Of Polyaniline Doped With CSA.* Journal Of Physics-Condensed Matter, 1996. **8**(17): p. 2991-3002.

13. Adams, P.N., Abell, L., Pomfret, S. and Monkman, A.P., *Polyaniline doped with AMPSA in DCA, To be published.* 1997.

14. Dailey, S., Halim, M., Rebourt, E., Samuel, I.D.W., Monkman ,A.P. *An Efficient Electron-Transporting Polymer for Polymer LEDs.* in *International Symposium on Optical Science, Engineering and Instrumentation.* 1997.

15. Reghu, M., Cao, Y., Moses, D., Heeger, A. J., *Metal-Insulator-Transition In Polyaniline Doped With Surfactant Counterion.* Synthetic Metals, 1993. **57**(2-3): p. 5020-5025.

16. Zuo, F., Angelopoulos, M., Macdiarmid, A. G., Epstein, A. J., *Transport Studies Of Protonated Emeraldine Polymer - a Granular Polymeric Metal System.* Physical Review B-Condensed Matter, 1987. **36**(6): p. 3475-3478.

17. Chiang, J.C., Macdiarmid, A. G., *Polyaniline - Protonic Acid Doping Of the Emeraldine Form to the Metallic Regime.* Synthetic Metals, 1986. **13**(1-3): p. 193-205.

18. Larkin, A.I., Khemelnitskii, D.E., Soviet Physics JETP, 1982. **56**: p. 647.

19. Jeong, S.K., Suh, J. S., Oh, E. J., Park, Y. W., Kim, C. Y., Macdiarmid, A. G., *Preparation Of Polyaniline Free Standing Film By Controlled Processing and Its Transport Property.* Synthetic Metals, 1995. **69**(1-3): p. 171-172.

20. Park, Y.W., Lee, Y. S., Park, C., Shacklette, L. W., Baughman, R. H., *Thermopower and Conductivity Of Metallic Polyaniline.* Solid State Communications, 1987. **63**(11): p. 1063-1066.

21. Abell, L., *To Be Submitted.* Macromolecules, 1997.

22. Stafström, S., Bredas, J.L., Epstein, A.J., Woo, H.S., Tanner, D.B., Huang, W.S., MacDiarmid, A.G., *Polaron Lattice in Highly Conducting Polyaniline - Theoretical and Optical Sudies.* Physical Review Letters, 1987. **59**: p. 1464.

23. Holland, E.R., *Transport Properties in Electrically Conductive Polymeric Materials*, in *Physics*. 1995, University of Durham: PhD Thesis.

24. Abell, L., Pomfret, S., Holland, E.R., Adams, P.N., Monkman, A.P. *Aspects of the Camphorsulphonic Acid Processing Route of Polyaniline*. in *Institute of the Plastic Engineers SPE/ANTEC*. 1996.

25. Abell, L., Devasagayam, P., Adams, P.N., Monkman, A.P. *Crystallinity and Stretch Orientation in Polyaniline Camphorsulphonic Acid Films*. in *Institute of Plastic Engineers SPE/ANTEC*. 1997.

26. Abell, L., Pomfret, S., Adams, P.N., Milton, A.C., Monkman, A.P., *Studies of Pre-Doped Polyaniline Films*. Synthetic Metals, 1997. **84**: p. 803 - 804.

27. Menon, R., Yoon, C. O., Moses, D., Heeger, A. J., Cao, Y., *Transport In Polyaniline Near the Critical Regime Of the Metal- Insulator-Transition*. Physical Review B-Condensed Matter, 1993. **48**(24): p. 17685-17694.

28. Kaiser, A.B., *Thermoelectric-Power and Conductivity Of Heterogeneous Conducting Polymers*. Physical Review B-Condensed Matter, 1989. **40**(5): p. 2806-2813.

29. Kaiser, A.B., *Physical Models For Electronic Transport In Highly-Conducting Polymers*. Abstracts Of Papers Of the American Chemical Society, 1991. **201**(APR): p. 175-PMSE.

30. Kaiser, A.B., *Metallic Behavior In Highly Conducting Polymers*. Synthetic Metals, 1991. **45**(2): p. 183-196.

31. Abell, L., Pomfret, S. J., Adams, P. N., Monkman, A. P., *Thermal studies of doped polyaniline*. Synthetic Metals, 1997. **84**(1-3): p. 127-128.

32. Mott, N.F., Davis, E.A., *Electronic processes in Non Crystalline Materials*. 1979, Oxford: Clarendon Press.

33. Kaiser, A.B., Liu, C.-J., Gilberd, P.W., Chapman, B., Kemp, N.T., Wessling, B., Partridge, A.C., Smith, W.T., Shapiro, J.S., *Comparrison of Electronic Transport in Polyaniline Blends, Polyaniline and Polypyrrole*. Synthetic Metals, 1997. **84**: p. 699-702.

34. Carter, S.A., Angelopoulos, M., Karg, S., Brock, P.J., Scott, J.C., *Polymeric anodes for improved polymer LED performance*. Applied Physics Letters, 1997. **70**: p. 2067 - 2069.

CHAPTER 3

CHAPTER 3

3. ELECTRON SPIN RESONANCE MEASUREMENTS OF CSA DOPED POLYANILINE FILMS.

3.1 AN INTRODUCTION TO ELECTRON SPIN RESONANCE.

3.1.1 THE BASIC THEORY OF ELECTRON SPIN RESONANCE.

Electron spin resonance (ESR) has been an important tool in chemical characterisation since 1945 when Zavoiski [1] reported the first ESR spectrum. Since these initial observations the subject grew rapidly, with virtually all the basic spectroscopic ESR techniques being formulated by physicists at the Clarendon laboratory in Oxford (early work summarised by [2,3]).

The interaction of spins with an applied magnetic field is the very essence of ESR spectroscopy. As the title of the technique suggests, the electron spin is probed at resonance to evaluate the properties of a material in terms of electronic structure. A brief introduction to ESR is given below but the reader is referred to one of the many comprehensive texts on the subject for strict derivations of the physics involved (see, for example, [4-6]).

It is widely accepted that electrons described quantum mechanically have spin angular momentum, **S**. The magnitude of the angular momentum is given by the square root of the eigenvalue of S^2. The eigenvalues for the projection of angular momentum on to a specified direction are M_S, the allowed values being integer steps from -S to +S. For an electron S=½, the values of M_S are, therefore, ±½. Perhaps the most obvious manifestation of electron spin is that electrons have a magnetic moment. This magnetic moment is predicted classically if the electron is considered as a charged spinning sphere. The calculated magnetic moment from this model is, however, almost exactly a factor of 2 too small compared to the observed moment. The classical model also shows that the magnetic moment is co-linear to the angular momentum (or, in classical terms, the axis of rotation).

The magnetic moment is directly proportional to the angular momentum, thus a magnetic moment operator for an electron, μ_e, can be defined as:

$$\mu_e = -g_e\mu_B\mathbf{S} \qquad \text{eqn. 3.1}$$

where $(g_e\mu_B)$ is the magnetogyric ratio. The Böhr magneton, μ_B, is the magnetic moment for a single unit of quantum mechanical angular momentum and g_e is the free electron g-factor (the factor by which the magnetic moment needs to be adjusted such that its value becomes that predicted classically). The negative sign in equation 3.1 indicates that the magnetic moment is anti-parallel to the spin angular momentum for an electron.

The energy, E, of a magnetic moment in a magnetic field, **B**, is given (classically) as:

$$E = -\mu.\mathbf{B}. \qquad \text{eqn. 3.2}$$

Quantum mechanically μ is replaced by the appropriate magnetic moment operator (equation 3.1), such that the Hamiltonian for a free electron in a magnetic field ,H_e, can be obtained. For the case where the field propagates in the z-direction the free electron Hamiltonian is:

$$H_e = g_e\mu_B S_z B \qquad \text{eqn. 3.3}$$

where B is the magnitude of the magnetic field **B**. Since the only operator in equation 3.3 is S_z, the eigenvalues of equation 3.3 are simply multiples of the eigenvalues of S_z. The energy of the magnetic moment in the field is, therefore, given as:

$$E = g_e\mu_B B M_S. \qquad \text{eqn. 3.4}$$

As mentioned earlier, $M_S = \pm ½$ for an electron. In the absence of a field there are two states that are degenerate, but a separation proportional to B is created by the application of an external magnetic field. Conventionally the different eigenstates (energy levels) corresponding to $M_S = +½$ and $M_S = -½$ are labelled α and β respectively (for the case where $S = ½$). Figure 3.1 illustrates the splitting of the degenerate energy levels by a magnetic field.

The separation between the two energy levels is, therefore, defined as:

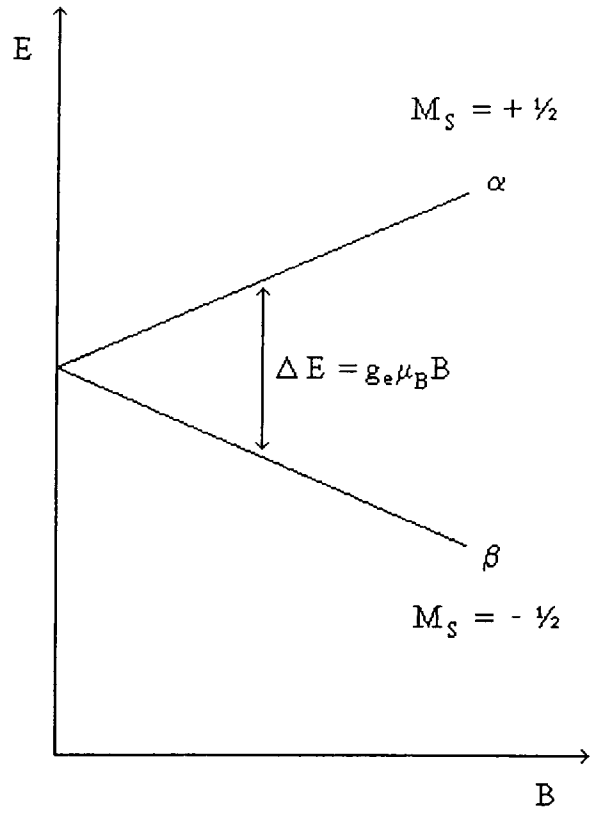

Figure 3.1. Diagram showing the splitting of degenerate energy levels for an electron, S = ½, in a magnetic field.

$$\Delta E = g_e \mu_B B. \qquad \text{eqn. 3.5}$$

Obviously this energy can be considered as being equal to a quantum of radiation such that $\Delta E = h\nu$, h being Planck's constant and ν the frequency of the radiation. Substitution of the physical constants, taking $g_e = 2.0023$ for a free electron, the frequency required is (almost exactly) 28 GHz/T. The most common type of ESR spectrometer uses fields of ~0.34T [4], thus $\nu \approx 9.5$ GHz. This frequency corresponds to a portion of the microwave region of the electromagnetic spectrum often termed the X-band, hence this type of ESR spectroscopy is also known as X-band ESR. ESR at other frequencies is also performed to probe different properties, but these are less common (the reader is again referred to the extensive texts [4-6] for more information about non-X-band ESR).

The classical description of ESR provides a useful illustration of magnetic resonance. Starting from Newton's third law for rotational motion:

$$\text{Rate of change of angular momentum} = \text{Torque}. \qquad \text{eqn. 3.6}$$

For an electron with angular momentum **S** and a magnetic moment μ in a field **B** equation 3.6 becomes:

$$\frac{d\mathbf{S}}{dt} = \mu \times \mathbf{B}. \qquad \text{eqn. 3.7}$$

Using equation 3.1 this becomes:

$$\frac{d\mu}{dt} = g_e\mu_B(\mathbf{B}\times\mu). \qquad \text{eqn. 3.8}$$

For a Cartesian axis system where **i**, **j** and **k** are unit vectors, with **B** along the z-axis such that **B** = B**k**. The cross product in equation 3.8 thus becomes:

$$\mathbf{B}\times\mu = B(\mu_x\mathbf{j} - \mu_y\mathbf{i}) \qquad \text{eqn. 3.9}$$

where μ_x and μ_y are the x and y components of μ. Equating the vector components on each side of equation 3.8 gives:

$$\frac{d\mu_x}{dt} = -g_e\mu_B B\mu_y,$$

$$\frac{d\mu_y}{dt} = g_e\mu_B B\mu_x,$$

$$\frac{d\mu_z}{dt} = 0. \qquad \text{eqn. 3.10}$$

The solutions to equation 3.10 are:

$$\mu_x = \cos(\omega_0 t),\ \ \mu_y = \sin(\omega_0 t),\ \ \mu_z = \text{constant}. \qquad \text{eqn.3.11}$$

where $\omega_0 = g_e\mu_B B$. The motion of a magnetic moment, μ, in a magnetic field, B, is thus described as the precession of μ about B at a frequency ω_0. This is known as Larmor

precession (where ω_0 is the Larmor frequency) after Larmor who discovered the result for a spinning magnet in a magnetic field in 1904.

Consider the effect of a second magnetic field, B_1, rotating about the z-axis at a frequency ω. Assuming that B_1 is small compared to B, (i.e. $B \gg B_1$) for the case where $\omega \neq \omega_0$. Since the precessing magnetic moment will pass in and out of phase with B_1 no net interaction occurs. In the case where $\omega = \omega_0$, however, the magnetic moment will experience a constant field, B_1, in the x-y plane. Thus precession of μ about B_1 will occur. Since B_1 is small compared to B, the precession frequency, ω_1, will be much less than ω_0, where ω_1 is given by:

$$\omega_1 = g_e \mu_B B_1. \qquad \text{eqn. 3.12}$$

The net effect of the additional field will be to cause the z-component of μ to oscillate between the two extremes +z and -z, where +z is the z-component in the absence of B_1 and -z is of the same magnitude but in the opposite direction. This occurs over the course of many Larmor precessions of μ about B and will continue until B_1 is removed or its frequency changed such that ω is no longer equal to ω_0.

The classical description of ESR is not satisfactory since it does not take into account that an exchange of energy between matter and radiation must occur in discrete quanta. The model does, however, provide an insight into the basic principles of ESR. Two important points should be stressed, firstly that an oscillating field in the plane orthogonal to the applied field with an oriented magnetic moment (and angular momentum) can cause a change in the projected value of the magnetic moment (and angular momentum) in the direction of the static field. Secondly, this reorientation can

only occur if the frequency of the oscillating field is at resonance with the natural (Larmor) frequency of the magnetic moment. For a full quantum mechanical description of ESR the reader is referred to the afore-mentioned texts [4-6].

Experimentally B_1 is provided by microwave radiation at a constant frequency and B is "swept" to match the energy separation of the levels with the quantum of radiation. The application of the sweeping field can locate the resonant frequency as B_1 is absorbed due to "z-flipping" at resonance (i.e., $\omega = \omega_0$). An ESR spectrometer thus requires a frequency-stable microwave source and a magnet that can provide a slowly sweeping field such that a spectrum can be recorded. The basic elements of an ESR spectrometer are shown in figure 3.2. Microwaves are channelled to the sample chamber (via a device called a circulator) along a waveguide. The sample chamber is a resonant cavity that has dimensions matching the wavelength of radiation such that a standing wave pattern is set up, effectively increasing the path length through the sample. Microwaves enter the sample chamber through a small, variable iris. At an appropriate iris setting, perfect matching can be achieved such that all the microwave power entering the resonant cavity is stored there in (eventually dissipating thermally) and no power is reflected from the cavity. As the applied field is varied such that resonance is achieved ($\omega = \omega_0$), microwave power is absorbed by the sample. The matching of the resonant cavity is, therefore, altered and microwave energy is reflected from it. The reflected microwave power passes (via the circulator) to the detector. This reflected microwave radiation is the ESR signal. In general, microwave detectors have a non-linear response at low incident powers, to overcome this the resonant cavity is set-up such that there is a slight mismatch and the ESR signal becomes the change in measured microwave intensity.

The output from the microwave detector is a d.c. signal which is not readily processible. This problem is solved by the modulation of the magnetic field. The field modulation is achieved by the addition of a second pair of coils, generally mounted on (or in) the sample chamber. An alternating current through the coils supplies a small alternating field superimposed upon the applied magnetic field. A standard frequency of modulation is 100kHz, lower frequencies lead to lower sensitivities, whilst it is difficult to obtain an oscillating field at the sample with higher frequencies. Provided that the amplitude of modulation is smaller than the linewidth of the absorption, the change in microwave power at the detector will have an oscillating component (at the modulation frequency) proportional to the slope of the absorption. It is this oscillating component that is taken as the ESR signal and it's phase (relative to the modulation frequency) depends on whether the ESR absorption has a positive or negative gradient. Comparison of the modulation frequency and the resultant oscillating component in a phase sensitive detector leads to the first derivative of the absorption spectrum.

It should be noted that the modulation amplitude must be small if the true absorption lineshape is to be observed. Increasing the modulation amplitude increases the intensity of the signal, but high amplitudes can lead to distortion of the lineshape. If this occurs, measurements of linewidths become invalid and resolution will be reduced, especially in the case of multi-line spectra.

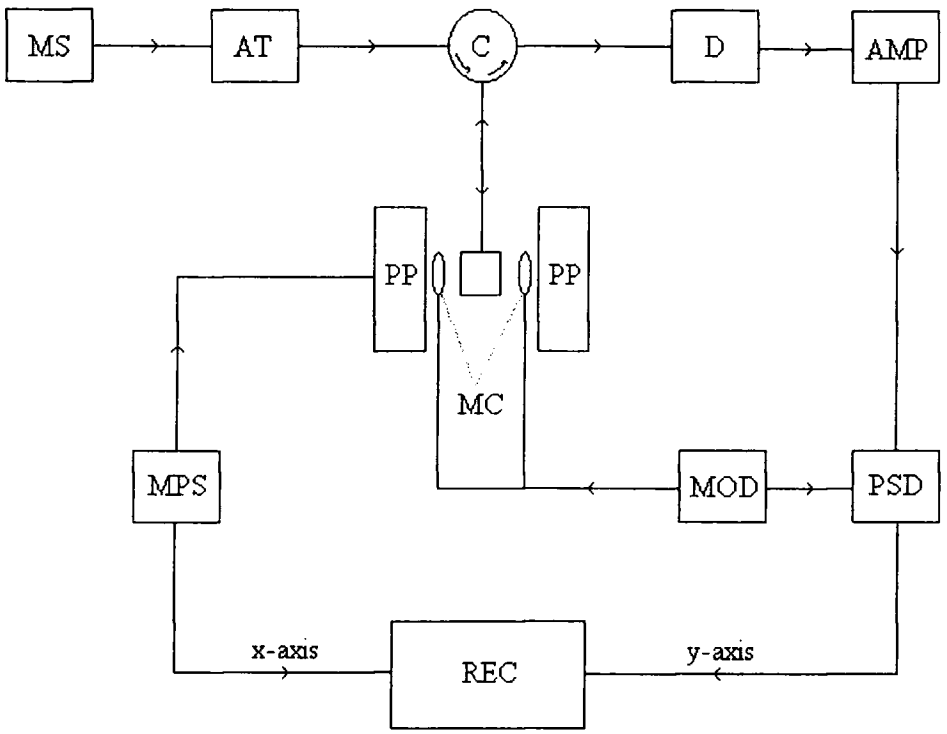

MS = Microwave source, AT = Attenuator, C = Circulator, D = Detector, AMP = Amplifier, PSD = Phase Sensitive Detector, MOD = Modulation Coil Power Supply and Reference, PP = Magnet Pole Piece, MC = Modulation Coil, MPS = Magnet Power Supply, REC = Spectrum Recorder.

Figure 3.2. Schematic diagram of a basic ESR spectrometer.

3.1.2 DETERMINATION OF THE SPIN CONCENTRATION.

It should be noted that ESR is only useful in characterisation of systems in which there are un-paired electrons. For doubly occupied electronic states the signal from each electron exactly cancels that of the other. As such ESR has been used to characterise some transition metals and organic radicals as these systems contain singularly occupied electronic orbitals. ESR can be used to measure the concentration of spins within a sample. Determination of the spin concentration is performed by comparison of the area under the ESR absorption peak with that of a known standard. It should be noted that the area under the absorption peak is found from the double-integral of the ESR spectral line as the recorded line is the first derivative of the actual absorption peak.

The ability to monitor the variation of the spin concentration with variables such as temperature and composition is one of the most useful properties of ESR spectroscopy. The change in shape of the ESR spectrum (namely peak position and linewidth) with the afore mentioned variables also provide information on the properties of the spin carrying species.

The study of charge carriers in conducting polymers by ESR was suggested initially with respect to *trans*-PA (see for example [7,8]). The dynamics of solitons could be studied in un-doped polyacetylene due to the inherent spin of the soliton defect (see chapter 1 section 1.4). As the charge transport models of highly conductive polyaniline are based upon the presence of polarons and/or bipolarons, it is obvious that

ESR provides a useful tool for probing microscopic conduction mechanisms. A wealth of reports regarding the study of polyaniline by ESR have been published (see for example [9-16]), generally reporting ESR of PANi powders with different pH values or HCl post-doped polyaniline films.

One of the major objectives of the numerous studies into the ESR of doped PANi is to determine whether polarons or bipolarons are responsible for charge transport. Electron spin resonance can easily determine whether polarons are present since polarons (like solitons) have an associated spin. Thus, the spin concentration would be expected to be proportional to the doping level if polarons alone were responsible for charge transport within conducting polymers. Similarly, if bipolarons dominate charge transport, the spin concentration would be expected to be independent of doping. The relevance of ESR spectroscopy as a method of characterising conducting polymers is therefore beyond doubt, especially with respect to polyaniline.

3.1.3 LINEWIDTH AND LINESHAPE ANALYSIS.

As mentioned earlier (section 3.1.1), the linewidth itself reveals information about the spin carriers within an ESR sample, narrow lines showing localised species which experience identical local fields. The shape of these narrow lines is referred to as "Lorentzian" as the mathematical Lorentzian line describes the shape of the peak [4-6]. The ESR spectra of localised spin carriers which experience slightly different local fields are not well described by the Lorentzian lineshape. Instead, the line is broadened as each spin exhibits a slightly different resonance frequency. These resonant

frequencies are distributed statistically around the resonant frequency of the most common species, and thus the line becomes "Gaussian" in shape [4-6]. Virtually all ESR spectra can, therefore, be considered as being composed of a Lorentzian and a Gaussian contribution to the overall lineshape.

For the case where spin carrying species were mobile, however, the linewidth would be reduced (compared to that of an identical material with localised spins) as the spin carriers would experience an averaged field. This phenomenon is known as motional narrowing. In conducting polymers where the charge carrying species are also spin carriers, motionally narrowed lineshapes are expected. Since conduction is thermally activated in all the models used to describe the low temperature conductivity of doped PANi (see chapter 2) it is expected that charge carrier mobility can be reduced at low temperatures. Thus, determination of whether the ESR signal is motionally narrowed can easily be demonstrated by studying the temperature dependence of the linewidth.

In the 1950's Dyson formulated a theory to explain the highly asymmetric ESR lineshape observed in some metals, e.g. Na and Be [17]. ESR spectra of conduction electrons in the most conductive metals (e.g., Cu, Au, Ag etc.) cannot be measured due to the rapid relaxation of the conduction electrons. This rapid relaxation leads to a broadening of the signal so great that the ESR signal can not be detected. In the less conductive metals (like those mentioned above) an ESR spectrum can be recorded, but the peak is not well described by a simple Lorentzian or Gaussian lineshape.

Dyson [18] proposed that the lineshape arose from the high mobility of the electrons. In these materials the oscillating magnetic field causes a macroscopic magnetisation which changes the penetration of the microwave field. Conducting

materials can thus be considered as having a "skin-depth," δ_s, which is probed by the ESR experiment. Near resonance the magnetisation becomes large and is carried through the material by the diffusion of the charge carriers. The charge carriers only lose their magnetisation through scattering events (e.g., scattering by phonons and other electrons). Thus, the charge carriers can diffuse into the bulk of the material taking their spin precession far beyond the skin depth region of the oscillating magnetic field which caused the spin alignment. The oscillating field, B_1 is therefore non-local to the classical skin-depth due to the diffusion of electrons.

The resultant line is a mixture of the absorptive and dispersive components of the Lorentzian line as the phase of the oscillating field changes as it propagates through the material. Since phase sensitive detectors are used in ESR spectroscopy, a mixture of absorptive and dispersive components will be detected from electrons at varying depths throughout the sample.

Consider materials of thickness d and skin-depth δ_s. For thin films, such that $d<\delta_s$, the signal will be totally absorptive and hence the lineshape will be that of a symmetric Lorentzian line. For thick films, where $d>>\delta_s$, the signal will be totally dispersive and the lineshape highly asymmetric. Between these two extremes the two components add to give an asymmetric (distorted) line.

The magnitude of this distortion is parameterised by the ratio A/B (often called the asymmetry factor), where A is the peak height above the baseline and B the peak height below the baseline. The work by Feher and Kip [17] on Na, Li and Be have shown that samples thinner than the microwave skin-depth have an asymmetry factor of unity (i.e., A/B = 1). The case where A/B = 1 also describes spins which are localised within the skin-depth of the sample. For spins distributed throughout the volume of the

material, however, A/B = 2.55 for the Lorentzian lineshape and A/B = 2 for the Gaussian lineshape. For mobile spins A/B > 2.55-2.7. The complete mathematical description of Dysonian lineshapes is particularly complex, as such only the relevant highlights have been given above, but it is obvious that Dyson's theory is important in the interpretation of the ESR spectra of conducting polymers.

3.2 EXPERIMENTAL PROCEDURE.

Samples of PANi-CSA films (prepared identically to those used by Holland *et al.* for conductivity measurements, see Chapter 2) were used in the ESR spectroscopy below, namely 30% to 100% doped PANi-CSA films. ESR measurements were made under the supervision of Dr. Andreas Petr at IFW (Institut für Festkörper und Werkstofforschung) Dresden. All the room temperature spectra were obtained using a Bruker ESP 300E ESR spectrometer which was set-up identically for each sample such that direct comparisons between the samples could be made. For reasons that will be explained in the next section a modulation amplitude of 20 Gauss was used for all the spectra taken. Although this large modulation amplitude undoubtedly introduced broadening of the absorption line, the fact that it is consistent between samples allows direct linewidth comparisons between the different samples.

The ESR spectra were measured in a double resonant cavity sample chamber, the sample occupying one of the cavities, with a reference (strong pitch, MgO) sample in the other. The reference sample was calibrated and it was known that there were 1×10^{15} spins per effective cm in the reference (this takes into account the physical length of sample under investigation). Samples 1 cm in height were cut from the polymer films and mounted in a "flat-cell" (figure 3.3) ESR sample tube that was positioned with the centre of the sample at the centre of the resonant cavity. ESR spectroscopy of powders is usually performed using round sample tubes of between 1mm and 2mm in internal diameter. The polyaniline films would need to be rolled if a round sample

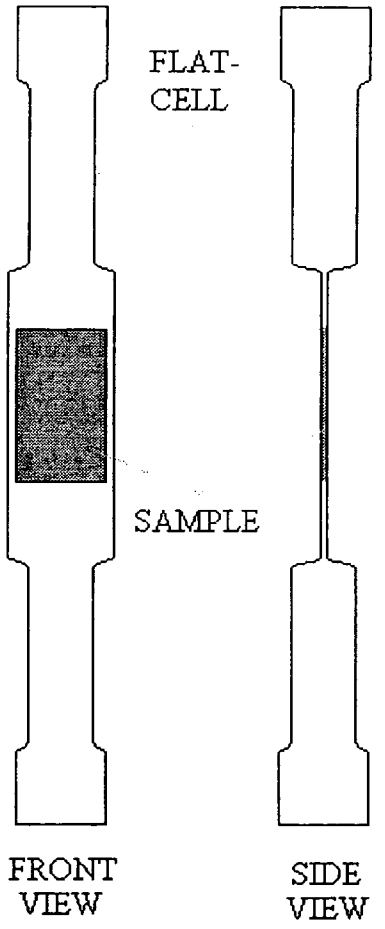

Figure 3.3. Schematic diagram showing a section of polyaniline film mounted in an ESR flat-cell sample tube.

tube was used, this would lead to screening of the inner section by the outer as the material is conductive. The samples were, therefore, inserted into a flat-cell sample tube which held the polyaniline samples flat such that the full surface of the material was exposed to the microwave radiation.

The spin concentrations were calculated using the specially designed transform programs of the spectrometer to calculate the double-integrals of the ESR spectra. The mass of the samples was accurately measured such that spin concentration could also be directly compared between samples. The absolute value of the spin concentration varies from spectrometer to spectrometer as reference methods are typically used. This technique is prone to errors arising from magnetic field and microwave frequency drift, differences in sample packing and dimensions and placement within the microwave cavity. Thus, the absolute spin carrier concentration can only (realistically) be evaluated to within an order of magnitude. In this work, however, the spin carrier concentration can be compared between samples since (virtually) identical conditions were used for each sample, thus any observed trends are likely to be characteristic of the material.

The temperature dependent ESR measurements were made using a Bruker ESP 100E spectrometer with a liquid Helium cooled sample chamber, under very similar conditions to those outlined above.

3.3 RESULTS AND DISCUSSION.

3.3.1 ROOM TEMPERATURE ESR MEASUREMENTS.

Figure 3.4 shows a typical room temperature ESR lineshape of a PANi-CSA film as measured in this work (the 80% doped sample). The line is (generally) Lorentzian in shape, but it is apparent that the lineshape in figure 3.4 is asymmetric with respect to the baseline. The asymmetry factor (A/B, as explained in section 3.1.3) as a function of doping level is plotted in figure 3.5. There is no discernible trend exhibited in figure 3.5, except for the fact that A/B is maximum for the 50% doped samples. The measured value of A/B = 2.5 at 50% doping is on the lower limit of the values expected for mobile spin carriers.

The 60% doped sample, however, has an asymmetry factor close to A/B = 1, suggesting that the spins probed by ESR are either localised, or that the sample is thinner than the classical skin-depth (i.e., $d < \delta_s$). The materials with other doping levels all exhibit some asymmetry, but the distortion is not large enough to be indicative of mobile spin carrying species.

If the fact that the most conductive material (namely the 60% doped sample) has an asymmetry factor close to unity is indicative of sample thickness being less than the classical skin-depth, then δ_s must be greater than 10μm (since the minimum sample thickness was 10μm). Classically the skin-depth is given by [18]:

$$\delta = (c^2 / 2\pi\sigma\omega)^{1/2} \qquad \text{eqn. 3.13}$$

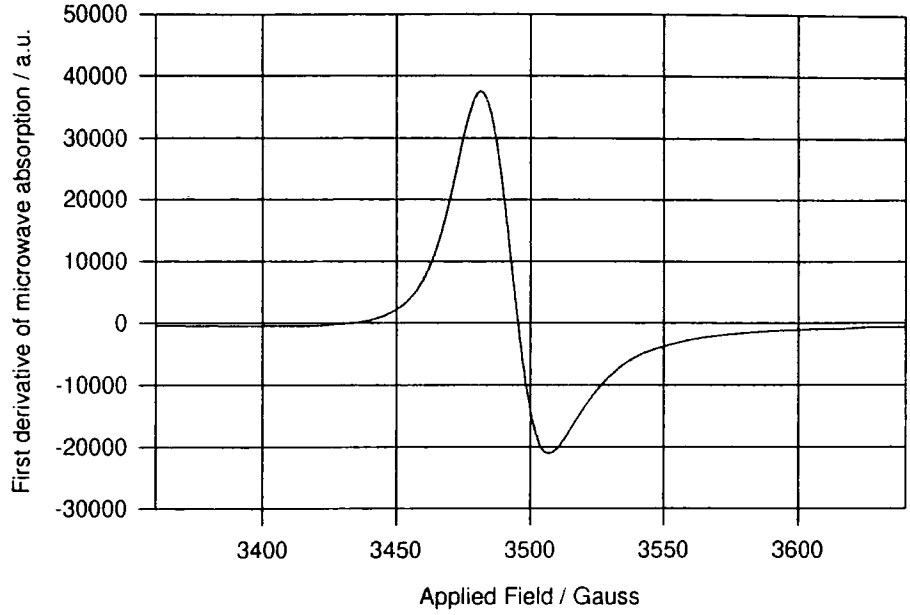

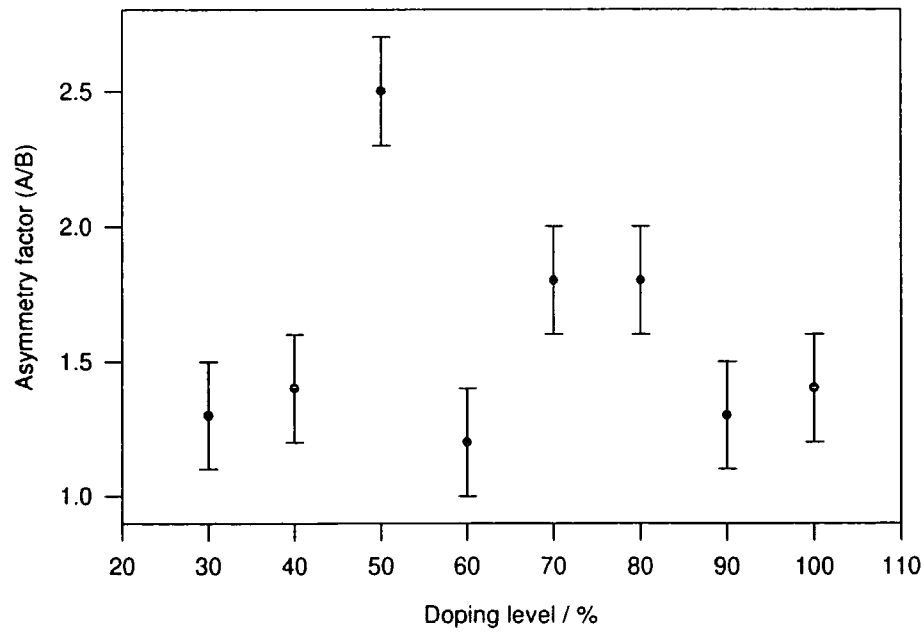

Top: Figure 3.4. First derivative ESR spectrum of 80% doped PANi-CSA.

Bottom: Figure 3.5. Asymmetry ratio (A/B) vs. doping level for PANi-CSA.

where c is the speed of light, σ the conductivity of the sample and ω the angular frequency of the electromagnetic radiation. This gives a minimum (classical) skin-depth of ~30μm for 60% doped PANi-CSA (where $\sigma \approx 300 Scm^{-1}$) for X-band microwaves. Thus, $d < \delta_s$ for all the samples used (typical sample thickness is between 10 and 20 microns). The observed distortion of the lineshape could, therefore, be due to some factor other than the Dyson effect.

Anomalies were also observed in the ESR of polyacetylene measured by Goldberg *et al.* [19] showing an asymmetric lineshape with A/B ~ 2.7 for highly doped samples. The conductivity of the PA samples was reduced as ammonia was added to the samples but the ESR signal remained unchanged, thus implying that the ESR signal arose from neutral spin defects and not the charge carriers. The results of Goldberg and co-workers question whether the distortion of the lineshape observed in PANi-CSA is Dysonian in origin.

It is useful to consider the metallic island model for the macroscopic conductivity of CSA doped PANi. Holland *et al.* [20] used a model where the charge transport within the metallic islands was described by Ohmic conduction. On a microscopic scale, therefore, the conductivity within the metallic regions could be greater than 1×10^5 Scm^{-1}. The skin-depth for a material with this conductivity would be less than 2μm. It is (theoretically at least) possible, therefore, that Dysonian distortion may explain the asymmetric ESR spectra of PANi-CSA materials, assuming that the size of the crystalline grains is greater than the skin-depth of the material within the crystalline regions (i.e., >2μm).

It is suggested that the asymmetric lineshapes observed in this work are not solely indicative of the Dyson effect occurring in PANi-CSA for two reasons. Firstly,

the magnitude of the asymmetry factor is not large enough to be characteristic of mobile spin carriers. Secondly, the anomalously low asymmetry factor of the most conductive sample (i.e., the 60% doped material) suggests that mobile polarons are not present or not detected within the material.

The spin concentration as a function of doping is shown in figures 3.6 and 3.7. The spin concentration per milligram of sample (figure 3.6) was converted into the spin concentration per four ring repeat unit of polyaniline (figure 3.7) within the sample. The fraction of polyaniline in a given sample was calculated assuming that only PANi and CSA were present within the sample, i.e. ignoring any solvation by either m-cresol or water. Although the presence of m-cresol and water is probable, it is almost impossible to determine the ratios present, hence (to a first approximation) the amounts are considered to be negligible.

It can be seen that there is a maximum in spin concentration (in both figures 3.6 and 3.7) for the 60% doped samples. This data suggests that the protonation of polyaniline leads to the creation of spin carriers, but only up to a doping density of ~60%. Above this limit there is either no further protonation or a process occurs whereby further protonation leads to the formation of bipolarons. Although not immediately obvious, both of these phenomena could lead to a reduction in the number of spins within the sample as a whole. If polaron formation is favourable within the metallic regions of doped PANi it is reasonable to assume that samples of greatest crystallinity will have the greatest spin concentration. Note that this explanation assumes that a 3-D polaron lattice (facilitating free carriers) is formed within the metallic grains. The formation of mobile polarons within the crystalline regions as a result of doping would also lead to the observed spin concentrations. Differentiating between the 3-D polaron lattice and mobile polarons as the observed spin carriers may

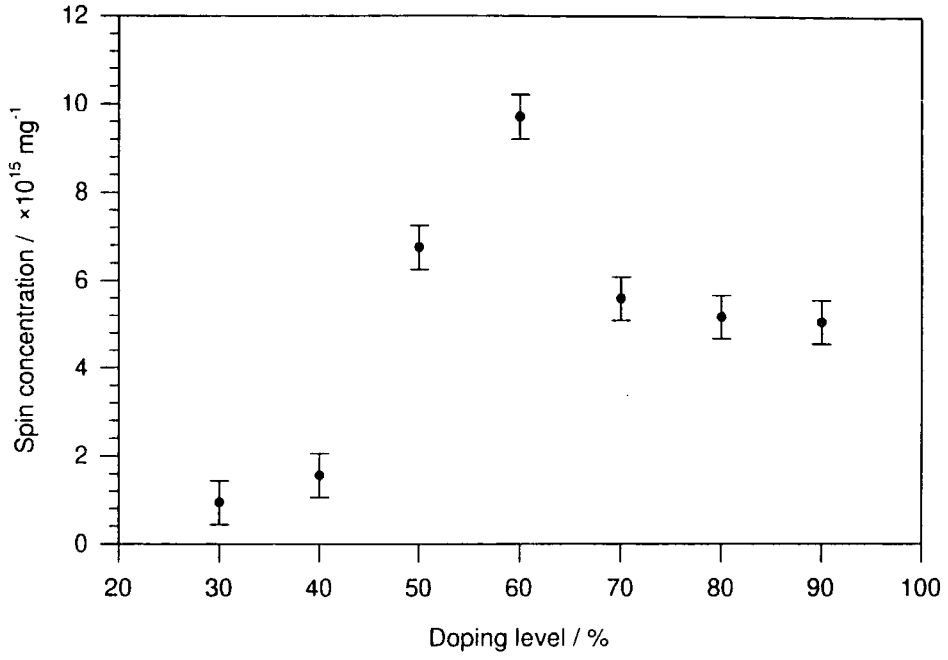

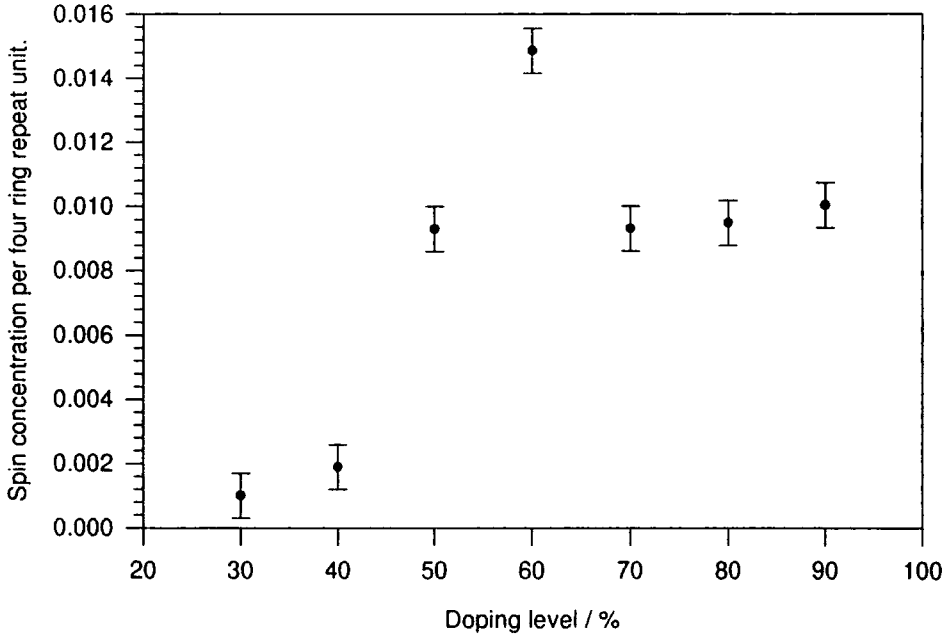

Top: Figure 3.6. Spin concentration per milligram of sample vs. doping level for PANi-CSA materials.

Bottom: Figure 3.7. Spin concentration per 4 ring repeat unit of polyaniline vs. doping level for CSA doped polyaniline.

be possible through analysis of the temperature dependence of the linewidth, since a motionally narrowed signal would be expected for mobile polarons, but not for the polaron lattice (see section 3.3.2).

The X-ray measurements of Abell *et al.* [21] have shown that there is a maximum in crystallinity for the 60% doped PANi-CSA materials. Addition of acid beyond this level, therefore, can be envisaged as reducing the fraction of metallic regions within the polymer. The spin concentration of the system is thus reduced if the polaron density in the crystalline regions is higher than that in the amorphous material. The formation of bipolarons at protonation levels greater than 60%, on the other hand, will lead to a reduction in the spin concentration due to the spinless nature of bipolarons (see chapter 1 section 1.5.2).

The linewidth as a function of doping (figure 3.8) shows a maximum between 50% and 60% doping. In the case of an imperfect crystal containing localised spin carriers, when a magnetic field is applied, each spin carrier will experience a field dependent on the crystallographic structure surrounding the spin. The resultant ESR line will be broadened as each spin carrier has a slightly different resonant frequency. If the spin carriers (in the same crystal) are delocalised, however, each will experience an average field and the Larmor frequencies will be very similar leading to a motionally narrowed lineshape.

The increase in linewidth with increasing doping (up to ~60%) suggests that the charge carriers are not mobile polarons since no motional narrowing is observed with doping. Above the 60% optimum (for conductivity) the decrease in linewidth can be attributed to the lowering of the overall crystallinity of the materials due to the presence of excess acid. This again assumes that polarons exist in the 3-D lattice. This linewidth analysis, however, is not conclusive as it is possible that mobile polarons would produce

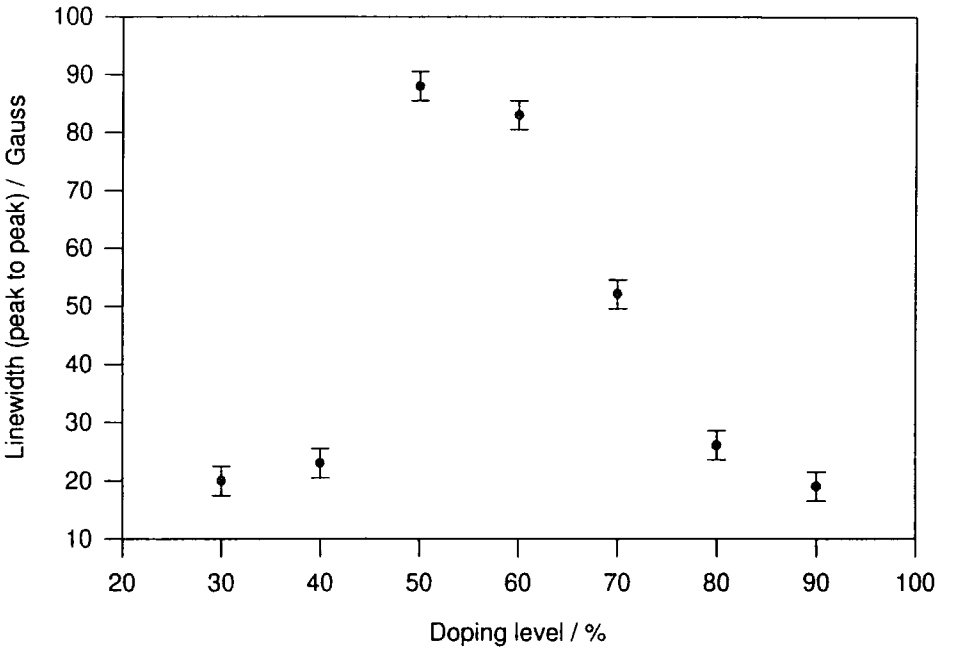

Figure 3.8. Linewidth as a function of doping for CSA doped PANi.

the same ESR spectra with respect to doping. Similar results to these have been observed in the ESR of doped polythiophene [22]. Schärli *et al.* [22] argue that the increase of line width with doping observed in polythiophene does not show that the spin carriers are localised. In terms of conducting polymers it is usually stressed that highly mobile spins (i.e., polarons) are expected to show narrow ESR signals due to motional narrowing. As a consequence, it has been suggested that linewidth is a direct measure of the quality of conducting polymers, i.e., the narrower the line the more perfect and longer are the polymer chains. Schärli suggests that these assumptions are only valid for broadening resulting from unresolved hyperfine splitting (due to spin carriers in different local environments). Metals in which conduction electron ESR spectra have been measured, however, usually have very large linewidths as a result of the rapid relaxation of the conduction electrons. Schärli [22] concludes that the ESR linewidth of conducting polymers is subject to two competing effects, motional narrowing and broadening due to fast relaxation. It is, therefore, difficult to draw any conclusions from the room temperature linewidth analysis.

3.3.2 TEMPERATURE DEPENDENT ESR MEASUREMENTS.

The temperature dependence of the spin concentration and linewidth were measured for the 30% and the 60% doped PANi-CSA samples. Figure 3.9 shows the first derivative ESR lineshapes with increasing temperature from 4K up to 296K. It is obvious from figure 3.9 that there is no great asymmetry in the ESR spectra of the

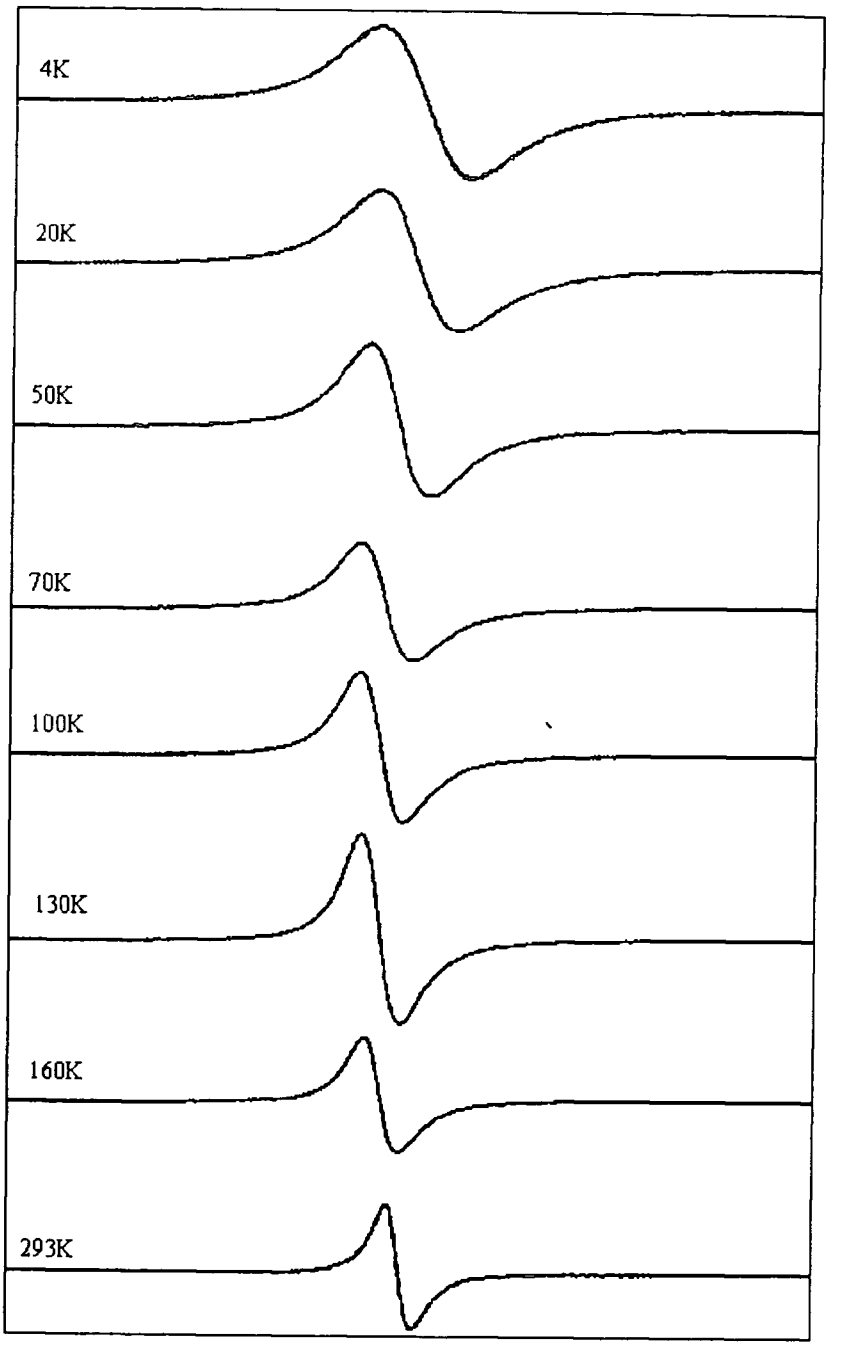

Figure 3.9. Temperature dependence of the first derivative ESR spectra of 60% doped PANi-CSA.

60% doped PANi-CSA at any temperature. There is, however, a discernible trend in which both the spin concentration and linewidth decrease with increasing temperature.

The normalised spin concentration as a function of temperature for both the 30% and 60% doped samples (given in figure 3.10) is normalised such that:

$$\text{Normalised spin concentration, } [S] = [S](T) / [S](300K) \qquad \text{eqn. 3.14}$$

where [S] = spin concentration. The linewidth (figure 3.11) is also normalised such that the linewidth at 300K = 1 for each sample.

It is apparent from figure 3.10 that the spin concentration of the 60% doped material is virtually independent of temperature, for temperatures greater than 20K at least. The 30% doped PANi-CSA, however, shows a strong dependence of the spin concentration with temperature, especially at temperatures less than 100K. This trend is also observed in the temperature dependence of the spin concentration in polythiophene, as measured by Schärli *et al.* [22]. Schärli points out that since the spin concentration is proportional to the magnetic susceptibility, χ, then the normalised spin concentration is equivalent to the normalised magnetic susceptibility, $\chi(T) / \chi(300K)$. Thus, there is a change from Curie susceptibility (1/T dependent) to Pauli susceptibility (temperature independent) with increasing doping (up to the optimum level of 60% doping giving maximum conductivity). Obviously, the temperature dependent ESR spectra of the other doping levels need to be investigated before this can be proved, but the fact that the data is in agreement with that of Schärli [22] is encouraging.

The temperature dependence of the linewidth, however, does not resemble that reported for polythiophene. Schärli *et al.* found that as doping was increased the

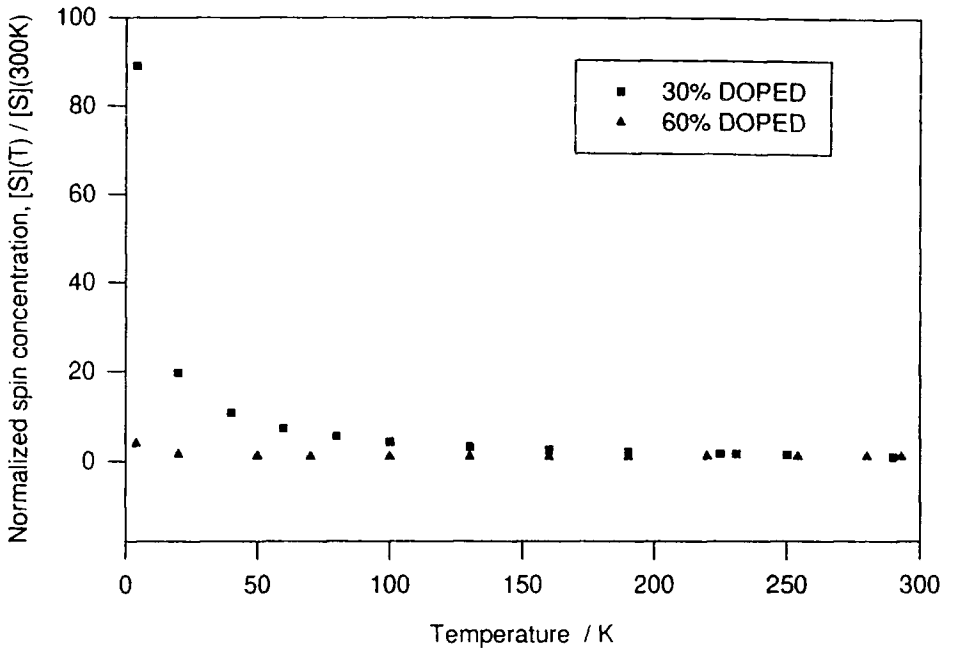

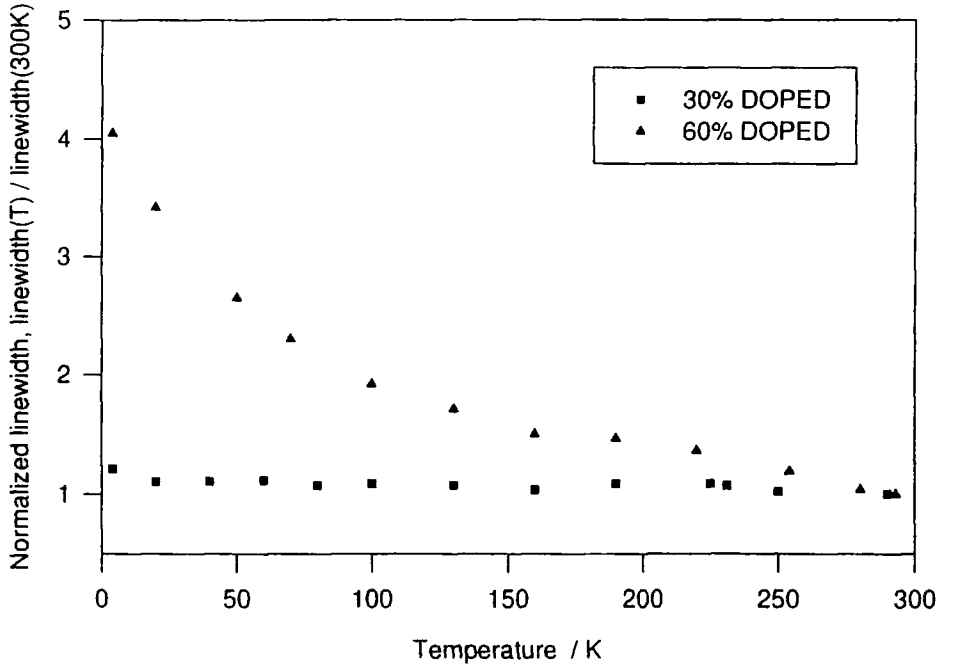

Top: Figure 3.10. Normalised spin concentration vs. temperature for doped PANi-CSA.

Bottom: Figure 3.11. Normalised linewidth as a function of temperature for doped PANi-CSA.

linewidth became proportional to temperature. Elliott [23] proposed that the ESR linewidth of a metal should become proportional to its resistivity, and hence Schärli concluded that the spin carriers probed by ESR in polythiophene were indeed metallic charge carriers. It can be seen from figure 3.11 that the temperature dependence of the ESR linewidth in the 30% doped material is almost temperature independent, whereas the (more conductive) 60% doped material has a linewidth that increases with decreasing temperature (almost as 1/T).

For the 60% doped PANi-CSA material it is apparent that there is some motional narrowing with increasing temperature, i.e., motion of the spin carriers is reduced at temperatures below 150K. This suggests that at least some (if not all) of the spin carriers observed by ESR are due to mobile spins (i.e., polarons) in the 60% doped material. The fact that this is not true for the 30% doped sample is indicative of there being few (if any) mobile spins within the material. It is proposed, therefore, that motional narrowing dominates the temperature dependent ESR signal of CSA doped PANi at the optimum 60% doping level as no line broadening (due to fast electron relaxation) with increasing temperature is observed (unlike polythiophene [22]).

3.4 CONCLUSIONS.

Early ESR measurements of polyaniline concentrated upon samples of pressed powder pellets, doped to different pH levels. It was found that there was a peak in spin concentration between pH values of 1 and -1 (see for example [9,24]). These results were supportive of the mobile polaron model as the maxima in the spin concentrations coincided with the maxima of the d.c. conductivities. Recently more in-depth studies have supported the theory that the polaron lattice model is a more likely explanation for both electrical and thermal conduction within the metallic clusters of heavily doped polyaniline (see for example [16]).

Other researchers ([13-15,25]), however, have presented data suggesting the presence of two charge carriers in doped polyaniline, i.e., both polarons and bipolarons. Kahol *et al.* [15] have studied the effects of moisture on HCl doped polyaniline powders using ESR spectrometry.

Kahol proposed a model where doped PANi consists of a highly ordered crystalline region at the core of the grain with a partially ordered layer forming the boundary between the metallic region and the amorphous material. Kahol's data shows that there is a decrease in the number of observable spins in the material that has been exposed to atmospheric moisture. Kahol attributes this to the conversion of polarons into bipolarons in the boundary layer due to the presence of atmospheric moisture and oxygen, thus concluding that an equilibrium between polarons and bipolarons exists.

The author, however, suggests that the presence of moisture and oxygen does not lead to the conversion of polarons into bipolarons within the partially ordered boundary

layer. It is instead proposed that a polaron may exhibit different properties in the metallic grains to one in the partially ordered region (i.e., polaron lattice within the metallic grains and partially delocalised (mobile) polarons in the partially crystalline layer surrounding the metallic grains). The presence of atmospheric moisture could alter the crystalline properties of the partially ordered layer, thus increasing the size of the polaron lattice and reducing the observed spin concentration. This theory, however, assumes that the spin carriers within the polaron lattice are truly metallic and hence have no observable ESR signal.

Other authors [13,16,25], however, have presented data supportive of Kahol's polaron-bipolaron equilibrium. Lux [25] proposes that Krinichnyi's [26] data is perhaps the strongest evidence for the presence of bipolarons in doped PANi powder samples. Lux states that the results of Krinichyi *et al.* show that below a pH value of ~1.5 the spin concentration is almost independent of pH, but the conductivity varies by a factor of more than 50 for different pH values (less than 1.5). There are, however, other explanations that differ with Lux's interpretation of the ESR data. The author suggests that the PANi-CSA data presented in this work shows the possibility of alternatives to Lux's bipolaron theory.

Lux [25] suggests that the variance in conductivity with pH can not simply be due to changes in mobility of polarons as the crystallographic structure is not expected to vary with doping. The X-ray diffraction experiments of Abell *et al.* [21], however, show that protonation level does have a great effect on the degree of crystallinity, for solution doped PANi at least. Hence, the assumption that doped powder samples of polyaniline do not exhibit crystallographic changes as a function of protonation is not necessarily valid.

Even if the crystallographic structure is very similar within the metallic regions of differently doped powder samples (with pH values of less than 1.5), it is possible that the nature of the amorphous material is greatly dependent upon the type of dopant and the presence or absence of moisture. It is widely accepted that the insulating (or semiconducting) barriers within doped polyaniline govern the overall conductivity. If the properties of the amorphous region (or the partially ordered region in Kahol's model) are pH or moisture dependent (as suggested by Kahol [15]) it is possible the conclusions about the formation of bipolarons suggested by Lux are incorrect. As no information was given about the experimental procedures used in the preparation of the materials studied by Krinichnyi *et al.* [26] it is difficult to interpret the results.

It is proposed that increased protonation leads to an increase in the size of a polaron lattice within the crystalline regions, up to the 60% doping limit. At low protonation levels the size of the metallic islands is small and hence the amorphous (barrier) regions govern conductivity. As protonation increases up to the optimum of 60%, the size of the metallic regions increases, as does the size of the partially ordered layer separating the metallic region from the amorphous layer. Further addition of acid (above 60% doping) leads to a reduction in the spin concentration as the acid does not protonate the polymer, hence no further polaronic species are created. The spin concentration is reduced due to the decreased crystallinity of the system as a result of the presence of excess acid (as supported by the X-ray crystallography of Abell *et al.* [21]).

This model, however, makes assumptions that may not be justifiable, firstly that a polaronic lattice forms the core of the metallic regions and that no ESR signal is observed from the metallic carriers within this region. Secondly, the observed ESR absorption is the sum of that from localised species in the amorphous polymer matrix,

and partially delocalised (mobile) polarons within the partially ordered region (Kahol's model). These assumptions are supported by the temperature dependent ESR measurements above, i.e., that only motional narrowing can be observed in the temperature dependence of the linewidth for the 60% doped material, not line broadening due to rapid electron relaxation. This is attributed to polarons in the partially ordered layer. The lack of temperature dependence in the linewidth of the 30% doped material indicates that the partially ordered region around the metallic islands is negligible at this doping level.

It is apparent that there is still controversy concerning the type of charge carriers present within doped PANi samples. The data presented above is believed to be the first ESR study of PANi-CSA materials. It is believed that the modified version of Kahol's model (above) can explain the observed ESR spectra and (possibly) other properties of PANi-CSA. The author is, however, reluctant to dismiss the polaron-bipolaron equilibrium model proposed by Lux without further investigation of the temperature dependent ESR of a full series of differentially doped PANi-CSA and PANi-AMPSA. Time constraints have (unfortunately) restricted the ESR investigation of solution doped polyanilines to that given above.

3.5 REFERENCES.

1. Zavoiski, E., Journal of Physics USSR, 1945. **9**: p. 211.
2. Bleany, B., Stevens, K.W.H., Reports of Progress in Physics, 1953. **16**: p. 108.
3. Bowers, K.D., Owen, J., Reports of Progress in Physics, 1955. **18**: p. 304.
4. Poole, C.P., *Electron Spin Resonance, A Comprehensive Treatise on Experimental Techniques*. Second ed. 1983, New York: Wiley-Interscience.
5. Atherton, N.M., *Principles of Electron Spin Resonance*. Physical Chemistry Series, ed. E. Horwood, Kemp, T.J. 1993, London: Ellis Horwood and Prentice Hall.
6. Wertz, J.E., Bolton, J.R., *Electron Spin Resonance, Elementary Theory and Practical Applications*. 1986, London: Chapman and Hall.
7. Mizoguchi, K., Macromolecular Chemistry, Macromolecular symposia, 1990. **37**: p. 53.
8. Nechtschein, M., Devereux, F., Genoud, F., Gugliemli, M. and Holczer, K., Physical Review B - Condensed Matter, 1983. **27**: p. 61.
9. Yoon, H., Jung, B. S., Lee, H., Synthetic Metals, 1991. **41**(1-2): p. 699-702.
10. Wan, M.X., Zhou, W. X., Li, Y. F., Liu, J. S., Solid State Communications, 1992. **81**(4): p. 313-316.
11. Mizoguchi, K., Nechtschein, M., Travers, J. P., Synthetic Metals, 1991. **41**(1-2): p. 113-116.
12. Mizoguchi, K., Kume, K., Solid State Communications, 1994. **89**(12): p. 971-975.
13. Raghunathan, A., Natarajan, T. S., Rangarajan, G., Dhawan, S. K., Trivedi, D. C., *Charge-Transport and Optical and Magnetic-Properties Of Polyaniline Synthesised With Use Of Organic-Acids*. Physical Review B-Condensed Matter, 1993. **47**(20): p. 13189-13196.
14. Genoud, F., Nechtschein, M., Santier, C., Synthetic Metals, 1993. **55**(1): p. 642-647.

15. Kahol, P.K., Dyakonov, A.J., McCormick, B.J., *An Electron-Spin-Resonance Study of Polyaniline and its Derivatives: Polymer Interactions with Moisture.* Synthetic Metals, 1997. **84**(1-3): p. 691-694.

16. Krinichnyi, V.I., *EPR and Charge Transport Studies of Polyaniline.* Physical Review B - Condensed Matter, 1997. **55**(24): p. 16233-16244.

17. Feyer, G.a.K., A.F., *Electron Spin Resonance Absorption in Metals. I. Experimental.* Physical Review, 1954. **98**: p. 337-348.

18. Dyson, F.J., *Electron Spin Resonance Absorption in Metals. II. Theory of Electron Diffusion and the Skin Effect.* Physical Review, 1954. **98**: p. 349-359.

19. Goldberg, I.B., Gowe, H.R., Newman, P.R., Heegar, A.J. and MacDiarmid, A.G., Journal of Chemical Physics, 1979. **70**: p. 1132.

20. Holland, E.R., Pomfret, S. J., Adams, P. N., Monkman, A. P., *Conductivity Studies Of Polyaniline Doped With CSA.* Journal Of Physics-Condensed Matter, 1996. **8**(17): p. 2991-3002.

21. Abell, L., Pomfret, S., Holland, E.R., Adams, P.N., Monkman, A.P. *Aspects of the Camphorsulphonic Acid Processing Route of Polyaniline.* in *Institute of the Plastic Engineers SPE/ANTEC.* 1996.

22. Schärli, M., Kiess, H. and Harbeke, G., *ESR of BF_4^- Doped Polythiophene.* Synthetic Metals, 1988. **22**: p. 317-336.

23. Elliott, R.J., Physical Review, 1954. **96**: p. 266.

24. Lux, F., Hinrichsen, G., Krinichnyi, V. I., Nazarova, I. B., Cheremisow, S. D., Pohl, M. M., *Conducting Islands Concept For Highly Conductive Polyaniline - Recent Results Of TEM-Measurements, X-Ray-Diffraction-Measurements, Epr-Measurements, Dc Conductivity-Measurements and Magnetic Susceptibility-Measurements.* Synthetic Metals, 1993. **55**(1): p. 347-352.

25. Lux, F., *Properties of electronically conductive polyaniline: a comparison between well-known literature data and some experimental findings.* Polymer, 1994. **35**: p. 2915 - 2926.

26. Krinichnyi, V.I., Roth, H.K., Lux, F., *Unpublished results.* 1993.

CHAPTER 4

CHAPTER 4

4. FARADAY ROTATION SPECTROSCOPY.

4.1 INTRODUCTION TO FARADAY ROTATION.

In 1846 Michael Faraday [1] discovered that the plane of plane-polarized light passing through a medium is rotated by the application of a magnetic field parallel to the propagation direction of the light. This discovery was heralded as "fundamental" by Zeeman in his book "Researches in Magneto-Optics" [2], which was dedicated to the memory of Michael Faraday. Over one hundred years after its initial discovery the "Faraday effect" was suggested as a method of characterizing the properties of inorganic semiconductors (see for example [3]). Recently Faraday rotation has been suggested as a non-destructive alternative to the Hall-Effect for the determination of carrier concentration and mobility at industrial level [4]. In this chapter the Faraday effect due to free carriers will be described with respect to both n-type and p-type semiconductors.

To understand how free carriers in a magnetic field alter the polarization plane of plane polarized light, it is useful to consider the polarized light as a sum of two circularly polarized waves, identical except for their electric wave vectors which rotate in opposite directions. The components of the two circularly polarized waves are:

$$F_x(t) = F_0\cos(\omega t); \qquad F_y(t) = F_0\sin(\omega t)$$

$$\text{and} \qquad F_x(t) = F_0\cos(\omega t); \qquad F_y(t) = -F_0\sin(\omega t) \qquad \text{eqn. 4.1}$$

where F_0 is a constant, ω is angular frequency and t is time (propagation along the z-axis). In a magnetic field (**B**) the motion of a free carrier (velocity **v**) is modified by the Lorentz force ($ev \times \mathbf{B}$) perpendicular to the field, [5] where e is the charge on the free carrier. Hence a free carrier moving with constant velocity describes a helical path about an axis parallel to **B** (motion in the direction of **B** is not affected, but the carrier describes a circle in the plane orthogonal to **B**). The orbital frequency of the carrier is thus:

$$\omega_c = e\mathbf{B}/m^* \qquad \text{eqn. 4.2}$$

where ω_c is the cyclotron frequency (by analogy with the orbits of charged particles in cyclotron accelerators) and m^* is the effective mass of the carrier. When plane polarized light propagates through a medium of free carriers in the Faraday orientation, (i.e. with the propagation direction parallel or anti-parallel to the applied magnetic field) one of the components of the polarized light has an electric vector rotating in the same direction as the circulating electrons. In the resonance case (when the angular frequency of the light $\omega = \omega_c$, the cyclotron frequency of the carriers) then the carriers will (classically) experience a force due to the circularly polarized component, thus increasing their radius of orbit. One of the circularly polarized components is, therefore,

attenuated by the circulating carriers, thus the light emerging from the medium has its' plane of polarization rotated by an angle θ.

To quantify the above illustration the motion of the carriers in the x and y directions are given in equations 4.3 and 4.4 below (for a field along the z-axis, such that the light propagation in equation 4.1 is parallel to **B**).

$$\frac{dv_x}{dt} + \frac{v_x}{\tau} = - \frac{e}{m^*} F_x(t) - \frac{ev_y B}{m^*} \qquad \text{eqn. 4.3}$$

$$\frac{dv_y}{dt} + \frac{v_y}{\tau} = - \frac{e}{m^*} F_y(t) - \frac{ev_x B}{m^*} \qquad \text{eqn. 4.4}$$

where τ is the mean free time between events causing scattering of the charge carriers. Elliott and Gibson [5] give the equations:

$$2n_0 k_0 = \frac{\sigma}{\omega \varepsilon_0} = \frac{\varepsilon_L}{\varepsilon_0}\left(\frac{\omega_p^2 \tau}{\omega}\right)\left(\frac{1}{1 + \tau^2(\omega \pm \omega_c)}\right) \qquad \text{eqn. 4.5}$$

$$n_0^2 - k_0^2 = \frac{\varepsilon_1}{\varepsilon_0} = \frac{\varepsilon_L}{\varepsilon_0}\left[1 - \left(\frac{\omega_p^2 \tau}{\omega}\right)\left(\frac{\omega \pm \omega_c}{1 + \tau^2(\omega \pm \omega_c)}\right)\right] \qquad \text{eqn. 4.6}$$

where n_0 and k_0 are the refractive index and extinction coefficient respectively. ε is the dielectric constant, where the subscripts 0, 1 and L refer to the free space permittivity, the real part of the dielectric constant due to free carriers (as opposed to the imaginary part) and the contribution to the dielectric constant by the lattice respectively. The ±

modifier preceding ω_c represents the two different circularly polarized components, conventionally the negative case refers to the component that rotates in the same sense as electrons in the field. The plasma frequency, ω_p, is representative of interactions between the charge carriers and is characteristic of the material. Elliott and Gibson [5] describe the plasma frequency in terms of a gas of "free" charged particles in a dielectric medium, a qualitative description follows.

Since the Coulomb interaction is very long range (with respect to a free electron gas in a metal, for example) a single particle is influenced by all the other particles, even those at long range. The coupling between the particles, therefore, allows collective motion and such a gas of charged particles interacting in this way is termed a plasma. The collective density fluctuations of the particles are called plasma oscillations, and the frequency is characteristic of the medium containing the particles. The plasma frequency can be obtained by consideration of the electric field created by the motion of the particles, and the force that this field exhibits on the charges. The force promotes motion of the plasma in the direction opposite to the motion creating the field, thus simple harmonic oscillations occur. For a mathematical description of the plasma frequency the reader is referred to the afore-mentioned text by Elliott and Gibson [5]. For this work, however, it will suffice to define the plasma frequency as:

$$\omega_p^2 = \frac{Ne^2}{\varepsilon m^*} \qquad \text{eqn. 4.7}$$

where N is the number of particles of charge e per unit volume (ε, e and m^* have the same meanings as before).

The contribution of free carriers to the dielectric constant of a material implies that (in the Faraday orientation) there are different effective refractive indices (and hence different phase velocities) for the different circularly polarized components of a plane wave propagating through the medium. The plane of polarization for electromagnetic radiation (of angular frequency ω) is thus rotated through an angle θ (in radians) given by[5]:

$$\theta = \frac{t\omega}{2c}\left(n_{0+} - n_{0-}\right) \qquad \text{eqn. 4.8}$$

where t is the thickness of the sample through which the light passed and c is the velocity of light. The different signs associated with the refractive indices, n_0, refer to the indices appropriate to the circularly polarized waves. To expand upon this equation certain conditions must be met, namely:

$$\omega\tau \gg 1, \qquad \omega > \omega_p, \qquad \omega > \omega_c. \qquad \text{eqn. 4.9}$$

These restraints ensure that k_0 is small compared to n_0 and thus $\left(n_0^2 - k_0^2\right) \approx n_0^2$ and that resonance effects around ω_p and ω_c can be ignored. Substitution of equation 4.9 into equations 4.5 and 4.6, and their subsequent insertion into equation 4.8 gives the Faraday rotation as [5]:

$$\theta = -t\left(\frac{\varepsilon_L}{\varepsilon_0}\right)^{1/2}\left(\frac{\omega_p^2\omega_c}{2c\omega^2}\right). \qquad \text{eqn. 4.10}$$

Replacing the cyclotron and plasma frequencies with equations 4.2 and 4.7 and using $\omega = 2\pi c/\lambda$, the Faraday rotation becomes:

$$\theta = -\left(\frac{1}{\varepsilon_L \varepsilon_0}\right)^{1/2}\left(\frac{t\lambda^2 N e^3 B}{8\pi^2 c^3 m^{*2}}\right) \qquad \text{eqn. 4.11}$$

where λ is the wavelength of the electromagnetic radiation. Perhaps a more useful definition of the angle through which the light is rotated is given by Moss, Burrell and Ellis [6] where the term $(1/\varepsilon_0\varepsilon_L)^{1/2}$ is replaced by $(1/\varepsilon_0 n)$ where n is the refractive index of the material, thus:

$$\theta = -\left(\frac{t\lambda^2 N e^3 B}{8\pi^2 c^3 \varepsilon_0 n m^{*2}}\right). \qquad \text{eqn. 4.12}$$

Inspection of equations 4.10 to 4.12 reveal the convention where θ is positive for a Faraday rotation due to negatively charged carriers (i.e. electrons) since e^3 is negative. It is obvious from equation 4.12 that measurement of θ will yield information about the nature of charge carriers in a given system, of particular note in this work is $\theta \propto N/m^{*2}$. For a material in which N can be determined (either experimentally or theoretically) the effective mass can be evaluated. The determination of m* is one of the major uses to which the Faraday effect has been used in semiconductor research.

A simpler way of defining the Faraday rotation of a material at a given wavelength is:

$$\theta = VBt \qquad \text{eqn. 4.13}$$

where V is the Verdet constant, derived from equation 4.12 as:

$$V = -\left(\frac{\lambda^2 N e^3}{8\pi^2 c^3 \varepsilon_0 n m^{*2}}\right). \qquad \text{eqn. 4.14}$$

It can be seen that $V \propto \lambda^2$ and measurements of θ over an extended spectral range show a λ^2 dependence for free carriers (see for example reference [6]).

Use of the Faraday effect at long wavelengths (such that $\omega^2\tau^2 \ll 1$) can give a direct measurement of carrier mobility, μ. An in depth mathematical derivation of this case is given by Rau and Caspari [7] with the result that:

$$\theta = \frac{\sigma\mu B}{2cn\varepsilon_0}. \qquad \text{eqn. 4.15}$$

It is obvious from equation 4.15 that carrier mobility can be measured easily by Faraday rotation on a material of known conductivity and refractive index. The condition $\omega^2\tau^2 \ll 1$ is met for inorganic semiconductors at microwave frequencies, hence this is not a simple "optical" measurement.

Another property exhibited by Faraday rotation measurements is to reveal information about the nature of electronic transitions in the sample. Comparisons between the spectral response of Faraday rotation and absorption of a given sample can

indicate the type of electronic states involved in the absorption. Marinelli *et al.* [8] report the Faraday rotation of yttrium iron garnet doped with silicon and cobalt. The data presented by Marinelli and co-workers show that the Faraday rotation of the sample is dispersive with respect to the absorption peak maximum at ~2.2μm. Marinelli [8] states that the dispersive nature of the Faraday rotation spectrum indicates that both the ground and excited states of the transition are singlets. An in-depth discussion of Faraday rotation as a tool to investigate the nature of optical transitions is given by Scott [9].

4.2 EXPERIMENTAL PROCEDURE.

Perhaps the simplest way to measure Faraday rotation is the extinction method. In this procedure a sample is placed between linear polarizers, the second polarizer is rotated such that the minimum intensity of light is transmitted through the system. The change in the measured angle of the second polarizer for a magnetic field applied parallel and anti-parallel to the light propagation direction is halved to give the Faraday rotation. This method has been used for visual measurements using polarizing microscopes. Paroli [10] has shown, however, that sensitivity is minimum around the extinction angle, and hence this method is not suitable for accurate determination of the Faraday rotation. It was shown by Paroli [10] that the sensitivity of a similar system is greatest for polarizers at 45° to each other; as such Marinelli *et al.* [8] suggested a "null-point" method to measure Faraday rotation over extended wavelengths. A modified version of Marinelli's experiment was designed and constructed as outlined below.

Figure 4.1 shows a schematic diagram of the system set-up to measure Faraday rotation in the visible and near IR range of the spectrum (wavelengths between 400nm and 1060nm). The equipment consists of a Bentham M300 monochromator with a Bentham PMC3B controller to monochromate the output from a Xenophot HLX tungsten filament bulb in a Bentham IL1 lamp housing. The power to the bulb was supplied by a Bentham 505 current stabilized filament lamp power supply. The monchromator also included two order sorting filters to remove second order diffracted light when working at wavelengths above 400nm and 750nm. The output

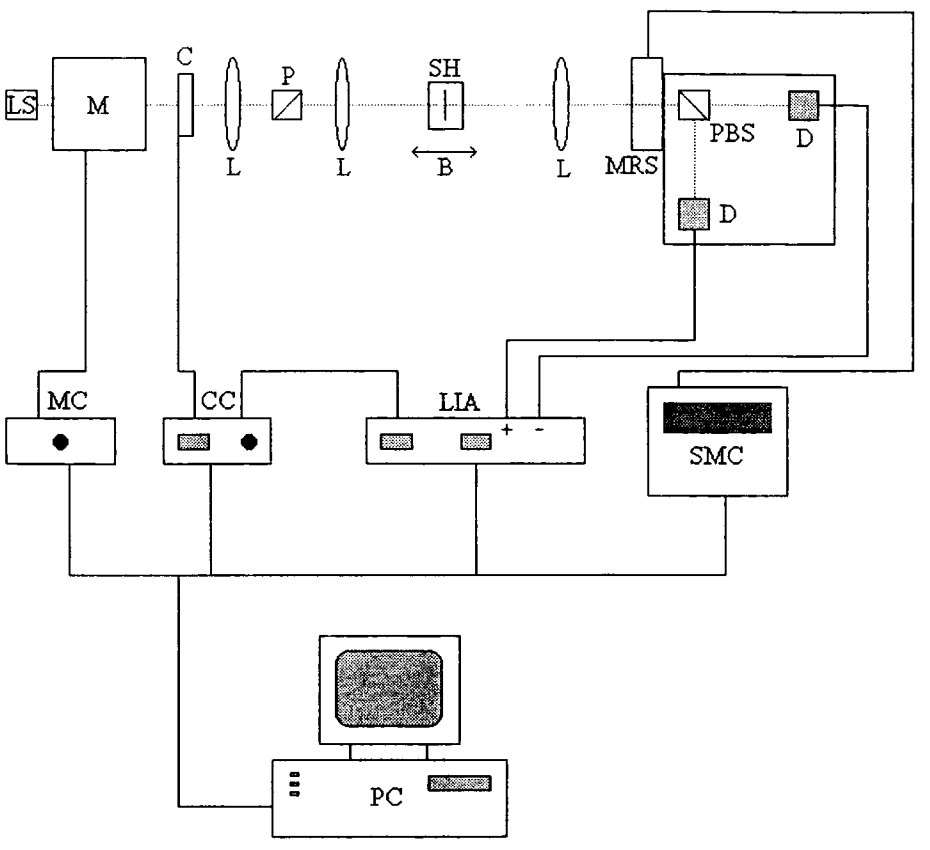

LS = Light Source, M = Monochromator, C = Chopper, L = Lens, P = Polarizer, SH = Sample Holder (fig. 4.2), B = magnetic field direction, MRS = Motorized Rotation Stage, PBS = Polarizing Beam Splitter, D = Detector, MC = Monochromator Controller, CC = Chopper Controller, LIA = Lock-In Amplifier, SMC = Stepper Motor Controller and PC = Personal Computer.

Figure 4.1. Schematic representation of the experimental set-up used to measure small angle Faraday Rotation.

from the monochromator was chopped at 173Hz by a Bentham 218 variable frequency optical chopper. This frequency was chosen as it gave the cleanest signal. The chopped, monochromatic output was focused by two glass lenses through a Glan-Thompson polarizer and into a specially designed mirror and sample housing (fig. 4.2).

The sample holder and associated mirrors were fixed between the pole pieces of a water cooled electro-magnet. A Glassman LV 60-18 d.c. power supply was used to power the magnet up to a maximum current of 18A, this corresponded to a maximum field of ~0.5 Tesla. The Glassman power supply was modified so that the polarity of the current (and hence the magnetic field) could be reversed simply.

The light emerging from the sample housing was focused by a third lens into a second Glan-Thompson polarizing beam-splitter. Two detectors (UV enhanced silicon photodiodes, Hamamatsu model S1337-1010BQ) were mounted on the escape paths for the two orthogonal components of light from the second Glan-Thompson polarizer. The circuitry and power supplies for the photodiodes were built especially for this application. The output from the detectors was fed to the inverting (B) and non-inverting (A) inputs of an EG&G 5210 lock-in amplifier, along with the reference frequency from the Bentham 218 optical chopper controller.

Consider the case where light passes through the first polarizer oriented such that the plane of polarization is vertical. The polarizing beam-splitter will thus be oriented at 45^{o} to the vertical to give A-B = 0 in the absence of a sample and magnetic field. To measure accurately the Faraday rotation of a given sample, the angle at which A-B = 0 is noted for parallel and anti-parallel field directions and the difference halved. This method of halving the angle for positive and negative field directions is

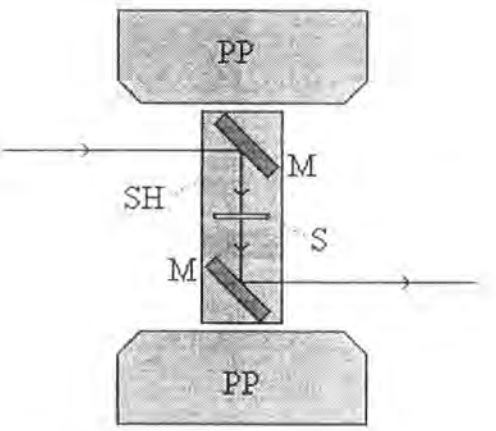

PP = magnet Pole Piece, M = aluminium Mirror, SH = Sample Housing and S = Sample.

Figure 4.2. Diagram showing the configuration of mirrors and sample within the sample housing. The sample housing was constructed from aluminium and the sample could be removed and replaced without altering the alignment of the mirrors.

the correct procedure for samples that have an associated birefringence. In the case of birefringent materials, light emergent from the sample is elliptically polarized not circularly polarized. It is the change in orientation of major axis of the ellipsoid that is defined as the Faraday rotation in this case. The above method, therefore, can be used on almost any sample that is transmissive in the range 400nm to 1060nm. The restriction to this range is due to the sensitivity of the photodiodes and the light transmitted through the monochromator.

The sensitivity of the above system is limited only by the precision at which the polarizer-detector mount can be rotated (theoretically at least). In the above system the polarizer-detector was mounted on a micrometer driven rotation stage. The micrometer was driven by a stepper-motor and gearbox controlled by a Bede Scientific Minicam IEEE/488 interface. Theoretically this system had a maximum resolution of 20660 steps per degree, i.e. 1 step $\approx 4.84\times10^{-5}$ degrees.

The monochromator controller and the lock-in amplifier had IEEE/488 interfaces and were linked to an IBM compatible 386PC, along with the Minicam stepper-motor controller. Programs were written in Turbo Pascal to control each individual unit, as well as a master program to run the experiment. Many revisions to the programming and the optical design of the experiment were made throughout this project. As is the case with many academic research experiments, the system was initially built using available equipment that was modified, supplemented and replaced over many months before the final system (above) was completed.

The final experiment was almost entirely computer controlled requiring only one input from the user after the experiment had been started (namely the reversal of the magnetic field polarity). The lock-in amplifier was set-up to read the magnitude and

phase of the signal in the A-B mode. The phase refers to which of A and B is the larger, for example if A » B the phase is 0^{o}, whereas for B » A the phase would be 180^{o}. The point where A = B gives a phase reading of 90^{o} from the lock-in amplifier. The phase reading of the lock-in amplifier is, effectively, a "flag" for the point when a given rotation of the detector mount changes A>B to B>A. Thus, the actual difference in voltage of A and B is useful only as a measure of the noise in the system. Noise was evaluated by taking multiple readings for a given position of the rotation stage and calculating the standard deviation from the mean. It is obvious that as A-B approaches zero, any noise associated with the experiment becomes more detrimental to the precision of the null-point determination.

The stepper-motor was always driven in the same direction to eliminate backlash errors. When a rotation of the stage in the opposite direction was needed, it was rotated well past the point of backlash and then forward to the requested setting. It was found that a great saving in experimental time could be achieved if the minimum rotation was set at 12 steps of the stepper motor. This also had the advantage that 12 steps were exactly equal to 0.03485 arcminutes of rotation.

The system (in its final form) could be programmed to locate the null-point (A-B=0) for a given wavelength, and repeat this for a series of wavelengths at a user defined interval. This null-point was, therefore, found for given points within the spectral range at a given (negative) field (e.g. -B). After completion of the negative field spectrum, the polarity of the magnetic field was changed (manually), and the same spectrum recorded for the opposite field (+B). The data was recorded as a text file and calculation of the Faraday rotation was done using standard spreadsheet and graph-plotting packages.

Samples were prepared from 60% doped PANi-CSA and 50% doped PANi-AMPSA solutions spun cast on 1mm thick, 12mm diameter synthetic (Spectrosil B) quartz discs (see Chapter 2 sections 2.1.2 and 2.2.1 for sample preparation techniques). The films were between 0.1μm and 1μm in thickness, allowing transmission of light over the entire spectral range of the Faraday rotation experiment. The system was calibrated using a clean quartz disc and the results were compared with literature values.

4.3 RESULTS AND DISCUSSION.

Research into the Faraday rotation of polyaniline was initiated in response to data reported by Yuan *et al.* [11] in 1995. The magnitude of the effect reported by Yuan was much larger than that observed in other magneto-optical materials, according to Yuan's publication. The above system was calibrated using a 1mm thick quartz sample, as mentioned earlier. It is apparent, however, that quartz does not contain free carriers, as such, the Verdet constant of quartz is not described by equation 4.14. Clarke [4] describes the Faraday rotation of a given sample as the sum rotation due to free and bound carriers:

$$\theta = a\lambda^{-2} + b\lambda^{2} \qquad \text{eqn. 4.16}$$

where a and b are rotation coefficients for bound and free carriers respectively. The Verdet constant for quartz, therefore, is proportional to $1/\lambda^2$.

The magnetic field intensity was calibrated using a Bell Gauss meter at the point where samples would be during an experiment. The field for a given coil current was thus measured as shown in figure 4.3. It is apparent that at a current of 18 amps there is some saturation and Joule heating of the magnet occurs. The variation in temperature of the magnet with differing coil currents created some initial problems. It was noticed that when there was no coil current, but the cooling water was running, moisture from the atmosphere condensed on the sample with obvious detrimental effects on the

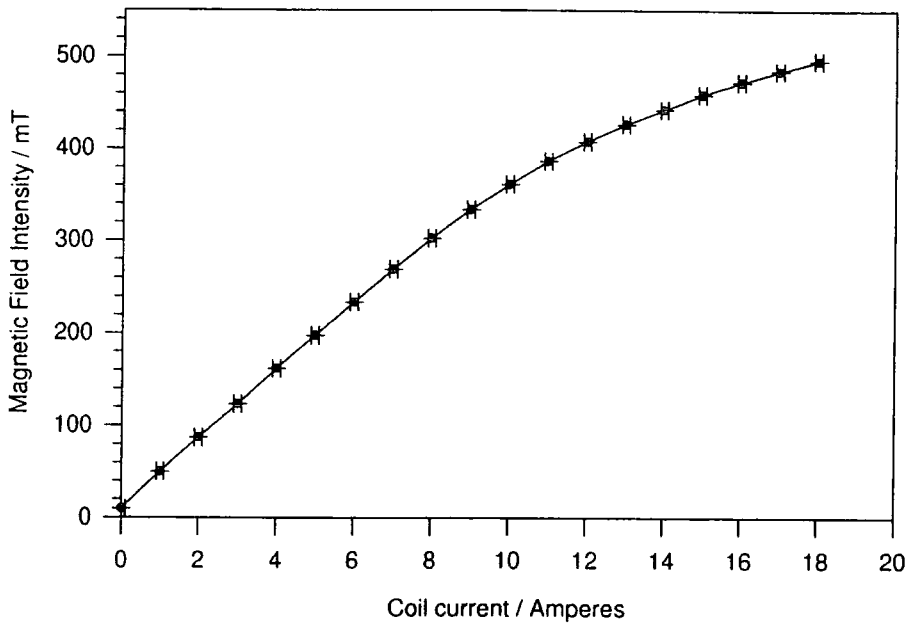

Figure 4.3. Calibration of magnetic field intensity vs. coil current.

measurement. The position of A-B=0 also exhibited some dependence on the magnitude of the current through the coils. The aluminium construction of the base plate fixing the sample housing to the base of the magnet was isolated as the root cause of these problems. It was found that the temperature of this base plate ranged from 15°C to 23°C for cooling water only and a coil current of 18amps respectively. This temperature variation created thermal expansion problems resulting in minute alterations of the alignment of the sample housing. The problem was resolved by manufacturing a polypropylene base plate to replace the aluminium one, thus insulating the sample housing from the temperature variations of the magnet. It should be noted that the magnet was always taken to saturation (18A) before being set to the desired coil current to reduce hysteresis effects.

Testing of the system was performed using the null-point location method described in section 4.2 (i.e., the point where the phase of the lock-in amplifier changes from <90° to >90°). The magnitude and phase of the signal from the lock-in amplifier (in A-B mode) as a function of detector rotation are shown in figures 4.4 and 4.5 respectively. It can be seen that the signal phase does indeed pass through 90° at the null-point and it is apparent that the system can be used to measure sub-arcminute rotations accurately.

After the final system had been tested such that there was reproducibility of the measurements made in the absence of a field, the Faraday rotation of a sample of Spectrosil B synthetic quartz was investigated. The field dependence of Faraday rotation in the sample at 436nm is shown in figure 4.6. The Verdet constant as a function of wavelength is shown in figures 4.7 and 4.8, along with the literature value for the Verdet constant of natural quartz at two wavelengths [12].

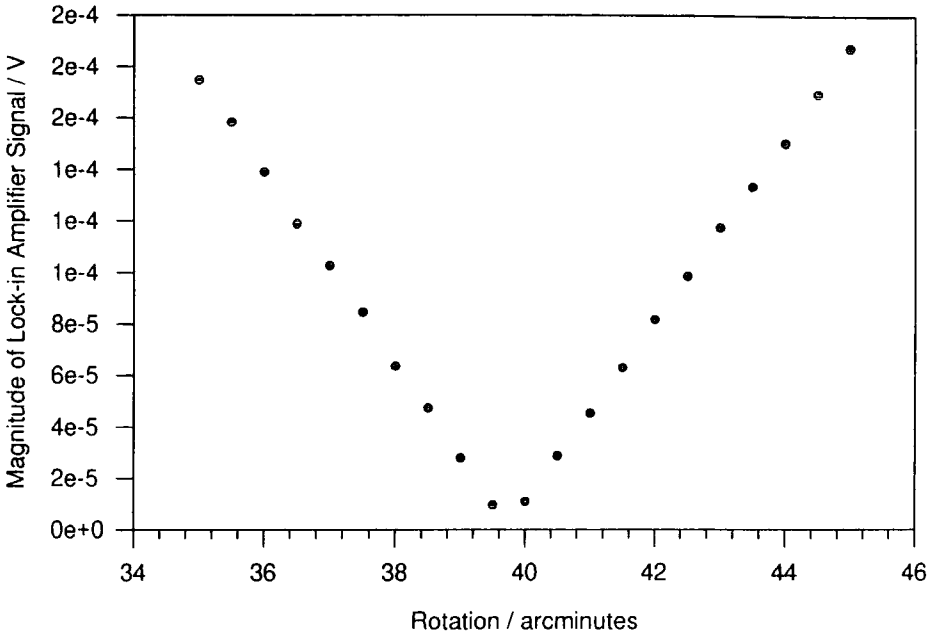

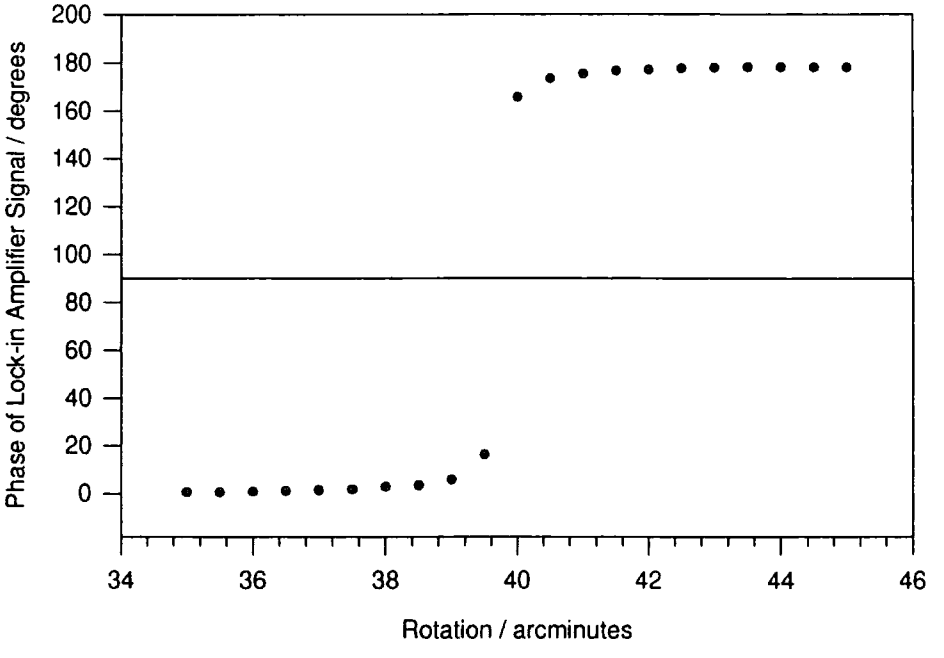

Top: Figure 4.4. Magnitude of the lock-in signal as a function of rotation for a quartz substrate at zero field.

Bottom: Figure 4.5. Phase of the lock-in signal as a function of rotation for a quartz substrate at zero field.

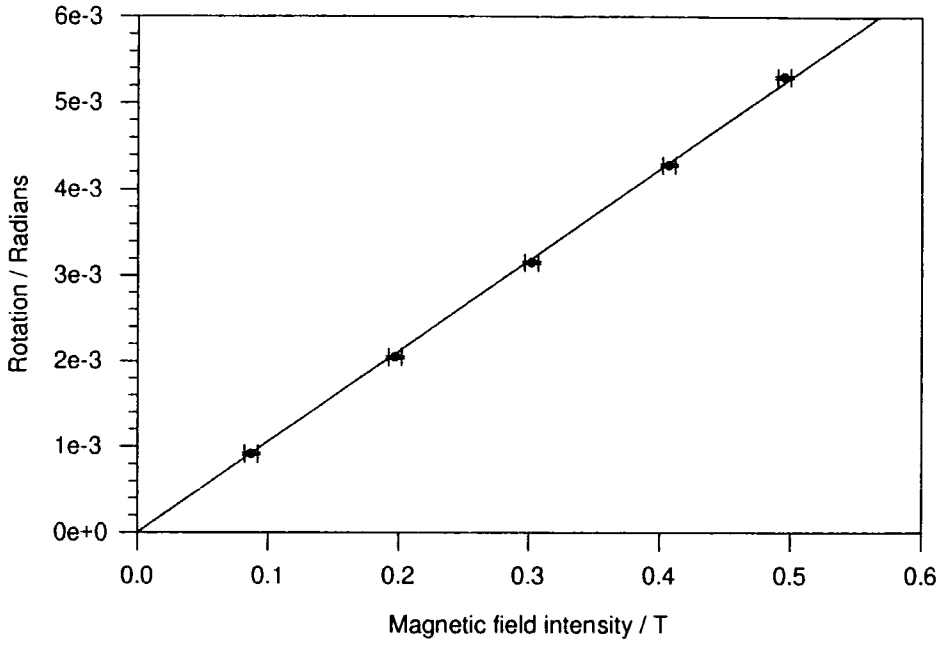

Figure 4.6. Faraday rotation of Spectrosil B quartz as a function of magnetic field at 436nm.

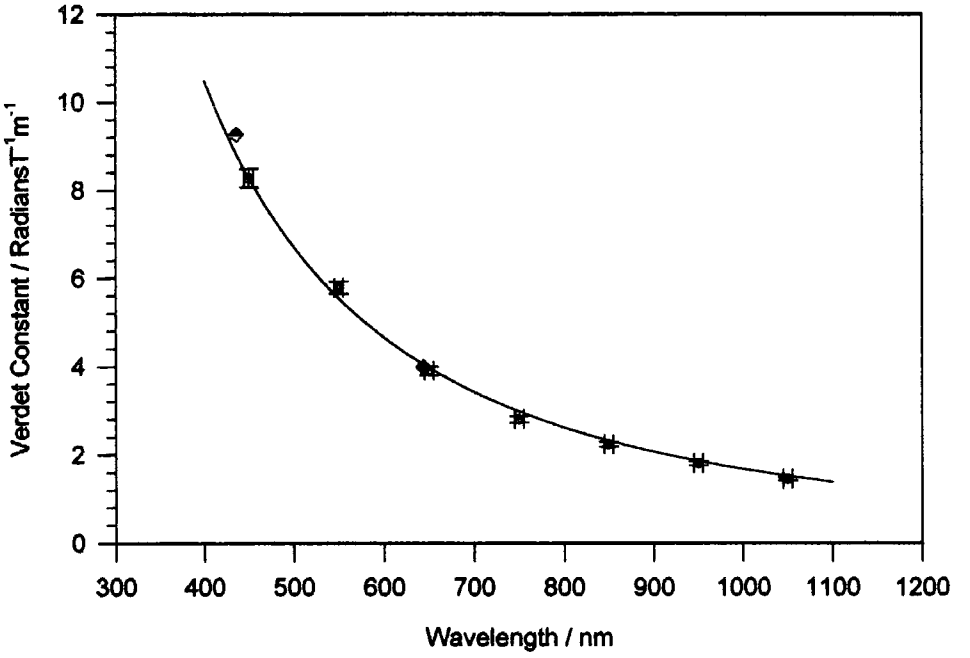

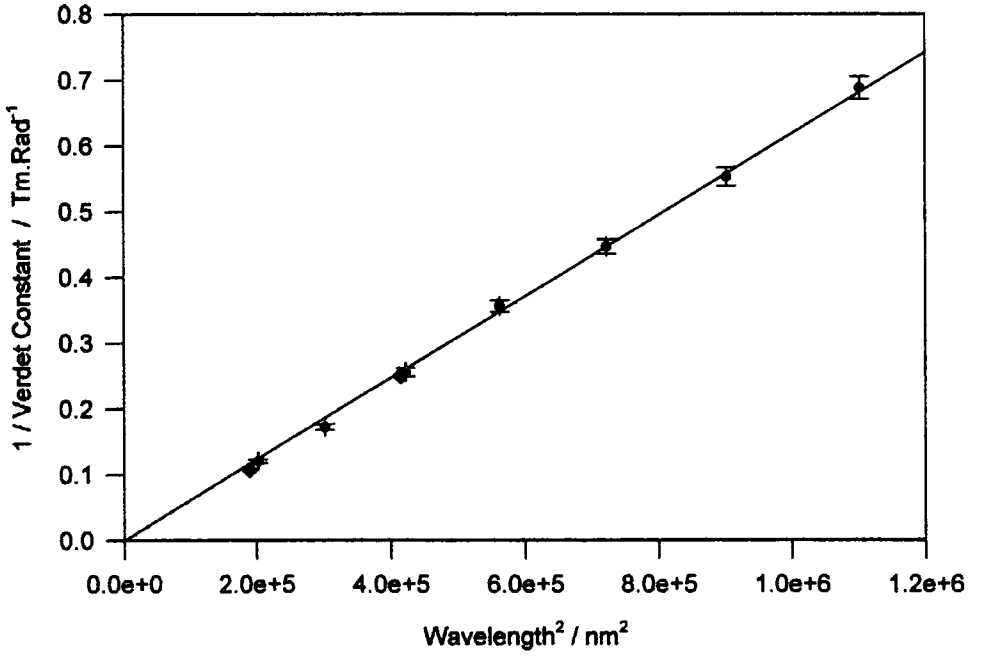

Top: Figure 4.7. Verdet constant as a function of wavelength for Spectrosil B quartz.

Bottom: Figure 4.8. $1/\lambda^2$ plot of figure 4.7. In both cases the diamond symbols represent literature values.

The $1/\lambda^2$ dependence of the Faraday rotation of quartz is easily observable in figures 4.7 and 4.8, thus indicating that the rotation is due entirely to bound carriers. A direct comparison between the experimentally determined and literature values for the Verdet constant of quartz is given in table 4.1, the experimental values are an extrapolation of the $1/\lambda^2$ fit to the data.

Wavelength / nm	Verdet Constant / rad/Tm (experimental)	Verdet Constant / rad/Tm (literature)
436	8.50	9.27
643.8	3.90	3.99

Table 4.1. Comparison of the experimentally measured Verdet constant of Spectrosil B quartz with the literature values for natural quartz.

Table 4.1 shows that the measured value of the Verdet constant for Spectrosil B quartz is slightly lower than the literature value for natural quartz. This difference is possibly due to the slight differences in the composition of the two materials. It is evident, however, that the equipment is sensitive enough to measure the Faraday rotation of quartz to within 10% of the literature values.

The Faraday rotation of polyaniline reported by Yuan *et al.* [11] is as large as 1×10^{-2} radians per nm for a field of 0.4T and a wavelength of 434nm, seven orders of magnitude larger than that of quartz. The measurement of Faraday rotation from a thin film of polyaniline deposited on a quartz substrate should, therefore, be simple using the above equipment. It was found, however, that the Faraday rotation of such a sample (<1μm thick doped PANi-CSA or PANi_AMPSA film on quartz) was almost indistinguishable from the Faraday rotation of the quartz substrate alone. Numerous experimental revisions performed on many different samples all showed the same result,

namely that the Faraday rotation of the quartz substrate was much greater than that due to the polyaniline. The author, therefore, disputes the claims of Yuan and co-workers. The data presented by Yuan *et al.* is probably translated from Chinese, however, and it is possible that a translation or transcription error has occurred. Yuan's publication is difficult to understand grammatically, supporting the possibility of a translation error in the work presented.

In this work it was found that the Faraday rotation of polyaniline was on the limit of detection for the above equipment. The Faraday rotation is proportional to the thickness of the sample, but due to the high absorption coefficient of polyaniline bulk films can not be measured by the above experiment. For thicker samples (~1μm in thickness) on quartz some effect could be measured due to the presence of a transmission window between 500 and 700nm. Outside this range the intensity of transmitted light became so small that noise inherent in the system made measurements impossible. Even within this transmission window reproducibility was low and interpretation of the results difficult.

Figure 4.9 shows the rotation as a function of wavelength for a 1.2μm thick sample in a 0.5T field. The results are fitted with a line representing the contribution to Faraday rotation from free and bound carriers. The fit is a modified version of equation 4.16 to account for the change in sign of the rotation, assuming that it arises from a zero-point (background subtraction) error and is not a true feature of the material. The equation of the fit to the data is given by:

$$\theta = (x + a\lambda^{-2}) + (x + b\lambda^{2}) \qquad \text{eqn. 4.17}$$

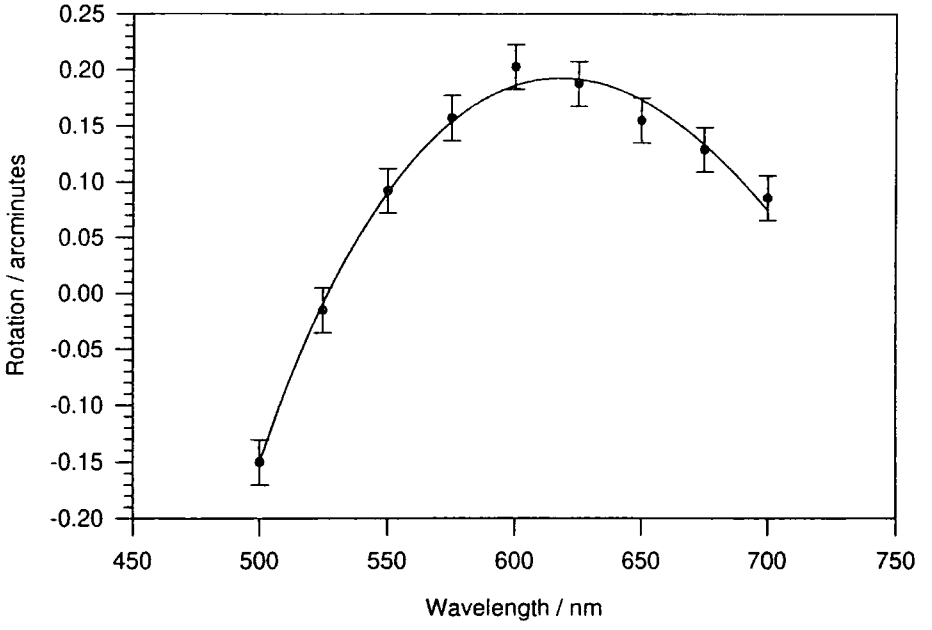

Figure 4.9. Preliminary Faraday rotation measurements from highly conductive polyaniline.

where x is a fitting constant and a and b have the same meaning as in equation 4.16. The author is doubtful as to the validity of this result due to its non-reproducibility and the large errors involved in trying to fit a model to so little data.

This preliminary result is, unfortunately, the only measurement of Faraday rotation in polyaniline that could be observed in the above experiment. If the trend in figure 4.9 is to be believed then the fact that the rotation is negative (assuming zero point error) supports the validity of positively charged carriers in polyaniline (see chapter 1 section 1.6).

The ratio of the effective mass of the charge carrier with the mass of an electron, m*/m, was calculated using the value of b from equation 4.17 as fitted to figure 4.7. Using equation 4.12 taking the value of N to be 4.8×10^{21} cm^{-3} from the calculations of Holland [13] for 60% doped PANi-CSA. The refractive index of polyaniline was taken as 2 (since it is probably between 1 and 3 intuitively) such that an estimate of m*/m could be made. From the calculations the value of m*/m was 800. In the author's opinion, it is therefore only possible to quote the result to the nearest order of magnitude, thus $m^*/m \approx 1\times10^3$. At first sight this is an alarmingly large value, but a publication by McCall and co-workers quotes a value of $m^*/m > 60$ [14]. It is, therefore, not unreasonable to take the value of $m^*/m = 1000$ as an upper limit, with a likely value being ~100.

To summarize, the major deductions that can be drawn from the Faraday rotation work present here are two-fold. Firstly, it has been shown that the data reported by Yuan *et al.* [11] cannot be reproduced. It is possible that Yuan and co-workers have measured Faraday rotation due to their substrate and not the deposited polyaniline film. This is supported by the fact that their films were synthesized electro-chemically onto a

transparent conducting substrate, most probably indium-tin-oxide (ITO) coated glass. Charge transport in ITO is via hole conduction, hence the Faraday rotation of ITO would be due to positive charge carriers, leading to a mis-interpretation of the results. Secondly, McCall *et al.* [14] cite ring rotation as the cause of the large charge carrier effective mass. Since the polaronic charge is bound to a configurational defect on the polymer backbone, the polymer must undergo significant conformational change as charge propagates along it. This implies that charge transport is mainly intra-chain and not due to a three dimensional polaron lattice. The author is reluctant to draw any conclusions from the measured value of m*/m due to the lack of reproducibility associated with this work. It is, however, obvious that further refinement of the experiment is needed to allow more accurate determinations of the Verdet constant and hence the effective mass of the charge carriers within doped polyaniline materials. It may then be possible to determine whether the 3-D polaronic model is an accurate description of charge transport or not.

Modification of the experiment to measure in the infra-red (assuming little absorption in that region) would lead to a greatly increased effect due to the λ^2 dependence of the Faraday rotation. This could be extended to a new experiment to measure the Faraday rotation at microwave frequencies where the low absorption coefficient of polyaniline in this region would allow measurements on thick polyaniline films, greatly increasing the ease of measurement. An increase in the sensitivity of the current system by using a high precision (worm-driven) rotation stage and higher intensity light (e.g. laser lines), combined with the use of a Wollaston polarizing beam-splitter may also lead to meaningful results. Time and monetary constraints, however, have not allowed the adaptation of the system to any of the above suggestions.

4.4 CONCLUSIONS.

Although the system designed and built to perform Faraday rotation spectroscopy was sensitive enough to measure (easily) a rotation of the magnitude reported by Yuan *et al.* [11], the results could not be reproduced. It is suggested that the signal measured by Yuan was due to the substrate (probably) ITO, in which holes are the majority charge carriers. The small amount of (non-reproducible) data obtained for the Faraday rotation of polyaniline supports McCall's [14] proposal that the effective mass of the charge carriers in polyaniline is at least 100 times the free electron mass. This leads to the conclusion that the observed charge carriers are not metallic, but partially localized polarons (or bipolarons). The formation of a polaron lattice, however, is not excluded by this theory, as long as the number of free carriers within the polaron lattice was many times smaller than the number of partially (and completely) localized polarons. This theory is supported by Kohlman *et al.* [15] who have suggested that as few as one in a thousand charge carrying species are responsible for the majority of charge transport in polyaniline. If this is the case, it is possible that the component of Faraday rotation due to free carriers may be very difficult to detect, (i.e., the localized charge carriers dominate the signal). This is especially true for the Faraday rotation measurements reported here where there is a significant contribution to the rotation from bound carriers. Faraday rotation experiments at microwave frequencies may provide a different value of m* since free carrier Faraday rotation is expected to dominate at longer wavelengths.

4.5 REFERENCES.

1. Faraday, M., *Experimental Researches.* Philosophical Transactions, 1846. **3**: p. 1.
2. Zeeman, P., *Researches in Magneto-Optics.* Macmillan's Science Monographs. 1913, London: Macmillan and Co.
3. Smith, S.D., Moss, T.S., Taylor, K.W., Journal of the Physical Chemistry of Solids, 1959. **11**: p. 131.
4. Clarke, F.W., *Nondestructive Determination of free-electron concentration and mobility in Hg(1-x)Cd(x)Te, n-type InSb and n-type GaAs.* Journal of Applied Physics, 1994. **79**(9): p. 4319-4326.
5. Elliott, R.J., Gibson, R.F., *Solid State Physics and its Applications.* Nature-Macmillan Physics Series. 1976, London: The Macmillan Press Ltd.
6. Moss, T.S., Burrell, G.J., Ellis, B., *Semiconductor Opto-Electronics.* 1973, London: Butterworth & Co.
7. Rau, R.R., Caspari, M.E., Physical Review, 1955. **100**: p. 632.
8. Marinelli, M., Milani, E., Paroli, P., *Measuring Faraday Rotation Over Extended Wavelength Ranges: A Simple Method.* Applied Optics, 1988. **27**(21): p. 4360.
9. Scott, G.B., *The Optical Absorption and Magneto-Optical Spectra of YIG*, in *Physics of Magnetic Garnets*, A. Paoletti, Editor. 1978, North-Holland: Amsterdam. p. 445.

10. Paroli, P., *An Introduction to Magneto-Optics*, in *Magnetic Properties of Matter*, F. Borsa, Tognetti, V., Editor. 1988, World Scientific: Singapore.

11. Yuan, R.K., Wu, W., Wang, Y.B., Qin, H., Wang, G.Q., *A New Type of Magneto-Optical Material and Device.* Synthetic Metals, 1995. **69**: p. 275-276.

12. *International Critical Tables of Numerical Data, Physics, Chemistry and Technology.*, ed. E.W. Washburn. 1926-33, New York: McGraw-Hill.

13. Holland, E.R., *Transport Properties in Electrically Conductive Polymeric Materials*, in *Physics*. 1995, University of Durham: Durham. p. 156.

14. McCall, R.P., Ginder, J.M., Leng, J.M., Ye, H.J., Manohar, S.K., Masters, J.G., Asturias, G.E., MacDiarmid, A.G. and Epstein, A.J., *Spectroscopy and Defect States in Polyaniline.* Physical Review B - Condensed Matter, 1990. **41**: p. 5202-5213.

15. Kohlman, R.S., Tanner, D. B., Ihas, G. G., Min, Y. G., MacDiarmid, A. G., Epstein, A. J., *Inhomogeneous insulator-metal transition in conducting polymers.* Synthetic Metals, 1997. **84**(1-3): p. 709-714.

CHAPTER 5

CHAPTER 5

5. INVESTIGATIONS INTO A POSSIBLE MAGNETIC DERIVATIVE OF POLYANILINE.

5.1 AN INTRODUCTION TO ORGANIC MAGNETIC MATERIALS.

Scientific insight and the discovery of new phenomena are driving forces in the search for molecular, organic, metallo-organic and polymeric magnets, in much the same way as conducting polymers. These materials undoubtedly have great technological applications for new and improved electrical, electronic and magnetic devices. The applications (for polymeric magnetic materials) [1,2] include magnetic and magneto-optic recording, as well as "soft" magnet applications. The major requirements of materials to complement (or even replace) conventional atomic-based magnetic materials are chemical stability and a paramagnetic-ferromagnetic transition temperature, T_c, above 300K (preferably closer to 400K). The anticipated properties of molecular/polymeric magnetic materials include transparency, solubility, and insulating behaviour, and are a direct result of the non-metallic nature of these materials [1-3].

Bulk magnets are sold on an energy density basis. Thus, even though the saturation magnetisation of the molecular/polymeric materials may exceed that of conventional magnets on a mole basis, their inherent low densities (and high molecular weights) indicate that their energy densities are unlikely to compare favourably to existing materials (e.g. $SmCo_5$ and $Nd_2Fe_{14}B$). Hence, unless an unusual niche can be

found, it seems unlikely that molecular/polymeric based magnets will have many bulk-magnetic applications.

The high permeability to mass ratio of molecular/polymeric materials makes them likely candidates to the class of soft magnetic materials (i.e., materials having a low coercive field). Applications of soft magnets include transformers, generators and motors, as well as d.c. and low frequency magnetic shielding. The major advantage of molecular/polymeric materials in this field would be their low density and hence light weight devices could be formed.

Conventional atom-based magnets have un-paired d- or f-orbital electrons creating spin sites with extended network bonding in two or three dimensions, hence they contain transition metal or lanthanide atoms. In recent years research into the preparation of a p-orbital based magnet has intensified [4,5], mainly as a result of the increasing number of optical and electrical properties exhibited by organic materials. As discussed in this work previously, one of the most prominent polymers with interesting electrical properties is polyaniline. Dervatives of polyaniline have, therefore, been investigated as candidates for magnetic materials [6-9]. Molecular/polymeric magnetic materials would enable "tuning" of the materials properties via conventional organic chemistry, along with the obvious benefits of simple fabrication and processing associated with molecular and polymeric materials (analogous to conducting polymers).

It is necessary to achieve long range ordering of spins in at least two dimensions to produce a ferromagnetic material, thus it is debatable whether an organic ferromagnetic (or even ferrimagnetic) polymer is theoretically plausible. In recent years, however, there have been increasing numbers of reports about magnetic organic polymeric materials and there are many groups world-wide which are actively

researching this area. There have also been reports of the ferromagnetic properties of biological polymers (e.g. DNA), although the magnetic behaviour in some of these bio-polymers was attributed to colloidal ferrites being present [10].

The first published paper reporting ferromagnetic behaviour in an organic polymer was released by a Soviet group (Ovchinnikov *et al.* [11]) in 1986, here a conjugated polymer with radical pendant groups was synthesised. This group attempted to polymerise the monomer 4,4-(butadiyne-1,4-diyl)-bis(2,2,6,6-tetramethyl-4-hydroxypiperidin-1-oxyl), **A** (figure 5.1). The synthesis gave a black material in which "...only an insignificant fraction of the crystallites have ferromagnetic properties." The ferromagnetic transition temperature was reported to be 440 ± 20K. Several focussed attempts to reproduce these results, however, have failed [12-14]. It is also unlikely that polymerisation of this molecule would lead to a ferromagnetic material as the spins of the two unpaired electrons in the monomer do not magnetically couple [14].

Post 1986 there have been numerous claims of magnetic responses from both organic and metallo-organic materials. These reports, in the main, have been unsubstantiated and often concerned materials of ill-defined composition and low magnetic yields [15]. The fact that the vast majority of these materials had a low saturation magnetisation raised questions about the origin of the magnetic behaviour, i.e. whether the magnetic response is due to extrinsic ferromagnetic impurities (such as Fe, Ni, Co, etc.) being present. In some cases extrinsic sources of ferromagnetic material had been introduced by mechano-chemical processes used to homogenise the material [16] (i.e., grinding in an iron mill). The researcher is thus obliged to provide a persuasive argument for the intrinsic origin of the low saturation magnetisation, often as the suggestion that the magnetic fraction of the material is only a small fraction of the bulk. When these claims were re-investigated it was often the case that extrinsic

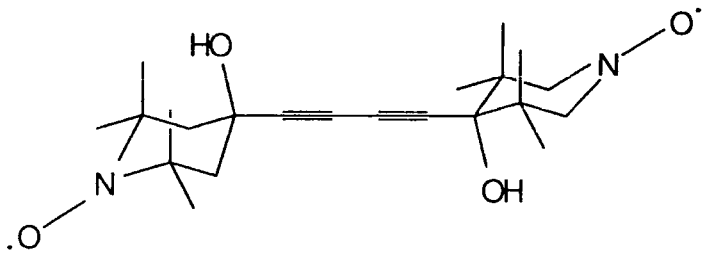

A

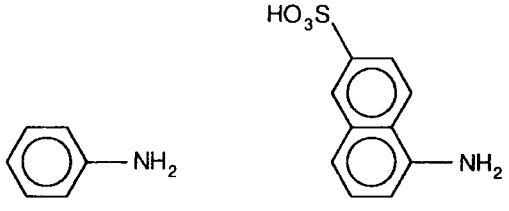

B **C**

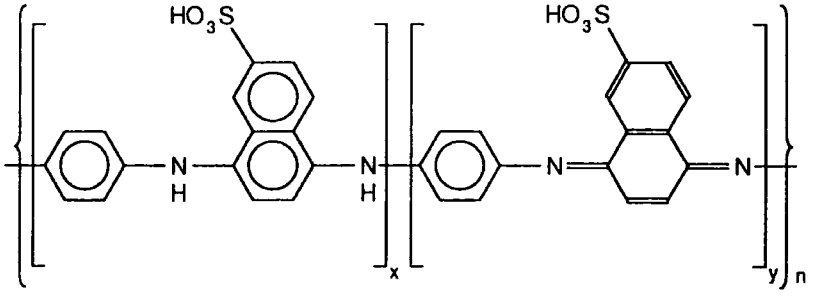

D

Figure 5.1. **A** = 4,4-(butadiyne-1,4-diyl)-bis(2,2,6,6-tetramethyl-4-hydroxypiperidin-1-oxyl), **B** = aniline, **C** = 5-amino-2-naphthalenesulphonic acid (ANSA), **D** = The Marcoussis polymer where case x=y=0.5.

sources of magnetic material are found. In cases where no extrinsic sources have been identified, verification of the magnetic behaviour has not been reported by independent laboratories. Hence, there has been no report, to date, of a polymeric material exhibiting ferro- (or even ferri-) magnetic behaviour that has been independently substantiated.

A recently released patent [17] and subsequent pre-print (from 1993 and still unpublished) by Galaj and Le Méhauté *et al.* [18], claims to have produced an entirely organic ferromagnet with a T_c above 300K. The oxidative copolymerisation of aniline, **B** (figure 5.1), and 5-amino-2-naphthalenesulphonic acid, (ANSA) **C** (figure 5.1), apparently gives an alternate copolymer which they have named the "Marcoussis" polymer, **D** (figure 5.1). This "polymer" is produced via an oxidative chemical reaction, in much the same way as polyaniline [19,20]. An investigation of this synthetic route is given here, along with a route used to prepare the monomer of the "Marcoussis polymer," and subsequent characterisation.

The Marcoussis polymer is claimed to be an alternate copolymer, produced by the oxidation of a 1:1 molar ratio of aqueous aniline and ANSA by potassium iodate. The copolymer fraction that is rich in naphthalenesulphonic acid groups is then extracted from the aniline rich chains by dissolution in aqueous ammonia and filtration. This allegedly gives a filtrate from which ferromagnetic blue crystals can be extracted by simple re-crystallisation. This process in itself is questionable as the ammonium salt, **E** (figure 5.2), of the Marcoussis polymer would be formed and it is the acid form, **D** (figure 5.1), which is reported to have ferromagnetic properties. It should be noted, however, that the synthetic route specified is given in patent form [17], hence it is more than likely to be written in such a way as to reduce the possibility of other researchers

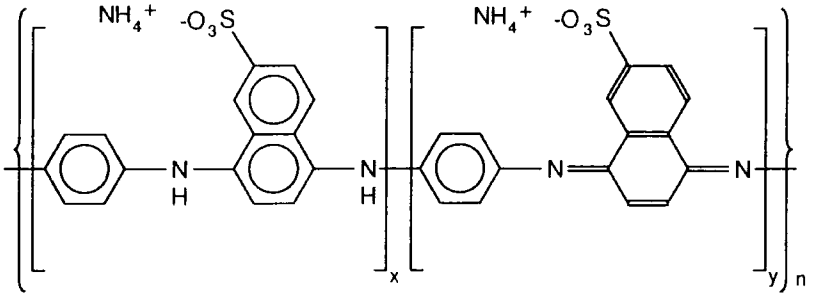

E

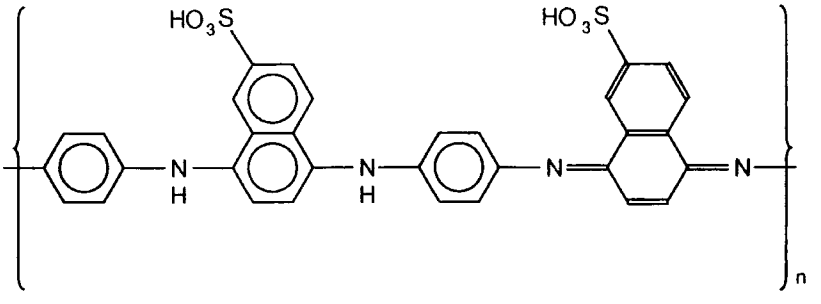

F

Figure 5.2. **E** = ammonium salt of the Marcoussis polymer, **F** = semi-oxidised (emeraldine) form of the Marcoussis polymer.

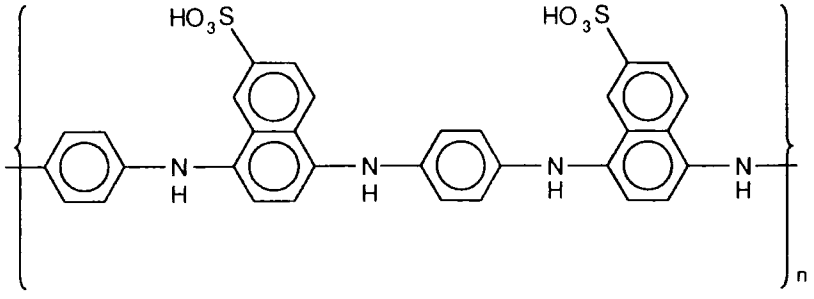

G

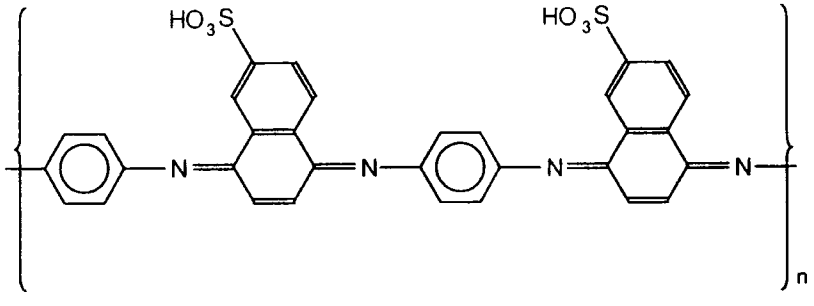

H

Figure 5.3. **G** = fully reduced (leuco-emeraldine) form of the Marcoussis polymer, **H** = fully oxidised (pernigraniline) form of the Marcoussis polymer.

making further advances than those who originally synthesised the polymer.

The report suggests that it is the semi-oxidised or "emeraldine" analogue, **F** (figure 5.2), of the Marcoussis polymer that exhibits ferromagnetism. The oxidation state of the polymer is, therefore, important in respect to the fully reduced (leuco-emeraldine) and fully oxidised (pernigraniline) analogues of the Marcoussis polymer, **G** and **H** (figure 5.3) respectively. The pre-print [18] goes on to suggest that "spiroconjugation" [21] may be present and account for the properties of the "...folded zwitterionic structure..." [18] that is suggested for the Marcoussis polymer. Spiroconjugation is intra-chain conjugation between atoms at different sites on a long chain or polymeric molecule [21]. This is most commonly displayed by helical molecules, hence the term spiroconjugation. Spiroconjugation is, however, an unlikely source of ferromagnetic properties since it would lead to delocalised spins. Hydrogen bonding between the sulphonate group and hydrogen atoms bonded to the nitrogen heteroatom may lead to a "trapping" of the spin carrier at the nitrogen site. Thus, the Marcoussis polymer could be considered as self-protonating and self-trapping the created spin carriers. This structure must also have long-range ordering of the trapped spins if a ferromagnetic material is to be produced.

5.2 EXPERIMENTAL PROCEDURES AND OBSERVATIONS.

5.2.1 ATTEMPTS TO COPOLYMERISE ANILINE AND AMINO-NAPHTHALENESULPHONIC ACID.

100ml of water were added to a 500ml beaker, to which 10g of 5-amino-2-naphthalenesulphonic acid, (ANSA), 4.2g of aniline, and 20ml of 96% sulphuric acid were added. This was stirred at room temperature to dissolve the "aniline sulphate" that formed upon the addition of the sulphuric acid. After half an hour the mixture consisted of purple suspension of ANSA in a pale pink solution (presumably dissolved ANSA). A second solution consisting of 7.25g potassium iodate in 180ml water, contained in a 250ml beaker, was prepared (dissolution of the potassium iodate took approximately 20 minutes). Over a 24 hour period the potassium iodate solution was added drop-wise to the solution in the 500ml beaker, this was achieved using a peristaltic pump (at a pump rate of approximately 8g per hour).

After the addition of the oxidant the reaction mixture took the form of a black precipitate in a red/brown solution. The suspension was filtered and the residue was washed using a small amount of water and dried in a vacuum desiccator. This yielded about 8g of a fine black powder.

Attempts to extract blue crystals from the black powder by dissolution of the black powder in ammonia, filtration, and re crystallisation of the filtrate (as explained in section 5.1 [17]) proved unsuccessful as the black powder was completely soluble in ammonia solution. Attempts to extract the acid form of the Marcoussis polymer via

acidification of the filtrate containing the ammonium salt, using an excess of 1 molar HCl, also failed to yield blue crystals.

Other similar reactions using different acids and oxidising agents were performed and are detialed in table 5.1 (below).

	Reaction	Result
1	5g 8-amino-2-naphthalenesulphonic acid, 2.1g aniline, 10ml sulphuric acid (96%) and 50ml water. After mixing the above solution for 1 hour, 3.63g of potassium iodate in 90ml of water were added dropwise over a 12 hour period. Collection of Product: The residue from this reaction was collected using a scintered glass filter. This residue was then dissolved in ammonia solution (30%) and filtered again. The filtrate was evaporated to dryness in a vaccuum oven (60°C).	The product from this reaction was determined to be unreacted amino-naphthalenesulphonic acid from FTIR spectroscopy. No desireable Product.
2	10g 5-amino-2-naphthalenesulphonic acid, 4.2g aniline, 100ml hydrochloric acid (10%). After mixing the above solution for 1 hour, 7.25g of potassium iodate in 180ml of water were added dropwise over a 12 hour period. Collection of Product: As above.	As above. No desireable Product.
3	10g 8-amino-2-naphthalenesulphonic acid, 4.2g aniline, 100ml hydrochloric acid (10%). After mixing the above solution for 1 hour, 7.25g of potassium iodate in 180ml of water were added dropwise over a 12 hour period. Collection of Product: As above.	As above. No desireable Product.
4	5.58g 5-amino-2-naphthalenesulphonic acid, 3.24g aniline hydrochloride, 21ml hydrochloric acid (12 Molar) and 75ml water. After mixing the above solution for 3 hours, 14.26g of ammonium persulphate in 40ml of water were added dropwise over a 24 hour period. Collection of Product: As above.	As above. No desireable Product.
5	5.58g 8-amino-2-naphthalenesulphonic acid, 3.24g aniline hydrochloride, 21ml hydrochloric acid (12 Molar) and 75ml water. After mixing the above solution for 3 hours, 14.26g of ammonium persulphate in 40ml of water were added dropwise over a 24 hour period. Collection of Product: As above.	As above. No desireable Product.

Table 5.1. Attempts to copolymerise aniline and amino-naphthalenesulphonic acid.

As it became apparent that the procedure given above [17] was not producing the Marcoussis polymer, oxidative polymerisations of simpler molecules were performed to try and devise a more successful synthetic route.

5.2.2 POLYMERISATION OF 1-AMINO-NAPHTHALENE.

5.2.2.1 USING THE STANDARD POLYANILINE REACTION.

Polymerisation of α-napthylamine, **J** (figure 5.4), to give a polymeric structure similar to polyaniline [19,20,22], (polynapthylamine, PNA, **K** figure 5.4), was attempted using the standard reaction used for polyaniline, as given below.

3.58g naphthylamine were added to 40ml of water which contained 2.5g of 12 molar hydrochloric acid. This suspension was stirred whilst a solution of 7.13g of ammonium persulphate in 20ml of water was added drop-wise over one hour using a tap funnel. Upon addition of the oxidant the solution turned from a lilac suspension to a dark blue suspension. After 24 hours the precipitate was filtered off, and washed in ammonia solution, this gave a purple/black powder after being dried under dynamic vacuum.

A large fraction of this powder was soluble in acetone, and suggests that the powder contains some very low molecular weight material, but is mainly unreacted α-naphthylamine.

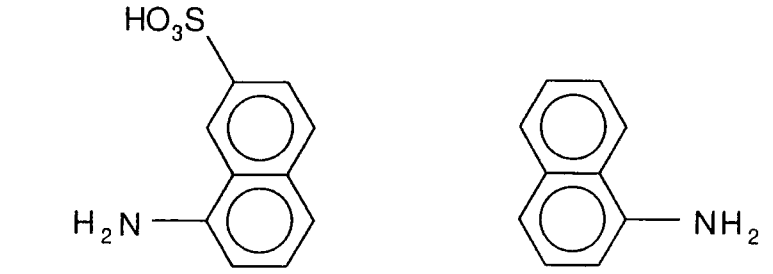

I J

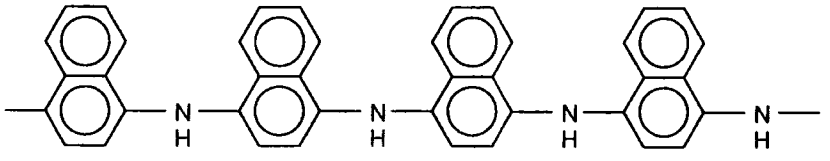

K

Figure 5.4. **I** = 8-amino-2-naphthalensulphonic acid, **J** = α-naphthylamine, **K** = polynaphthylamine (PNA).

5.2.2.2 USING THE MOON ROUTE.

Moon *et al.* [24] reported polymerisation of α-napthylamine, **J** (figure 5.4), to give a polymeric structure similar to polyaniline (polynapthylamine, PNA, **K** figure 5.4), this synthetic route is outlined below.

0.54g naphthylamine were dissolved in 30ml acetonitrile and stirred, 15ml of methanol were added whilst stirring. Another solution consisting of 3ml of 96% sulphuric acid and 0.03g of iron (II) sulphate heptahydrate (as a catalyst) in 70ml of water was prepared. The latter solution was added to the former, with stirring. Initially a pale precipitate formed in the purple solution, which re-dissolved upon addition of all of the second solution. To this mixture 1.08g of 27.5% hydrogen peroxide solution were added using a glass pipette. This immediately turned the solution from a pink/lilac colour to a clear brown colour and after 24 hours a brown precipitate had formed. The reaction mixture was filtered using a sintered glass filter and the residue was washed using water, methanol and 28% aqueous ammonia solution, followed by repeated washing with methanol. The brown coloured powder was then dried in a vacuum desiccator.

The synthesis requires twice the amount (by molar ratio) of oxidising agent than is used in production of polyaniline to achieve a similar yield. To produce the emeraldine form of polyaniline (PANi) an oxidant is required in a quantity such that for every aniline monomer there are 2.5 electrons available. This route produces the emeraldine (semi-oxidised) form of polyaniline. This is also the ratio used by Moon *et al.* to produce poly(1-amino-anthracene) from the anthracene monomer, **L** (figure 5.5). But in the case of naphthylamine yields of less than 50% were produced for this ratio.

Only with 5 electrons per monomer unit did the yield approach the 95% region. This suggests that the polymeric material produced (if indeed it is polymeric) might not be the emeraldine analogue of polynaphthylamine.

Attempted oxidation of the material produced by the polymerisation using ammonium persulphate did not alter the materials UV-visible spectra. The same is true for the UV-visible spectra after an attempted reduction of the material using phenyl-hydrazine. It can thus be deduced that the material produced by the Moon reaction gives a very stable product.

This reaction, however, deserves attention with respect to the copolymerisation of aniline and ANSA to give the Marcoussis polymer. The reaction shows that the simple copolymerisation of the two molecules is not likely to give a well-defined alternate copolymer, more probably a random block copolymer with many defects. This is suggested by the relative inertness of naphthylamine, and the knowledge that ANSA is stabilised by the presence of the sulphonic group. Alternatively, it could be suggested that the sulphonic group may stabilise the non-backbone ring of the naphthalene group in such a way as to negate the effects present in PNA (assuming that the product of the Moon reaction is indeed PNA). Hence it is obvious that the next step is to attempt to polymerise ANSA.

Attempts to produce PNA using different conditions (as listed in table 5.2 below) failed to give any substance other than the brown material produced by the Moon reaction.

	Reaction	**Result**
1	4.83g α-naphthylamine hydrochloride, 25ml water, 25ml methanol and 5ml hydrochloric acid (12 Molar) were mixed together. To this 3.35g of sodium dichromate dihydrate in 10ml water and 10ml methanol were added over 4 hours. Collection of product: The residue was filtered from the reaction medium and washed with water, ammonia solution (28%) and then repeatedly with methanol.	Approximately 2g of product were collected. The product was determined to be short chain oligomers of α-naphthylamine by UV-visible and FTIR spectroscopy.

2	3.58g α-naphthylamine were dissolved in 50ml acetonitrile with 20ml methanol and 30ml water. 15g og 96% sulphuric acid were added such that a pH value <0 was achieved. To this mixture 0.2g of $FeSO_4.7H_2O$ were added. 7.97g of 27% hydrogen peroxide solution were added dropwise over a two hour period. Collection of product: As above.	A similar yield of the same type of product described in the polymerisation attempt via the Moon route (above) was recovered.
3	3.58g α-naphthylamine were dissolved in 60ml acetonitrile with 30ml methanol and 30ml water. To this mixture 0.2g of $FeSO_4.7H_2O$ were added. 6.2g of sodium dichromate dihydrate in 10ml acetonitrile with 5ml methanol and 5ml water were added dropwise over a one hour period. Collection of product: As above	A yield >90% of short chain PNA was produced. (FTIR and UV-visible spectroscpoy characterisation.)

Table 5.2. α-naphthylamine polymerisation attempts using variations Moon's route.

It should be noted that the presence of $FeSO_4.7H_2O$ may not be required for the reaction using the dichromate oxidant system. This is due to the fact that Cr^{3+} ions are a product of the reaction and could act to self-catalyse the reaction. It is apparent, however, that the presence of transition metal ions is to be avoided if an entirely organic product is to be obtained.

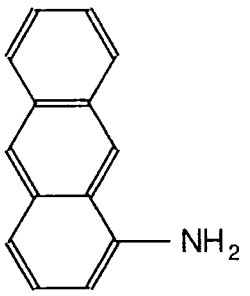

L

Figure 5.5. **L** = 1-amino-anthracene.

5.2.3 POLYMERISATION OF AMINONAPHTHALENESULPHONIC ACID.

5.2.3.1 USING THE STANDARD POLYANILINE ROUTE.

Using the same basic method as used for polyaniline [19,20,22] polymerisation of ANSA was attempted.

5.58g of ANSA were placed in 40ml of water which also contained 2.5g of 12 molar hydrochloric acid. Over a one hour period 7.13g of ammonium persulphate, dissolved in 20ml of water, were added drop-wise using a tap funnel.

This reaction did not change after 24 hours and the re-captured precipitate was identified (by FTIR and UV-visible spectroscopy) as being the initial reactant.

5.2.3.2 USING THE MOON ROUTE.

5.58g of ANSA were added to 60ml of acetonitrile. This mixture was stirred and 30ml of methanol along with 30ml of water were added and gave a suspension of the ANSA. To this 20g of 96% sulphuric acid were added and the mixture stirred vigorously. 6.2g of sodium dichromate were dissolved in 20ml acetonitrile with 10ml of water and 10ml of methanol. The dichromate solution was added drop-wise to the ANSA suspension over a 30 minute period (using a tap funnel) and the reaction was stirred for 24 hours. The suspension was then filtered and washed with water. The

residue was then dissolved in aqueous ammonia solution. This solution yielded a purple precipitate upon standing, and this was collected on a sintered glass filter, and dried in a vacuum desiccator.

The purple powder was insoluble in a wide range of organic solvents and water. The Powder did, however, react with aqueous acid solutions and the product dissolved. This suggests that the powder is in fact an ammonium salt of ANSA.

5.2.4 THE SYNTHESIS OF 5-(1,4-AMINO-ANILO)-2-NAPHTHALENESULPHONIC ACID, THE "MARCOUSSIS MONOMER".

The molecule 5-(1,4-amino-anilo)-2-naphthalenesulphonic acid, (AANSA) **M** figure 5.6), could be vitally important in understanding the properties displayed by the Marcoussis polymer. It has been suggested that if the Marcoussis polymer is indeed ferromagnetic, then the monomer should exhibit similar properties. Hence, the production of this molecule is of great interest. A two step reaction process for this molecule was formulated using a similar reaction (Bucherer reaction) to that reported by Rieche and Seeboth [25], the reaction is outlined below.

9g of sodium hydroxide were dissolved in 50ml of water and the solution was cooled to room temperature. 91.2g of sodium bisulphite were dissolved in 150ml of water. These solutions were added to a round bottomed flask along with 50g of ANSA and the reactants were refluxed at approximately 90°C for two days.

After two days the reaction was cooled to room temperature and hydrochloric acid was added to the solution to give a pH of less than 7 to remove excess sodium bisulphate. During the addition of HCl, nitrogen gas was bubbled through the reaction medium, to remove the resultant sulphur dioxide:

$$NaHSO_3 + HCl \Rightarrow NaCl + SO_2 + H_2O. \qquad \text{eqn. 5.1}$$

The mixture was then evaporated (using a rotary evaporator) to precipitate out the inorganic salts. These salts were then filtered out of the reaction medium using a sintered glass filter. The filtrate was then stirred and a saturated solution of potassium acetate (80g in 80ml of water) was added drop-wise using a tap funnel. After this addition the solution was allowed to stand and the potassium salt of the organic intermediate, **N** (figure 5.6), slowly precipitated from the solution. The precipitation was aided by the drop-wise addition of ~80ml of ethanol and after 2 hours a light brown suspension had formed. The precipitate was collected by filtration using a sintered glass filter and the residue was washed with ethanol and ether and allowed to dry on the filter. The powder was then dried in a vacuum desiccator and gave a pale yellow powder of **N** (figure 5.6). From this batch of the ketone intermediate, **N**, several attempts to produce 5-(1,4-amino-anilo)-2-naphthalenesulphonic acid were undertaken.

The first method used 1.91g of **N**, placed in 25ml of ethyleneglycol along with 1.81g of 1,4-phenylenediamine dihydrochloride in a round bottomed flask and refluxed at ~120°C for 6 hours. The reaction medium was cooled to room temperature and a solution of 10g of potassium hydroxide in 50ml of water was prepared. The reaction mixture was added to the potassium hydroxide solution and stirred. The resultant

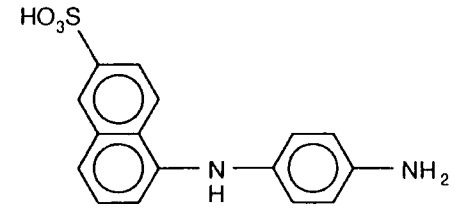

M

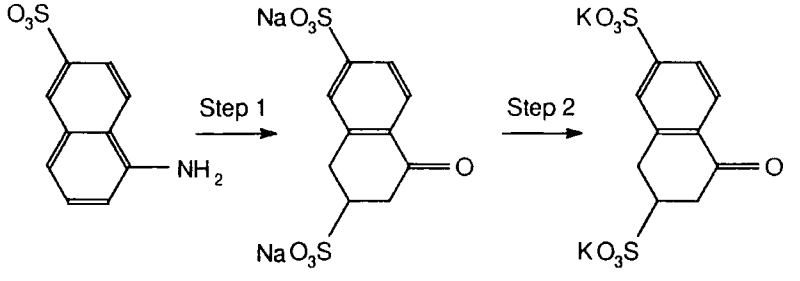

N

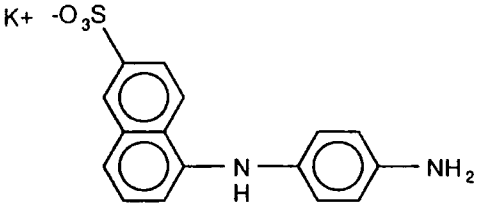

O

Figure 5.6. **M** = the Marcoussis monomer, 5-(1,4-amino-anilo)-2-naphthalenesulphonic acid (AANSA). The formation of **N** (ketone intermediate of the Bucherer reaction) via: Step 1 = NaOH, $NaHSO_3$, H_2O and heat; Step 2 = CH_3COOK and H_2O. **O** = The potassium salt of the Marcoussis monomer.

suspension was filtered (using a sintered glass filter) and the residue was washed with a small amount of ethanol and then with ether.

By the above method approximately 0.15g of potassium 5-(1,4-amino-anilo)-2-naphthalenesulphonate, **O** (figure 5.7), was collected, i.e., ~9% yield. To increase the yield of the reaction phosphorus pentoxide can be added to the ethyleneglycol to remove any water present in the reaction medium. Hence, a second (large batch), reaction was performed using 25g of **N** in 325ml of ethyleneglycol with 23g of phenyldiamine dihydrochloride and 5g of P_2O_5. (Note that it is advisable to add the P_2O_5 to the ethyleneglycol before the addition of the other substances, as it reacts violently with the small amount of water present in the liquid.) The reaction was then carried out at ~120°C for 24 hours and added to a saturated solution of potassium hydroxide (300g in 800ml of water) as before. The suspension was filtered, washed and dried (as before) and gave ~19.5g of **O** (figure 5.6), i.e., approximately 85% yield. (Note, however, that this may be an over estimate as the product could contain water of crystallisation.)

To produce a more pure sample of **O**, 9.2g of the salt were placed in 50ml of water and refluxed for 30 minutes under nitrogen. The resultant solution was then cooled slowly, allowing the product to re-crystallise. Via this process 3.15g of re-crystallised **O** were collected (by filtration on a glass filter and washing with ether).

Initial attempts to produce longer chain material from the potassium salt of the Marcoussis monomer all proved fruitless. These attempts included the standard polyaniline route as well as the Moon method, even including an attempt to synthesise a dimer of **O** using an iron catalysed hydrogen peroxide oxidation system, similar to that used by Moon. The polymerisation attempts are described in table 5.3 (below).

	Reaction	Result
1	0.53g of the potassium salt of the "Marcoussis monomer" were added to 10ml of water with 0.88g of 12Molar hydrochloric acid. To this solution 0.189g of sodium dichromate dihydrate in 25ml of water were added dropwise over a 2 hour period. Collection of product: The residue from the resultant mixture was recovered using a sintered glass filter. The solid was washed with water and dried in a vacuum dessicator.	The product was determined by NMR spectroscopy to be the initial monomer in the acid form (see section 5.3.4, below).
2	29ml water, 0.82ml 12Molar HCl and 1.69g of H_2O_2 were mixed together, and 0.5g of the potassium salt of the "Marcoussis monomer" were added. The mixture was stirred and 0.05g of $FeSO_4.7H_2O$ added to catalyse the reaction. Collection of product: As above.	As above.
3	0.25g of the potassium salt of the "Marcoussis monomer" were added to 2.5ml of 96% H_2SO_4, and this mixture added to 12.5ml water. To the mixture were added 0.061g of potassium iodate in 22.5ml of water over a 30 minute period. The reaction mixture was left to stir for 16 hours. Collection of product: as above	As above.
4	0.25g of the potassium salt of the "Marcoussis monomer" were added to 2.5ml of 96% H_2SO_4, and this mixture added to 15ml water. To this 0.25g of ammonium persulphate in 1ml of water were added dropwise over a one hour period. Collection of product: as above	As above.
5	0.5g of the potassium salt of the "Marcoussis monomer" were added to 30ml water, 15ml of acetonitrile and 15ml of methanol with 10g of 96% sulphuric acid. To this 0.53g of sodium dichromate dihydrate in 10ml of water, 5ml of acetonitrile and 5ml methanol over a 30 minute period. Collection of product: As above.	As above.

Table 5.3. Attempts to polymerise the Marcoussis monomer.

The acid form of the monomer, **M** (figure 5.6), can easily be produced from the potassium salt by simply acidifying an aqueous solution of **O** with HCl to give a 1 molar acid solution. This yields a pale brown precipitate of the acid form. This appearance was unexpected, due to the fact that the Marcoussis polymer is reportedly blue, hence doubts were raised about the composition of this acid material. As previously noted, the oxidation state of the Marcoussis polymer is expected to be important in its chemical and magnetic properties. Hence oxidation and/or reduction of the molecule **M** could produce a material with very different properties.

The acid form of **M** could only be dissolved in dimethylsulphoxide (DMSO) out of wide range of common solvents tried. A small amount of the material was placed in DMSO to give a saturated solution and the solution was refluxed at ~150°C in an attempt to re-crystallise the material. After 30 minutes at this temperature the solution had changed from a pale pink/red to a dark blue. Upon cooling a small amount of crystals were produced and ~7mg of these were recaptured.

To the remaining AANSA-DMSO solution 20ml of water were added to try and precipitate further the blue material. This was partially successful and resulted in the collection of 60mg of a fine blue powder after filtration and drying in a vacuum desiccator. It is possible that in the attempt to re-crystallise the AANSA (under an oxygen atmosphere) has resulted in an oxidised material being formed.

Further attempts to oxidise AANSA using "red lead" and other metal-ion based oxidants lead to the production of a purple solution. UV-vis spectroscopy of these indicate that a 5-(1,4-amino-anilo)-2-naphthalenesulphonate salt has formed and (as previously observed) this ion seems to be stable under oxidising conditions. Hence, oxidation of AANSA in DMSO was tried using hydrogen peroxide, and this resulted in a blue/black solution from which no product could be isolated.

5.3 CHARACTERISATION RESULTS AND DISCUSSION.

5.3.1 COPOLYMERIZATION ATTEMPTS.

Figure 5.7 shows a UV-vis spectrum of amino-naphthalenesulphonic acid (ANSA), note the presence of the peak at ~320nm, this is attributed to the presence of benzene rings (i.e., the benzenoid absorption peak). Figure 5.8 shows the UV-vis spectrum of the product isolated from the copolymerisation attempt described in section 5.2.1. There is an absence of further peaks in figure 5.8 (between 450nm and 550nm) where an absorption due to quinoid groups would be expected if the material contained quinoid groups, showing that no quinoid structures are present. The lack of quinoid groups indicates that there is no emeraldine analogue of the suggested Marcoussis polymer present from the copolymerisation reaction, opposing the results obtained by Galaj *et al.* [17].

It can be seen from comparisons of UV-vis spectra (figures 5.7 and 5.8) that the only fraction of the reaction mixture that could be isolated after completion of the reaction is, in fact, unreacted ANSA. All of the other variations of the copolymerisation experiment also yielded the same results. It is hard, therefore, to deduce how Galaj *et al.* [17] managed to produce what they have named the Marcoussis polymer. Other reactions were thus investigated to try and determine whether another synthesis route would lead to the production of the Marcoussis polymer.

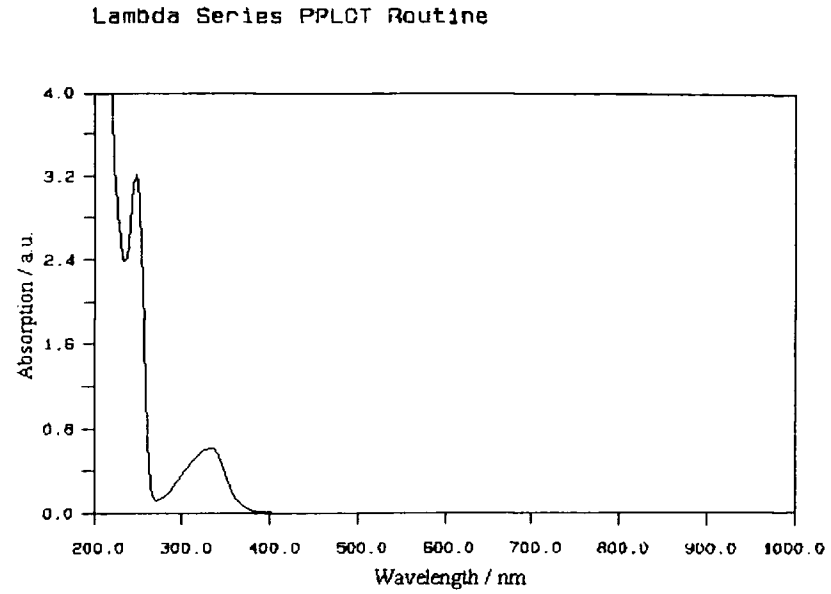

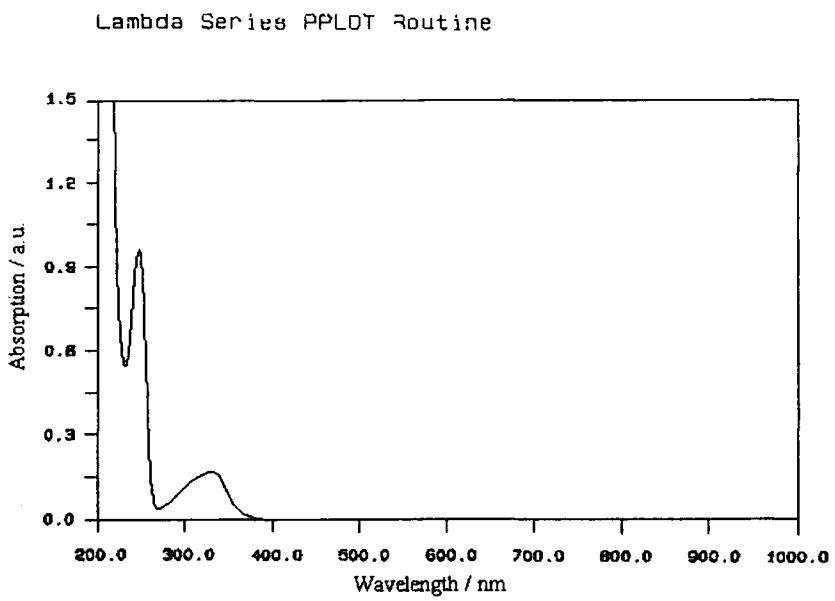

Top: Figure 5.7. UV-vis spectrum of ANSA in ammonia solution.

Bottom: Figure 5.8. UV-vis spectrum of products from attempted copolymerisation of ANSA and aniline.

5.3.2 POLYMERISATION OF 1-AMINO-NAPHTHALENE.

From comparisons of the UV-visible spectra of α-naphthylamine (figure 5.9) and the reaction product (figure 5.10), it is apparent that the persulphate polymerisation route [22] gives a material that has an extended absorption at ~500nm. This has been attributed to the presence of quinoid groups in the product. It can also be seen, however, that there is still a larger absorption at ~320nm due to the presence of benzenoid rings.

In the emeraldine form of polyaniline the peak intensities are approximately equal (by comparison of peak height) for the ratio of 1:3 for quinoid and benzenoid groups respectively. This suggests that in the products of the reactions outlined in section 5.2.2 there is a proportion of short chain oligomers. If an emeraldine analogue of poly(amino-naphthalene) was formed there would be a ratio of 1:7 quinoid groups to benzenoid groups. The resultant UV-vis peak intensities would therefore be expected to be approximately 1:2 for the quinoid and benzenoid absorptions respectively. The observed peak intensities in figure 5.10 are closer to 1:5, indicating that an emeraldine analogue has not been synthesised. This, however, assumes that the absorption coefficient of the benzenoid rings in amino-naphthalene (or poly(amino-naphthalene)) is the same as that of aniline (or polyaniline).

It is suggested that low molecular weight oligomers have been produced and this is supported by the observation that polymeric films could not be cast from a number of

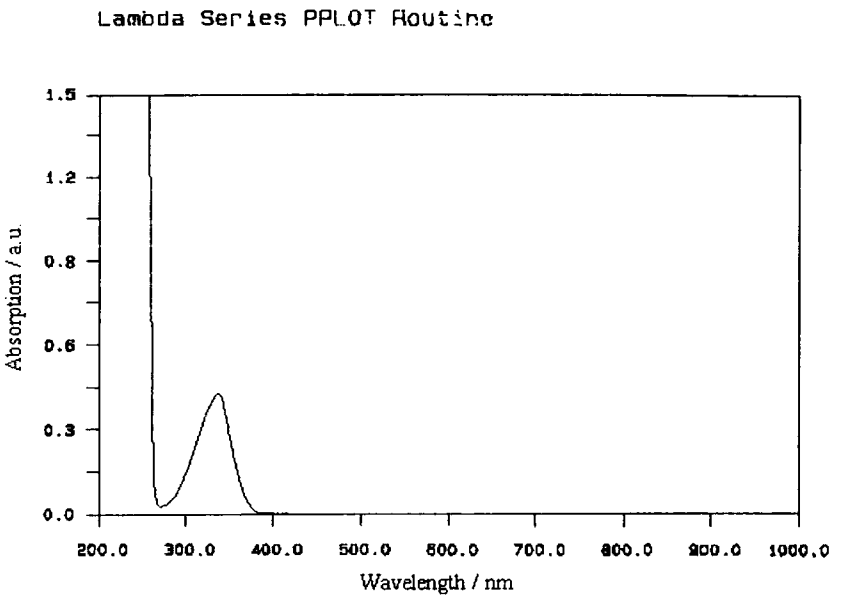

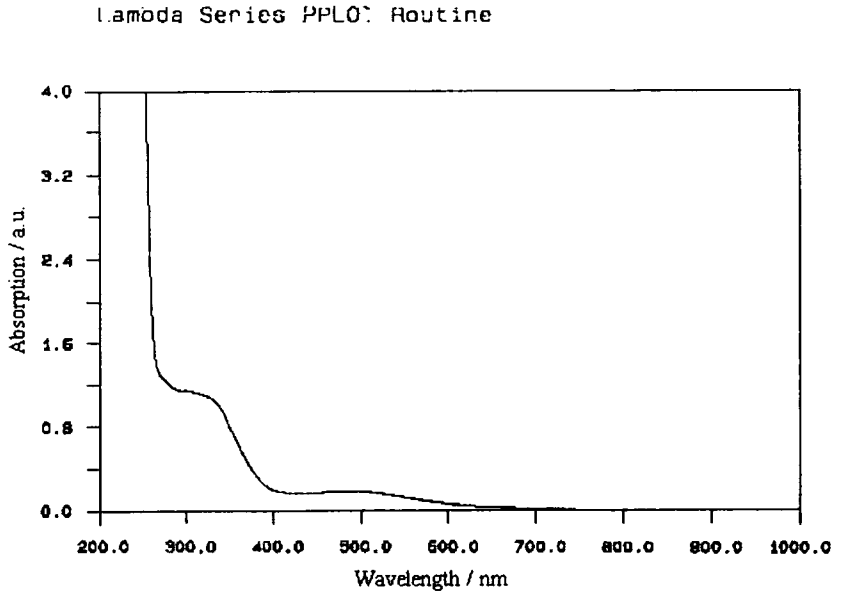

Top: Figure 5.9. UV-vis spectrum of α-naphthylamine in N-methyl-pyrrolidinone

Bottom: Figure 5.10. UV-vis spectrum of polymeric material (in N-methyl-pyrrolidinone) produced by the oxidative polymerisation of α-naphthylamine using ammonium persulphate.

different solutions of the product. Very similar results to those given below were also observed for the Moon synthesis route, also indicating that only low molecular weight material could be synthesised. It is the author's opinion that very little material greater than three repeat units was produced since the ratio between the quinoid and benzenoid peaks is so small. It is believed that most of the product was unreacted monomeric starting material.

It is apparent that neither of the synthetic routes attempted in section 5.2.2 provided a viable procedure for the synthesis of a (high molecular weight) polymer. It is thus suggested that the route outlined by Galaj *et al.* [17] for the copolymerisation of ANSA and aniline is unlikely to yield high molecular weight material containing a large fraction of ANSA. This is supported by the suggestion that the stability of the naphthalene ring is increased by the presence of the sulphonic group.

5.3.3 POLYMERISATION OF AMINO-NAPHTHALENESULPHONIC ACID.

The spectra in figures 5.11 and 5.12 clearly show that the persulphate oxidation of ANSA yields a product that has a much lower quinoid absorption (when compared to the benzenoid absorption) than would be expected if the product was polymerised in an analogous way to polynapthylamine (see section 5.3.2). It can thus be deduced that the majority of the product is unreacted ANSA, and that only a small fraction has yielded any desirable product. No spectra of the material produced by the Moon route (section 5.2.3.2) have been recorded as no solvent has been found for it.

The results show that the production of polymers from oxidative polymerisation experiments (analogous to that of the polyaniline) is not efficient, throwing doubt upon the route suggested by Galaj *et al.* [17] for the Marcoussis polymer. This is probably due to the stability of the molecule owing to the presence of the sulphonic group, as suggested in section 5.2.2.2 and 5.3.2.

The lack of progress experienced in oxidative polymerisation and copolymerisation reactions lead to the investigation into whether the Marcoussis polymer could be produced via a slightly different route. The manufacture of the Marcoussis monomer (as outlined in section 5.2.4) was undertaken to investigate whether oxidative polymerisarion of such a molecule would lead to the production of the Marcoussis monomer.

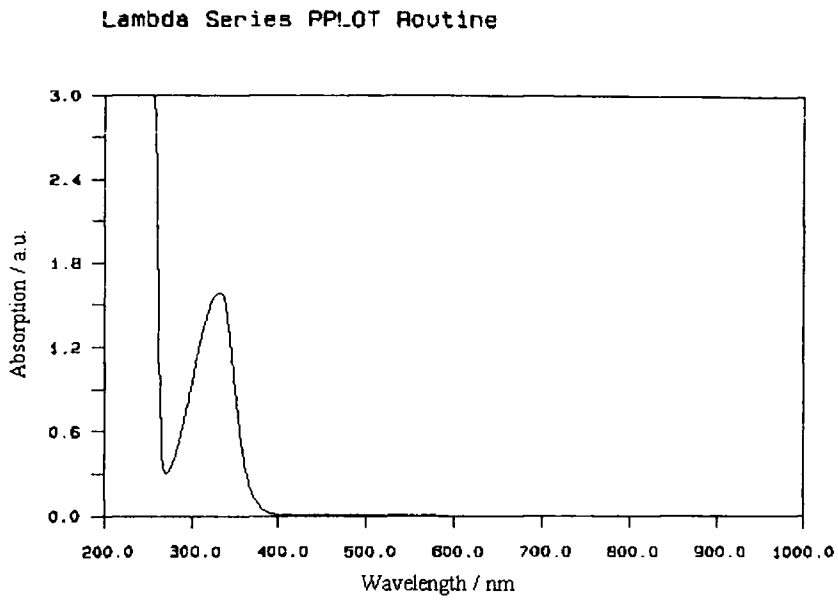

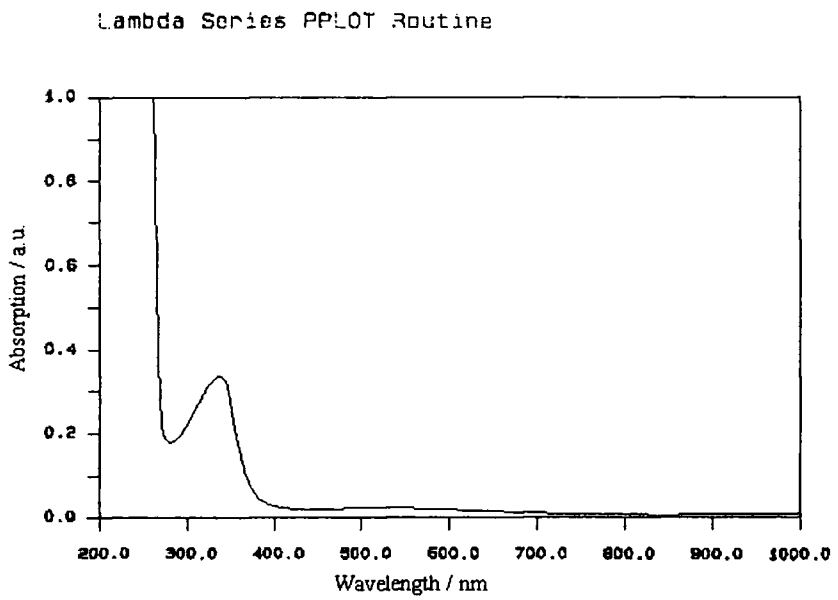

Top: Figure 5.11. UV-vis spectrum of amino-naphthalenesulphonic acid (ANSA) in N-methyl-pyrrolidinone (NMP).

Bottom: Figure 5.12. UV-vis spectrum of ammonium persulphate oxidised ANSA in NMP

5.3.4 THE MARCOUSSIS MONOMER.

^{1}H- and ^{13}C-NMR spectroscopy along with IR and mass spectroscopy were performed on the product of the two step reaction outlined in section 5.2.4. The results showed that the material was indeed the potassium salt of the Marcoussis monomer (AANSA), and that no waters of crystallisation were present. (See Appendix A for ^{1}H-NMR and ^{13}C-NMR spectra of the material.)

Oxidative polymerisation attemps performed on the monomer yielded no product (see table 5.3), except for the blue crystalline material produced by the refluxing of the monomer in DMSO under atmospheric conditions. UV-visible spectra of the material (in DMSO) gave approximately equal peak intensities for the benzenoid and quinoid absorptions. This result, however, was later shown to be indicative of the formation of polyaniline derivatives due to the decomposition of the Marcoussis monomer under the reflux conditions. It is believed that the crystalline nature of the material was due to the presence of potassium salts of other decompostion products. The oxidation of the Marcoussis monomer in DMSO using hydrogen peroxide also gave similar results. It is proposed, therfore, that the material studied by Galaj *et al.* was also the result of degradation products.

Vibrating sample magnetometry (VSM) was performed on the product of refluxing the Marcoussis monomer to determine whether any ferromagnetism was associated with the material. Approximately 7mg of the material were placed in a PTFE sample holder used in the VSM measurement. The vibrating sample magnetometry measurements taken from the crystals are shown in figures 5.13 and 5.14 respectively.

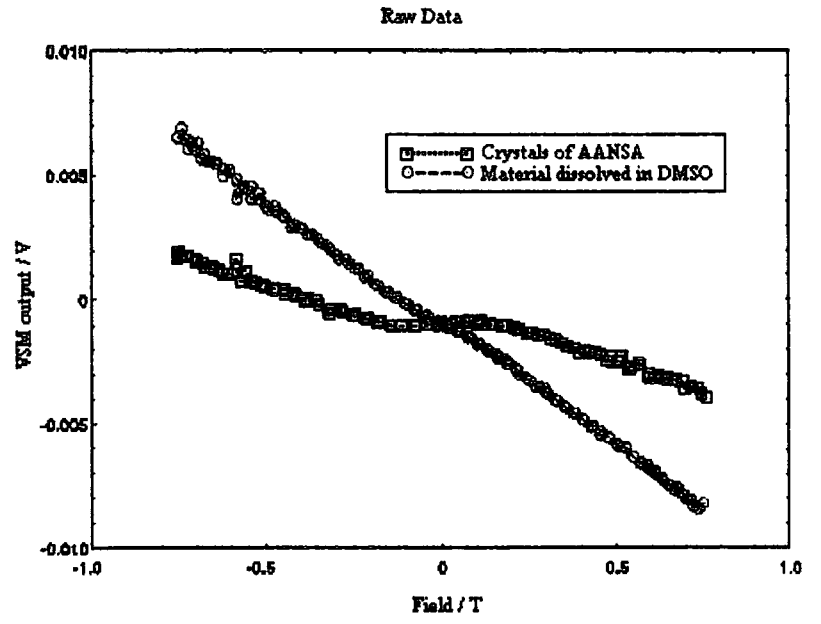

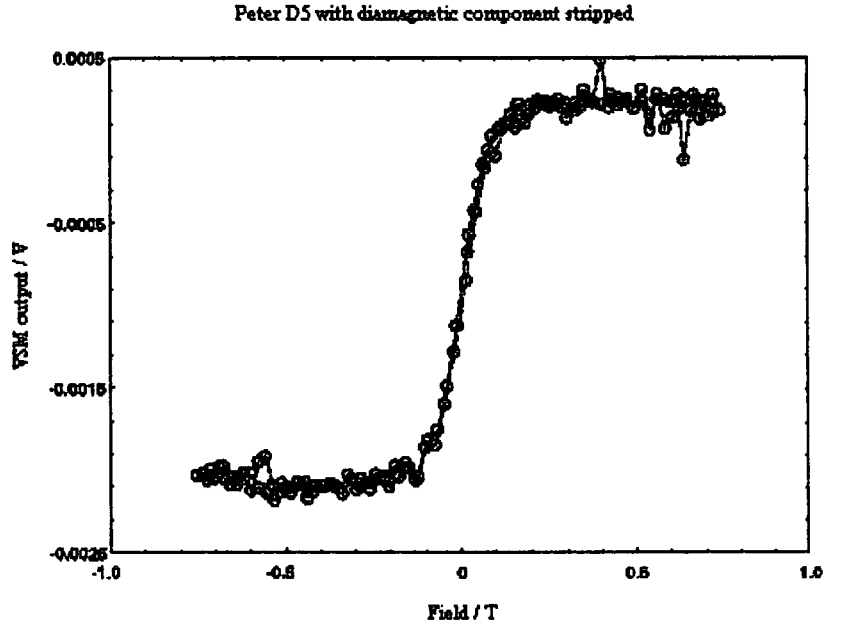

Top: Figure 5.13. Raw VSM data for AANSA in both solid and solution states.

Bottom: Figure 5.14. Solid state AANSA VSM data with the diamagnetic component subtracted.

Figure 5.13 shows the raw data from the VSM experiment for the crystals and a solution of the crystals formed by the addition of 0.5ml of DMSO. It can be seen that there is a diamagnetic component (negative slope) due to the PTFE sample holder. The data shown in figure 5.14 shows the resultant line of the crystalline material, with the negative slope from the diamagnetic PTFE subtracted. The fact that the solution of the material displays no ferromagnetic component suggests that the signal can not be caused by the presence of ferromagnetic metal particles as these are insoluble in DMSO.

From this data it can be seen that there is a definite ferromagnetic component present in the crystalline material. Elemental analysis of the material (performed by Durham university chemistry department), however, isolated a fraction of iron impurities that could easily account for the observed magnetic signal. This suggests that the results of Galaj *et al.* are incorrect. It is suggested that the observed ferromagnetic signal is the result of iron oxides in the material. Iron oxides are indeed soluble in DMSO.

The author believes that similar ferromagnetic impurities caused the observed ferromagnetic material that Galaj *et al.* [17,18] claimed to be entirely organic. It is, therefore, suggested that the Marcoussis polymer is not ferromagnetic. The appearance of the Marcoussis polymer itself causes concern as it is reported to be crystalline on a macroscopic scale [17,18], unlike any other high molecular weight polymer.

The observation that there has been no report of the Marcoussis polymer in any scientific journal to date also suggests that the original claims may have been withdrawn. The author suggests that ESR measurements on the Marcoussis monomer would show whether localised spins (capable of ferro- or ferri-magnetic interaction) are present. The absence of such spins would strongly indicate that the polymer would not

be magnetic, but the possibility of the extended molecule exhibiting different properties in different oxidation states must exist. After all, the properties of polyaniline are greatly dependent on the oxidation state and protonation level. Time constraints and the priority given to the other projects in this work have not allowed further investigation of the Marcoussis monomer, but it is the author's opinion that the Marcoussis polymer (could it be synthesised) would not be ferromagnetic.

5.4 CONCLUSIONS.

The inability to synthesise the Marcoussis polymer has meant that no investigation into the properties of the spin carriers could be performed. It has been shown that the reports of the Marcoussis polymer being an entirely organic ferromagnetic material are unsubstantiated and (in this work at least) non-reproducible. It is obvious, however, that all the required synthetic procedures were not available, thus further publication of the work by Galaj *et al.* [17,18] may lead to different results. In the absence of further experimental information, it is proposed from the results of this work that the Marcoussis polymer is not intrinsically ferromagnetic and that the ferromagnetic species observed by Galaj and co-workers were extrinsic.

5.5 REFERENCES.

1. Miller, J.S., *The Quest for Magnetic Polymers - Caveat Emptor (A).* Advanced Materials, 1992. **4**: p. 298-300.
2. Miller, J.S., *Molecular/Organic Magnets - Potenial Applications.* Advanced Materials, 1994. **6**: p. 322-324.
3. Miller, J.S.a.E., A.J., *Organometallic Ferromagnets.* Phil. Trans. R. Soc. Lond., 1990. **330**: p. 205-215.
4. Tanaka, K., Yoshizawa, K., Takata, A., Yamabe, T., *Magnetic Property Measurement of Simple Alkylene-Aromatic Polymers.* Synthetic Metals, 1990. **39**: p. 103-108.
5. Murry, M.M., Kaszynski, P., Kaisali, D.A., Chang, W., Dougherty, D.A., *Prototypes for the Polaronic Ferromagnet. Synthesis and Characterisation of High-Spin Organic Polymers.* Journal of the Americam Chemical Society, 1994. **116**: p. 8152-8161.
6. Yue, J., Wang, Z.H., Cormack, K.R., Epstein, A.J. and MacDiarmid, A.G., *Effect of Sulphonic Acid Group on Polyaniline Backbone.* Journal of the American Chemical Society, 1991. **113**(2665-2671).
7. Kawai, T., Mizobuchi, H., Yamasaki, N., Araki, H., and Yoshino, K., *Optical and Magnetic Properties of Polyaniline Derivatives Having Ionic Groups.* Japanese Journal of Applied Physics, Part 2, 1994. **33**: p. L357-L360.
8. Mizobuchi, H., Kawai, T., Yoshino, K., *Ferromagnetic Behavior Of Self-Doping Type Polyaniline Derivatives Depending On Oxidation-State.* Solid State Communications, 1995. **96**(12): p. 925-929.
9. Mizobuchi, H., Kawai, T., Araki, H., Yamasaki, N., Yoshino, K., and Sakamoto, A., *Unique pH Dependent Optical and Magnetic Properties of Self-Doping type Copolymers of Aniline and aminonaphthalene Derivatives with Sulphonic Groups.* Synthetic Metals, 1995. **69**: p. 239-240.
10. Blyumenfeld, L.A., Dolk. Akad. Sci. Nauk. S.S.S.R., 1962. **148**: p. 361.

11. Ovchinnikov, A.A., Mdvedeva, T.V., Korshak, Y.V., Spector, V.N., Shapiro, A.M., Pisma Zh. Eksp. Teor. Fiz., 1986. **4**: p. 309.

12. Sandman, D.J., Hamill, G.P., Levinson, P.G., Rossoni, P.G., Yost, E.A., Papaefthymiou, MRS Symp. Proc., 1990. **173**: p. 567.

13. Jones, M.T., Braig, K., Singh, M., Sandman, D.J., Synthetic Metals, 1991. **41-43**: p. 3301.

14. Miller, J.S., Glatzhofer, D.T., Laversanne, R., Chittipeddi, S., Vaca, P., Brill, T.B., Timken, M.D., O'Connor, C.J., Zhang, J.H., Calabrese, J.C., Epstein, A.J., Chem. Mater., 1990. **2**: p. 60.

15. Miller, J.S., *The Quest for Magnetic Polymers - Caveat Emptor (B).* Advanced Materials, 1992. **4**: p. 435-438.

16. Miller, J.S., Epstein, A.J., *Organic and Organometallic Molecular Magnetic Materials - Designer magnets.* Angew. Chem. Int. Ed. Engl., 1994. **33**: p. 385-415.

17. Galaj, S., LeMéhauté, A., Genies, E., *Entirely Organic Ferromagnetic material.* 1992: Patent, France.

18. Galaj, S., LeMéhauté, A., Tsobnang, F., Cotteville, D., Léaustic, A., Clément, R., Cagan, V., Guyot, M., Tiller, A.R., Wimmer, E., Genies, E., Fayet, J.C. and Villeret, B., *Purely Organic Ferromagnets with High Curie Temperature.* Nature (Unpublished Pre-print), 1993.

19. Lux, F., *Properties of electronically conductive polyaniline: a comparison between well-known literature data and some experimental findings.* Polymer, 1994. **35**: p. 2915 - 2926.

20. Adams, P.N., Laughlin, P.J.,Monkman, A.P., Kenwright, A.M., *Synthesis of High Molecular Weight Polyaniline.* Polymer, 1996. **37**: p. 3411-3417.

21. Maslak, P., *Spiroconjugation: an Added Dimension in the Design of Organic Molecular Materials.* Advanced Materials, 1994. **6**: p. 405-407.

22. Adams, P.N., Apperley, D.C., Monkman, A.P., Polymer, 1993. **34**: p. 328.

23. Monkman, A.P., Adams, P., *Structural Characterization Of Polyaniline Free Standing Films.* Synthetic Metals, 1991. **41-43**(3): p. 891-896.

24. Moon, D.K., Osakada, K., Maruyama, T., Kubota, K., Yamamoto, T., *Synthesis Of Poly(1-Aminonaphthalene) and Poly(1-Aminoanthracene) By Chemical Oxidative Polymerization and Characterization Of the Polymers.* Macromolecules, 1993. **26**(25): p. 6992-6997.

25. Rieche, A.a.S., H., *Reactions of Naphthols and Naphthylamines with Bisulphates (Bucherer Reaction).* Ann. Chem., 1960. **38**: p. 43-56.

CHAPTER 6.

6. CONCLUSIONS.

6.1 CONCLUSIONS.

6.2 REFERENCES.

6. CONCLUSIONS.

The data presented in this thesis can (in the author's opinion) be considered as supporting a simple model describing charge transport in solution doped polyaniline materials. First, the conclusions from each chapter are described below. The proposed model for charge transport in solution doped polyaniline is then given, with the support for the proposal from each experimental chapter being established.

The temperature dependent conductivities of PANi-AMPSA (Chapter 2) and PANi-CSA (Holland *et al.* [1]) show that the heterogeneous metal-FIT model [1-4] proposed by Holland [1] (along the lines of Kaiser [2-4]) provides the best fit to the experimentally observed data. Thus, it is suggested that solution doped PANi is indeed a disordered granular metal in which highly conductive metallic islands are randomly distributed in an insulating or semiconducting amorphous polymer matrix.

Clearly the conductivities of the solution doped polyanilines investigated here (PANi-CSA and PANi-AMPSA) have marked differences. These (the author suggests) are a result of the dissimilar physical composition and crystallinity induced by the acid-solvent combinations in each case. Perhaps the most intriguing difference between PANi-CSA and PANi-AMPSA observed in this work is the doping level required to achieve optimum conductivity. It is uncertain whether this is a result of protonation to greater than the 50% theoretical optimum in both cases. Alternatively, if the PANi-CSA material is atypical of solution doped polyaniline in that the crystal structure of the 60% doped material allows better charge transport than when PANi-CSA is 50% doped. In the latter of these possible explanations the presence of excess CSA promotes a more

highly crystalline structure (up to ~60%doping) but does not lead to increased protonation of the polymer backbone.

Another notable difference between conductivities of the PANi-AMPSA and PANi-CSA systems is the discontinuous temperature dependent conductivity of the former between 240 K and 260 K. The effect has been attributed to a phase transition that increases the vibrational and/or rotational degree of freedom of the polymer chains above the transition temperature. The increased phonon density above ~260 K causes the conductivity to display a stronger negative temperature coefficient than that observed between 100 K and 240 K.

It is suggested that conductivity through the "metallic grains" of the material is changed at this discontinuity. This is supported by the fitting of Holland's heterogeneous metal-FIT model to the discontinuity (section 2.3.2). The best fit to the data does not change the parameters of the FIT contribution (except the minimum metallic conductivity parameter, B, which is effectively an extrapolation of the line back to T=0) but does require a modification to the metallic term. It should be noted, however, that the fitting parameters may be just mathematical necessities for the heterogeneous metal-FIT model.

The thickness dependent conductivity measurements also highlight the differences between PANi-CSA and PANi-AMPSA. In these results the AMPSA doped material displays a smaller dependence of conductivity on thickness than PANi-CSA. The CSA doped material shows a rapid fall of conductivity as the sample thickness is reduced below 100nm. Two possible explanations for the PANi-CSA of thickness dependence are proposed. Firstly, the size of the crystallites in PANi-CSA is large enough that the observed thickness dependence is a result of the material changing from

a 3-D array of metallic islands to a 2-D system. The other suggestion is that the physical properties of the PANi-CSA in m-cresol solution reduce the size and/or number of crystallites during the spinning of films less than 100nm thick. The fact that the same thickness dependence is not shown by PANi-AMPSA films is probably a reflection of the fact that PANi-AMPSA in dichloroacetic acid solution is not influenced by either of the above effects (for film thickness' greater than ~30nm thick, at least).

The investigation of the thin-film polyaniline layers has also shown that PANi-AMPSA has the potential to be used as an electrode in the manufacture of polymeric LEDs. The replacement of ITO coated glass by polyaniline is expected to increase device performance [5].

Electron spin resonance results (Chapter 3) support a modified version of the model suggested by Kahol *et al.* [6,7]. Kahol proposed that a partially ordered layer separates a highly ordered metallic core from the amorphous region, thus providing the possibility of different charge carriers and/or mobilities in each of the three different layers (i.e., ordered, partially ordered and amorphous). The ESR results detailed in this work may be indicative of the modifications Kahol's model outlined in Chapter 3. Namely that the highly ordered region contains a polaron lattice in which there are "free" carriers. It is proposed that the "semi-ordered layer" surrounding the metallic core contains partially delocalised "mobile" polarons, whereas only trapped (localised) polarons are present in the amorphous matrix. The relative size of each of these regions is determined by the dopant type (which in turn determines the solvent used) and protonation level. It is also suggested that the solution concentration, drying temperature and atmosphere may have important roles in determining the crystalline properties of the resultant film.

Initial questions are raised about the validity of the model described above when the results of the ESR spectroscopy are first analysed. The anomalous lack of any real Dysonian asymmetry [16] for the 60% doped PANi-CSA material does not fit well with the model proposed above. If mobile polarons are present in a semi-ordered layer that encapsulates the polaron lattice at the core of the crystallites, a highly distorted ESR lineshape would be expected according to Dyson's theory [16]. The lack of Dysonian distortion is further compounded by the fact that the temperature dependent ESR shows that mobile spin carriers are present due to the observation of motional narrowing with increasing temperature. The most plausible explanation for these apparently contradictory results is that the core of the crystalline region is not a polaron lattice. The observed ESR signal, therefore, might be due to highly mobile polarons within the crystallites, and it is these mobile polarons that are responsible for metallic conduction within the highly ordered region. This explanation, however, infers that the mobile polarons are of such high mobility that Dyson's effect can not be observed.

To determine whether mobile polarons or a polaron lattice is responsible for charge transport within the core of the crystallites it is proposed that temperature dependent ESR spectroscopy is performed on AMPSA doped PANi. As previously mentioned, the discontinuity in the temperature dependent conductivity of PANi-AMPSA has been attributed to the freezing out of a vibrational or rotational degree of freedom as the temperature is reduced below ~240 K. If this transition introduces an increased phonon density to a polaronic lattice (above ~260 K) then the temperature dependence of the conductivity would be increased as conduction through the metallic regions is affected by increased phonon scattering at increased temperatures. Since ESR absorption by the carriers in the polaron lattice is expected to be negligible, a

discontinuity in the temperature dependent ESR would not be expected. If mobile polarons are responsible for charge transport through the high conductivity regions of the crystallites, however, a discontinuity in the linewidth of the temperature dependent ESR would be expected at around 250 K. The temperature dependent linewidth (in this case being used as a measure of motional narrowing) would be discontinuous as the polaron mobility was reduced with increasing temperature between ~240 and 260 Kelvin.

The ESR data alone, however, can not determine whether bipolarons are present within the material. If the majority charge carriers within the highly ordered regions were bipolarons there would be no observable ESR signal from this region, thus the formation of a polaron lattice may not be a justifiable assumption. Hence, the existence of a polaron-bipolaron equilibrium (see for example [6-10]) can not be ruled out.

The temperature dependent ESR results do show, however, that there must be (partially) mobile polarons in the most conductive PANi-CSA materials since a motional narrowing effect is observed. The reduction in the number of charge carriers that display motional narrowing in the 30% doped material leads the author to believe that the modified Kahol model suggested (above) is correct. It is proposed that the major difference between the 30% and 60% doped PANi-CSA material is the relative size of the highly ordered and partially ordered regions. That is, the 30% doped material has smaller (or fewer) crystallites in which the semi-ordered layer is negligible when compared to the 60% doped PANi-CSA.

The small amount of (non-reproducible) data obtained for the Faraday rotation of polyaniline (Chapter 4) supports McCall's proposal that the effective mass of the charge carriers in polyaniline is at least 100 times the free electron mass [11]. This leads to the

conclusion that the charge carriers observed by Faraday rotation are not metallic, but partially localized polarons (or bipolarons). The Faraday rotation spectroscopy undertaken has, however, shown that the results of Yuan *et al.* [12] are not reproducible. The rotation observed by Yuan *et al.*, in the author's opinion, is that of the transparent conductive substrate (probably ITO coated glass) upon which Yuan deposited the films electrochemically.

The numerous attempts to synthesise the Marcoussis polymer (as described in Chapter 5) have cast significant doubt on the claims of Galaj *et al.* [13, 14] that the Marcoussis polymer is an intrinsically ferromagnetic material. The similarities in the described appearance of the Marcoussis polymer as synthesised by Galaj *et al.* [13, 14] and the iron oxide contaminated material investigated in this work suggest that the two materials are the same. The possibility that the Marcoussis polymer, if it could be synthesised, might display ferromagnetic properties can not be discounted as there is obvious doubt about how accurately the synthesis route described in the patent reflects the work of Galaj *et al.* [13, 14]. The lack of further publications, however, has led the author to conclude that Galaj and co-workers have not been able to reproduce their initial results, thus suggesting that the Marcoussis polymer is not intrinsically ferromagnetic.

From the above summaries of each chapter the author proposes that the modified Kahol model (Chapter 3) can be considered as describing the composition of solution doped polyaniline materials. The fitting of Holland's heterogeneous metal-FIT model to the discontinuity observed in the conductivity of PANi-AMPSA suggets that only the metallic contribution to conduction is affected. This provides support for the

assumption that a metallic polaron lattice exists as it appears that the "barrier" regions are unaffected by the phase transition. As noted above and in (Chapter 2) the complexity of Holland's metal-FIT equation may lend itself to the fitting of almost any curve of the general shape of the temperature dependent conductivity of PANi-AMPSA. As such the author is cautious to cite the fitting of discontinuity with the metal-FIT model as proof of the proposed modifications to Kahol's model. Indeed the proposed model contains three distinct conductivity environments: a polaron lattice encapsulated in a less ordered layer containing mobile polarons, dispersed in an amorphous matrix. This is indicative of the need for a third term, describing conductivity through the partially ordered region, to added to Holland's metal-FIT model, or replacing the metallic term with one that combines the conductivities of both ordered and semi-ordered regions within the "metallic" grains. This however may lead to such a complex equation with so many variables that the fitting of any curve of the same general shape becomes possible.

In the authors opinion the best way to determine the validity of the proposed model would be temperature dependent ESR investigation of PANi-AMPSA. The ESR results given in this work may support the existance of a polaron lattice within the highly conductive crystallites, and mobile polarons in the semi-ordered region. If the temperature dependent ESR of PANi-AMPSA shows no discontinuity around the temperature of the phase transition observed by the conductivity measurements then further support for the proposed model would be gained (see Chapter 3 and above). It is the author's hope that a full investigation of the ESR properties of PANi-CSA and PANi-AMPSA is undertaken to confirm or deny the validity of the proposed model.

The limited results yielded by the Faraday rotation experiment do not negate the assumption that a three-dimensional polaron lattice is formed in the highly ordered crystallite core. If the work by Kohlman *et al.* [15] is to be believed, then it may not be possible to detect the free carrier contribution to Faraday rotation in the visible spectrum. Faraday rotation in the microwave region (assuming the existence of a transmission window) may show that conduction in solution doped polyaniline is dominated by a small fraction of metallic free carriers. If free carrier Faraday rotation could be detected, the polaron lattice theory would be supported.

Taking all the above into consideration the author proposes that solution doped polyaniline systems are composed of three distinct regions. A highly ordered region containing a polaron lattice in which there are "free" carriers. A semi-ordered layer surrounding the metallic core contains mobile polarons. The crystalline islands are dispersed in an amorphous matrix which also contains trapped (localised) polarons. The relative size of each of these regions is determined by the dopant type (which in turn determines the solvent used) and protonation level. The physical properties of the doped polyaniline solution (viscosity, drying rate etc.) used to produce films and fibres is important with respect to the relative size of the three layers in the resultant material. The conductivity of solution doped polyaniline is well modelled by Holland's metal-FIT equation, but is obvious that a third term may need to be added to accurately describe the model proposed here.

6.2 REFERENCES.

1. Holland, E.R., Pomfret, S. J., Adams, P. N., Monkman, A. P., *Conductivity Studies Of Polyaniline Doped with CSA.* Journal Of Physics-Condensed Matter, 1996. **8**(17): p. 2991-3002.
2. Kaiser, A.B., *Physical Models For Electronic Transport In Highly-Conducting Polymers.* Abstracts Of Papers Of the American Chemical Society, 1991. **201**(APR): p. 175-PMSE.
3. Kaiser, A.B., *Metallic Polymers - Interpretation Of the Electronic Transport-Properties.* Synthetic Metals, 1991. **43**(1-2): p. 3329-3334.
4. Kaiser, A.B., *Metallic Behavior In Highly Conducting Polymers.* Synthetic Metals, 1991. **45**(2): p. 183-196.
5. Carter, S.A., Angelopoulos, M., Karg, S., Brock, P.J., Scott, J.C., *Polymeric anodes for improved polymer LED performance.* Applied Physics Letters, 1997. **70**: p. 2067 - 2069.
6. Kahol, P.K., Dyakonov, A.J., McCormick, B.J., *An Electron-Spin-Resonance Study of Polyaniline and its Derivatives: Polymer Interactions with Moisture.* Synthetic Metals, 1997. **84**(1-3): p. 691-694.
7. Kahol, P.K., Guan, H., McCormick, B. J., *Moisture Effects On the Magnetic State In Polyaniline.* Physical Review B-Condensed Matter, 1991. **44**(18): p. 10393-10395.
8. Raghunathan, A., Natarajan, T. S., Rangarajan, G., Dhawan, S. K., Trivedi, D. C., *Charge-Transport and Optical and Magnetic-Properties Of Polyaniline*

Synthesized With Use Of Organic-Acids. Physical Review B-Condensed Matter, 1993. **47**(20): p. 13189-13196.

9. Krinichnyi, V.I., *EPR and Charge Transport Studies of Polyaniline.* Physical Review B - Condensed Matter, 1997. **55**(24): p. 16233-16244.

10. Lux, F., *Properties of electronically conductive polyaniline: a comparison between well-known literature data and some experimental findings.* Polymer, 1994. **35**: p. 2915 - 2926.

11. McCall, R.P., Ginder, J.M., Leng, J.M., Ye, H.J., Manohar, S.K., Masters, J.G., Asturias, G.E., MacDiarmid, A.G. and Epstein, A.J., *Spectroscopy and Defect States in Polyaniline.* Physical Review B - Condensed Matter, 1990. **41**: p. 5202-5213.

12. Yuan, R.K., Wu, W., Wang, Y.B., Qin, H., Wang, G.Q., *A New Type of Magneto-Optical Material and Device.* Synthetic Metals, 1995. **69**: p. 275-276.

13. Galaj, S., LeMéhauté, A., Genies, E., . 1992: France.

14. Galaj, S., LeMéhauté, A., Tsobnang, F., Cotteville, D., Léaustic, A., Clément, R., Cagan, V., Guyot, M., Tiller, A.R., Wimmer, E., Genies, E., Fayet, J.C. and Villeret, B., *Purely Organic Ferromagnets with High Curie Temperature.* Nature (UNPUBLISHED), 1993.

15. Kohlman, R.S., Tanner, D. B., Ihas, G. G., Min, Y. G., MacDiarmid, A. G., Epstein, A. J., *Inhomogeneous insulator-metal transition in conducting polymers.* Synthetic Metals, 1997. **84**(1-3): p. 709-714.

16. Dyson, F.J., *Electron Spin Resonance Absorption in Metals. II. Theory of Electron Diffusion and the Skin Effect.* Physical Review, 1954. **98**: p. 349-359.

APPENDIX A.

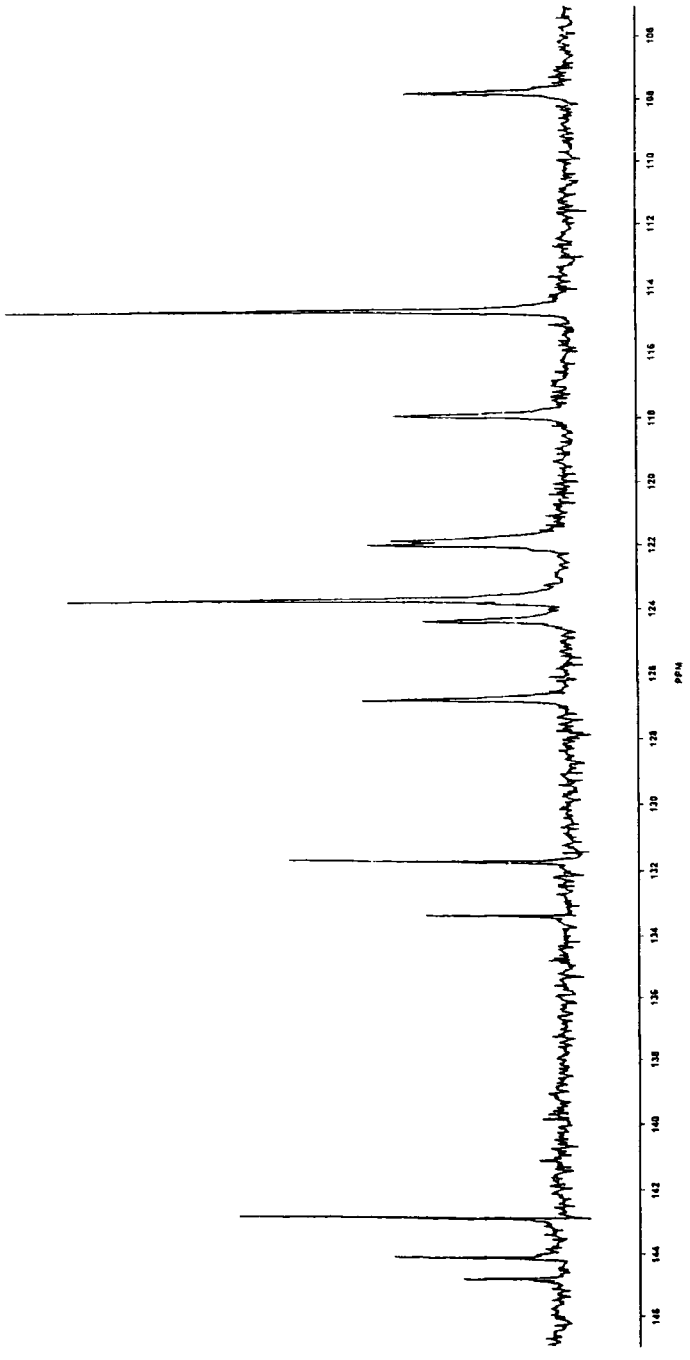

Figure A1.1. ^{13}C-NMR Spectrum of the potassium salt of the Marcoussis monomer.

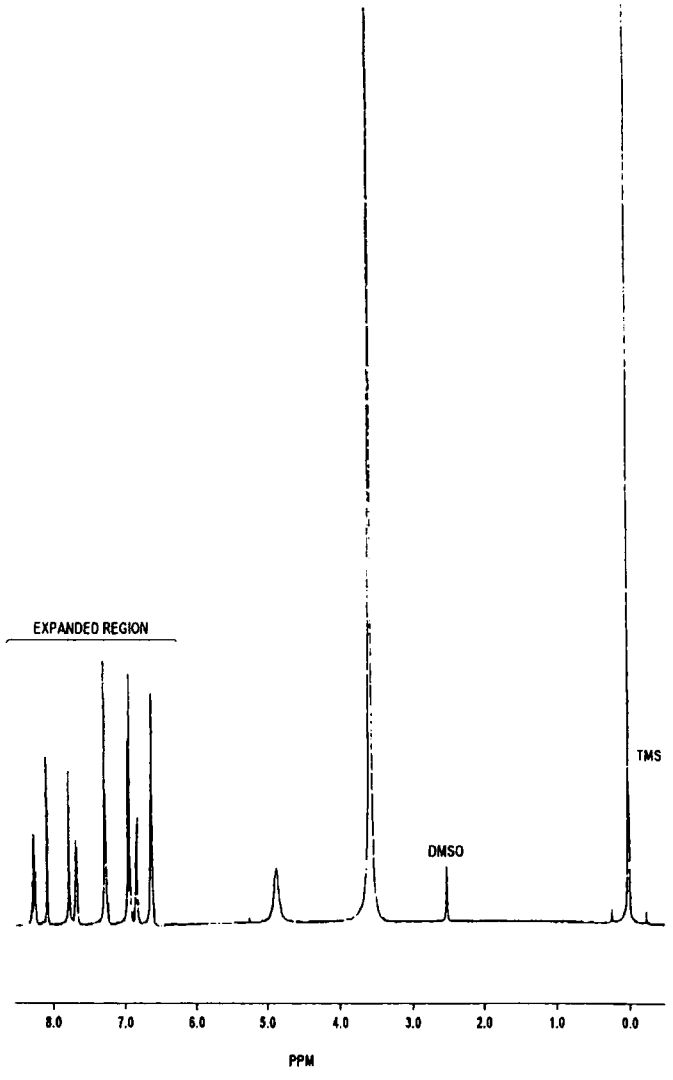

Figure A1.2. ^{1}H-NMR Spectrum of the potassium salt of the Marcoussis monomer.

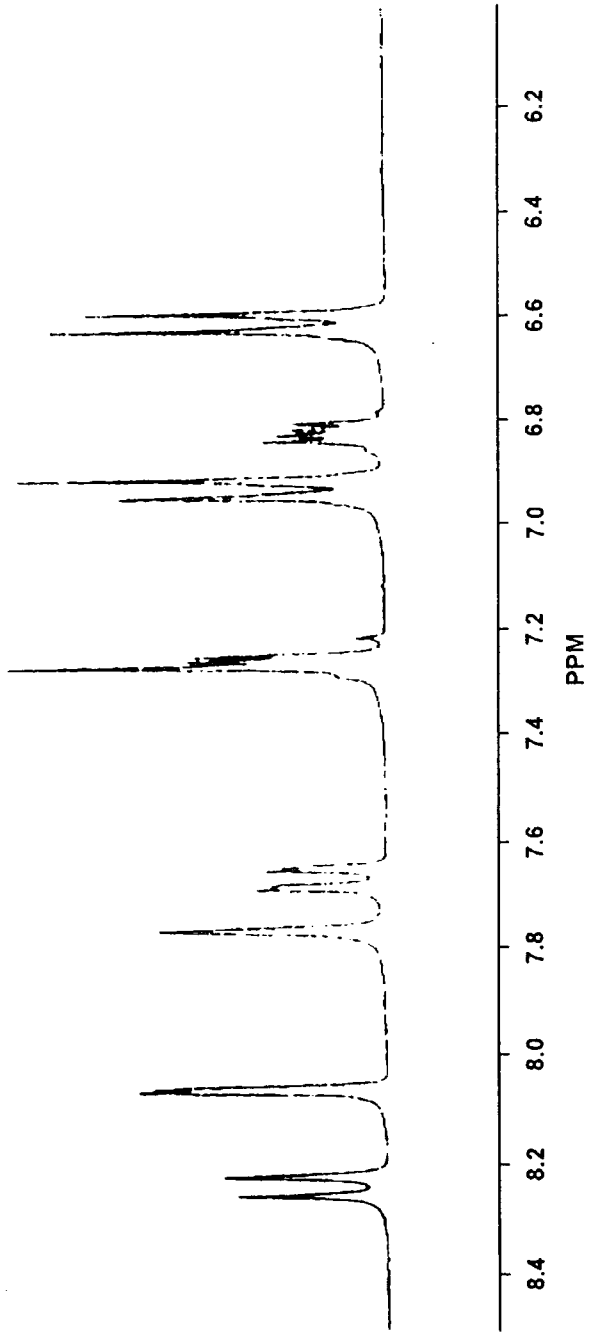

Figure A1.3. Expanded region of the ^{1}H-NMR spectrum of the potassium salt of the Marcoussis monomer.